Water–montmorillonite systems: Neutron scattering and tracer through-diffusion studies

Inauguraldissertation
der Philosophisch-naturwissenschaftlichen Fakultät
der Universität Bern

vorgelegt von
Martina Bestel
aus Deutschland

Leiter der Arbeit: Prof. Dr. L.W. Diamond (Institut für Geologie)
Co-Leiter: Dr. M. A. Glaus (Paul Scherrer Institut)
Co-Leiter: Dr. T. Gimmi (Institut für Geologie & Paul Scherrer Institut)
Co-Leiter: Dr. L. R. Van Loon (Paul Scherrer Institut)
Co-Leiterin: Dr. F. Jurányi (Paul Scherrer Institut)

Water–montmorillonite systems: Neutron scattering and tracer through-diffusion studies

Inauguraldissertation
der Philosophisch-naturwissenschaftlichen Fakultät
der Universität Bern

vorgelegt von
Martina Bestel
aus Deutschland

Leiter der Arbeit: Prof. Dr. L.W. Diamond (Institut für Geologie)
Co-Leiter: Dr. M. A. Glaus (Paul Scherrer Institut)
Co-Leiter: Dr. T. Gimmi (Institut für Geologie & Paul Scherrer Institut)
Co-Leiter: Dr. L. R. Van Loon (Paul Scherrer Institut)
Co-Leiterin: Dr. F. Jurányi (Paul Scherrer Institut)

Von der Philosophisch-naturwissenschaftlichen Fakultät angenommen.

Bern, 06.05.2014 Der Dekan: Prof. Dr. S. Decurtins

Abstract

Designs for deep geological respositories of nuclear waste include bentonite as a hydraulic and chemisorption buffer material to protect the biosphere from leakage of radionuclides. Bentonite is chosen because it is a cheap, naturally occurring material with the required properties. It consists essentially of montmorillonite, a swelling clay mineral. Upon contact with groundwater such clays can seal the repository by incorporating water in the interlayers of their crystalline structure. The intercalated water exhibits significantly different properties to bulk water in the surrounding interparticle pores, such as lower diffusion coefficients (González Sánchez *et. al.* 2008).

This doctoral thesis presents water distribution and diffusion behavior on various time and space scales in montmorillonite. Experimental results are presented for Na- and Cs-montmorillonite samples with a range of bulk dry densities (0.8 to 1.7 g/cm^3). The experimental methods employed were neutron scattering (backscattering, diffraction, time-of-flight), adsorption measurements (water, nitrogen) and tracer-through diffusion. For the tracer experiments the samples were fully saturated via the liquid phase under volume-constrained conditions. In contrast, for the neutron scattering experiments, the samples were hydrated via the vapor phase and subsequently compacted, leaving a significant fraction of interparticle pores unfilled with water. Owing to these differences in saturation, the water contents of the samples for neutron scattering were characterized by gravimetry whereas those for the tracer experiments were obtained from the bulk dry density.

The amount of surface water in interlayer pores could be successfully discriminated from the amount of bulk-like water in interparticle pores in Na- and Cs-montmorillonite using neutron spectroscopy. For the first time in the literature, the distribution of water between these two pore environments was deciphered as a function of gravimetric water content. The amount was compared to a geometrical estimation of the amount of interlayer and interparticle water determined by neutron diffraction and adsorption measurements. The relative abundances of the 1 to 4 molecular water layers in the interlayer were determined from the area ratios of the (001)-diffraction peaks.

Depending on the characterization method, different fractions of surface water and interlayer water were obtained. Only surface and interlayer water exists in Na-montmorillonite with water contents up to 0.18 g/g according to spectroscopic measurements and up to 0.32 g/g according to geometrical estimations, respectively. At higher water contents, bulk-like and interparticle water also exists. The amounts increase monotonically, but not linearly, from zero to 0.33 g/g for bulk-like water and to 0.43 g/g for

interparticle water. It was found that water most likely redistributes between the surface and interlayer sites during the spectroscopic measurements and therefore the reported fraction is relevant only below about -10 ºC (Anderson, 1967). The redistribution effect can explain the discrepancy in fractions between the methods.

In a novel approach the fractions of water in different pore environments were treated as a fixed parameter to derive local diffusion coefficients for water from quasielastic neutron scattering data, in particular for samples with high water contents. Local diffusion coefficients were obtained for the 1 to 4 molecular water layers in the interlayer of $0.5 \cdot 10^{-9}$, $0.9 \cdot 10^{-9}$, $1.5 \cdot 10^{-9}$ and $1.4 \cdot 10^{-9}$ m²/s, respectively, taking account of the different water fractions (molecular water layer, bulk-like water).

The diffusive transport of ^{22}Na and HTO through Na-montmorillonite was measured on the laboratory experimental scale (i.e. cm, days) by tracer through-diffusion experiments. We confirmed that diffusion of HTO is independent of the ionic strength of the external solution in contact with the clay sample but dependent on the bulk dry density. In contrast, the diffusion of ^{22}Na was found to depend on both the ionic strength of the pore solution and on the bulk dry density. The ratio of the pore and surface diffusion could be experimentally determined for ^{22}Na from the dependence of the diffusion coefficient on the ionic strength. Activation energies were derived from the temperature-dependent diffusion coefficients via the Arrhenius relation. In samples with high bulk dry density the activation energies are slightly higher than those of bulk water whereas in low density samples they are lower. The activation energies as a function of ionic strengths of the pore solutions are similar for ^{22}Na and HTO. The facts that (i) the slope of the logarithmic effective diffusion coefficients as a function of the logarithmic ionic strength is less than unity for low bulk dry densities and (ii) two water populations can be observed for high gravimetric water contents (low bulk dry densities) support the interlayer and interparticle porosity model proposed by Glaus *et al.* (2007), Bourg *et al.* (2006, 2007) and Gimmi and Kosakowski (2011).

Acknowledgements

The Swiss National Science Foundation (SNF), the University of Bern and the Paul Scherrer Institut are acknowledged for the financial support of this Ph.D. thesis.
I would like to express my gratitude to my thesis supervisor Prof. Larryn W. Diamond for his encouragement and advice. I am indebted to Dr. Martin Glaus for sharing his huge knowledge and patience with very constructive explanations. I thank Dr. Luc R. Van Loon for his support and the possibility to finish the Ph.D. thesis. I appreciated the contribution of Dr. Thomas Gimmi; thank you for the very helpful explanations! I acknowledge Dr. Fanni Jurányi for giving me the opportunity to work on this interesting project. My gratitude is also extended to Dr. Georg Kosakowski for useful discussions. Thank you to Dr. Cecile Marcelot-Garcia for help with Morpheus also to Dr. Michaela Zamponi and Dr. Joachim Wuttke for their help with Spheres. I thank Dr. Enzo Curti for providing a figure. S.A.R.M. (Nancy, France) and Dr. Michael Plötze are acknowledged for measurements. Prof. André Maes is thanked for his effort as external referee.

Many thanks to Sabrina Frick and Werner Müller for their help in the laboratory! I am grateful to Matthew Watson for preparing the first samples.

The LES members are greatly thanked for accommodating me well during the last 6 months of my Ph.D. work. Thanks for a nice time to Jenna, Bruno and Amir. I wish you all the best!

I thank Julien and Cecile for nice lunch and coffee breaks. I thank Silvio for reading the introduction of this thesis! Thanks to Eva & Fernando, Carmen & Juan Luis and Gwen & Thibault for the nice weekends. I enjoyed the dinners and discussions during the hard period! Together with Gwen I started the Ph.D. and I benefited also from the time together with her, summer students and Henar in the guest house where I met my boyfriend Alexandre ☺.

My dear Alexandre I thank you so much for your love, understanding, patience, encouragement and as well very helpful discussions. This work would have not been possible without your support! Many warm thanks are as well extended to the famille Trisorio! Merci beaucoup pour tous vos encouragements! Mein besonderer Dank gilt meinen Eltern, meinen Schwestern Andrea und Heike und meiner Oma für die wertvolle Unterstützung während der Doktorarbeit. Ganz ganz lieben Dank!

Table of Contents

List of Figures

List of Tables

List of Symbols

A_s	[m^2/g]	specific surface area
A	[mol/l]	molar concentration
$A_{dif}^{\Delta t_i}$	[Bq]	activity diffused through a clay pellet during time Δt_i
∇C	[mol/m^4]	concentration gradient in x,y,z-direction
dC/dx	[mol/m^4]	concentration gradient in x-direction
C_t^{dsb}	[mol/m^3]	tracer concentration in the downstream boundary reservoir at time t (days)
C_t^{usb}	[mol/m^3]	tracer concentration in the upstream boundary reservoir at time t (days)
d	[Å]	d-spacing of the wet clay
d_0	[Å]	d-spacing of the dry clay
D_l	[m²/s]	local diffusion coefficient
D_a	[m²/s]	apparent diffusion coefficient
D_e	[m²/s]	effective diffusion coefficient
$D_{e,\,IP}$	[m²/s]	effective diffusion coefficient for the interparticle pores
$D_{e,\,IL}$	[m²/s]	effective diffusion coefficient for the interlayer pores
D_f	[m²/s]	filter diffusion coefficient
D_p	[m²/s]	pore diffusion coefficient
D_0	[m²/s]	diffusion coefficient in bulk water
E	[meV]	energy transfer
ΔE	[µeV]	energy resolution
E_a	[kJ/mol]	activation energy
G	[-]	geometrical facor describing the diffusion path (tortuosity, pore connectivity, pore-size variability)
j_{tot}	[mol/m^2/s]	total diffusive flux
j_{IL}	[mol/m^2/s]	diffusive flux in the interlayer pores
j_{IP}	[mol/m^2/s]	diffusive flux in the interparticle pores
K_d	[cm^3/g]	equilibrium distribution coefficient
l	[Å]	mean jump length
M	[g/mol]	molar mass
m_{ILW}	[g]	mass of water in the interlayer pores
m_{IPW}	[g]	mass of water in the interparticle pores
m_n	[g]	mass of neutron
m_w	[g]	mass of total water of a sample
m_s	[g]	solid mass
n_{BLW}	[%]	fraction of bulk-like water
n_{ILW}	[%]	fraction of interlayer water
n_{SW}	[%]	fraction of surface water
n_W	[%]	fraction of molecular water layer
Q	[$Å^{-1}$]	scattering wave vector
q	[-]	electrostatic constraints
R	8.314 J/K/mol	gas constant
S	[cm^3/cm^3]	degree of saturation

T	[K]	temperature
t_{bt}	[days]	break through time
V_{sample}	[cm^3]	volume of the sample
w	[g/g]	gravimetric water content per dry solid mass
w_{BLW}	[g/g]	gravimetric bulk-like water content per dry solid mass
w_{IPW}	[g/g]	gravimetric interparticle water content
w_{ILW}	[g/g]	gravimetric interlayer water content
w_{SW}	[g/g]	gravimetric surface water content per dry solid mass
W	[#]	number of molecular water layer
α	[-]	rock capacity factor
Γ^T	[meV]	lorentzian line width from translational diffusion
δ	[-]	constrictivity
δ_{ILW}	[-]	constrictivity near basal surfaces
ε	[cm^3/cm^3]	total porosity
ε_{IL}	[cm^3/cm^3]	interlayer porosity
ε_{IP}	[cm^3/cm^3]	interparticle porosity
κ	[-]	capacity ratio for sorption
λ	Å	wavelength
μ_s	[-]	surface mobility
ρ_w	[g/cm^3]	pore water density (assumed to be 1 g cm^{-3} in all compartments)
ρ_{bd}	[g/cm^3]	bulk dry density
ρ_s	[g/cm^3]	solid density
τ	[-]	tortuosity
τ_S	[-]	tortuosity of the surface pathway
τ_t	[ps]	residence time for translational jump diffusion
$\hbar$	$6.68 \cdot 10^{-16}$ eV·s	Planck constant

List of Abbreviations

BET	Brunauer-Emmet-Teller
BLW	Bulk-like water from FWS
CEC	Cation exchange capacity
DDL	Diffuse Double Layer
D_2O	Deuterated water
dsb	downstream boundary
EGME	Ethylene glycol monoethyl ether
FRM II	Forschungsneutronenquelle Heinz Maier-Leibnitz
FWS	Fixed window scans
HDO	Partly deuterated water
HTO	Partly tritiated water
ICP-MS	Inductively coupled plasma mass spectrometry
ILW	Interlayer water
IPW	Interparticle water
NSE	Neutron spin echo
PSI	Paul Scherrer Institut
QENS	Quasielastic neutron scattering
SINQ	Swiss Spallation Neutron Source
SW	Surface water clearly influenced by surfaces as determined from FWS opposed to interlayer water determined from diffraction.
tof	time of flight
TOT	Crystalline Tetrahedra-Octahedra-Tetrahedra clay sheets
usb	upstream boundary
W	Molecular water layer

1. Chapter 1: Introduction

1.1 Motivation

Bentonite consists of various aluminium phyllosilicate minerals. Most of these minerals (~80 %) are smectites, with the largest fraction being montmorillonite. Smectites have nanoporous interlayers, where water can be intercalated in the atomic structure as structural water. The structural water has properties different to bulk water in the surrounding interparticle pores (Low, 1976). Smectites have numerous applications due to their manifold properties. One particularly interesting property is their ability to swell upon contact with water, resulting in a low hydraulic conductivity, leaving diffusion as main dynamic transport mechanism. It is for this hydraulic self-sealing capacity that bentonite is envisaged to be part of the multi-barrier system in a geological repository for high-level nuclear waste and spent fuel in Switzerland (Fig. 1; Nagra, 2009) as well as in other countries (Czech Republic, Finland, Japan, Republic of Korea, Spain, Sweden, and USA). Such repositories are to be sited in deep geological formations that sustain tunnelling and the excavation of caverns. The waste packages are placed in the caverns on a base of compacted bentonite and the remaining space is filled with pelletized clay and surrounded by cement or clay to provide another barrier (buffer or backfill). When groundwater enters such barriers, the clay reacts as an absorbent and it swells. Thus, the combination of waste packaging and bentonite buffer within an engineered repository, all surrounded by a stable geological formation, serves as a multi-barrier to protect the biosphere from contamination by radionuclides.

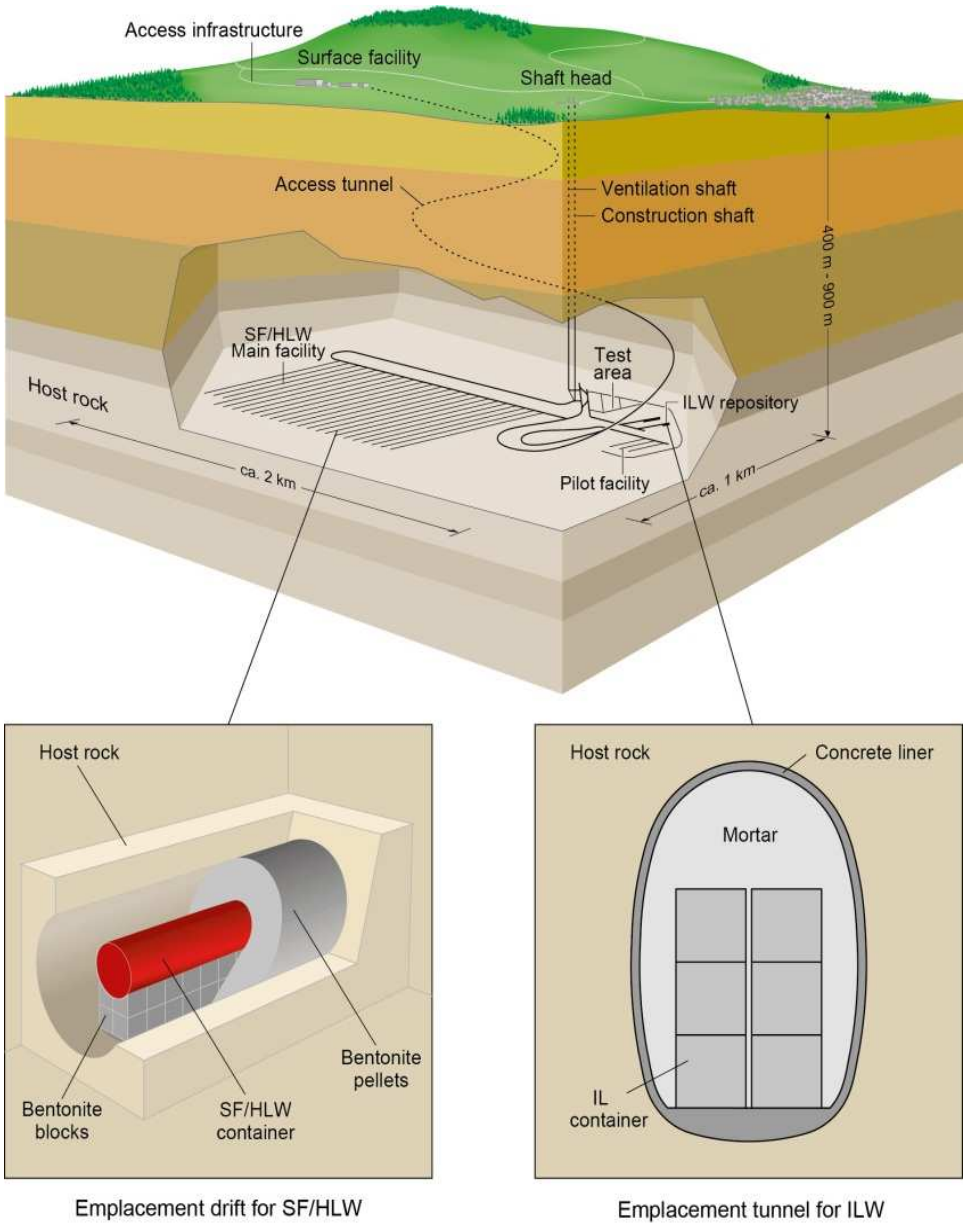

Figure 1. Possible layout for the deep geological disposal of vitrified high-level radioactive waste (HLW), spent fuel (SF) and intermediate-level waste (ILW) in Opalinus clay (Nagra, 2009).

Because diffusion is the main transport mechanism for the propagation of radionuclides through bentonite, diffusion coefficients in such swelling clays have to be quantified in order to

predict the long-term behavior of the repository. While cations undergoing cation exchange are found to diffuse preferentially in the interlayer or diffuse double layer (DDL) (Glaus *et al.*, 2007), anions are excluded from interlayers (Van Loon *et al.*, 2007).

The motivation of this Dissertation was to investigate the diffusive behavior at atomic and laboratory scales, based on the structural properties of the smectites. The diffusion of structural water and the molecular transport of radionuclides through the pores could be studied over a range of temporal and spatial scales.

1.2 Background

1.2.1 Swelling clay-water systems

Montmorillonite is a negatively charged 2:1 swelling clay mineral, meaning that an octahedral sheet (O) is sandwiched between two tetrahedral (T) silica sheets (Fig. 2). A negative charge in the O-sheet exists due to isomorphous substitution of Mg^{2+} for Al^{3+}. The charge deficiencies are balanced by counter cations sitting in the interlayer between TOT layers. When swelling clay is in contact with water, pores are saturated in order of increasing layer distance, that is, first the interlayer (atomic scale) and second the interparticle pores (micro- and mesoscopic scale) (Sing *et al.* 1995; Salles *et al.*, 2010). The intercalation of molecular water layer in the interlayer occurs stepwise (where *W* denotes the number of water molecule layers) and leads to variable basal lattice spacings (d-spacing, Å) in the c direction (i.e. swelling), depending on the type of counter cations. Cations are surrounded by adsorbed water molecules and can either move (e.g. Ca^{2+}, Na^{+}) or cannot move (e.g. Cs^{+}) to the central region between clay layers during progressive hydration (Sposito, 1984, Hensen *et al.*, 2002). In the literature a distinction is drawn between outer sphere complexes, with strongly hydrated cations like Ca^{2+}

or Na^+ (Sposito *et al.*, 1999), and inner sphere complexes with less hydrated cations adsorbed at the contact plane, like Cs^+ (Sposito *et al*., 1999). Crystalline swelling occurs between d-spacings of 10-22 Å and osmotic swelling occurs with diffuse double layers beyond d-spacings of 22 Å (Norrish, 1954; Kozaki *et al*., 1998; Muurinen et al., 2004; Saiyouri *et al.*, 2004; Holmboe *et al.*, 2012).

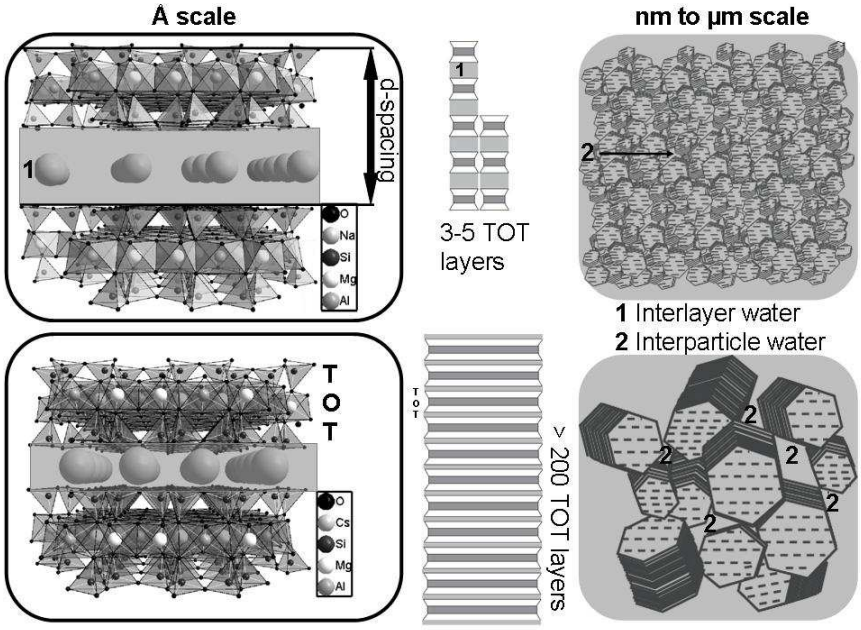

Figure 2. Left: schematic representation at the atomic scale of arrangements of tetrahedral (T) - octahedral (O) - tetrahedral (T) aluminosilicate sheets. The aggregates are stacked together (center) to form the particles. Right: schematic representation shows the clay particles with surrounded interparticle pores at the microscopic scale. Note the different structure for Na-montmorillonite (top) and Cs-montmorillonite (bottom).

In the diffuse double layer model (DDL) of Gouy (1910) and Chapman (1913) the clay surface is envisaged as a negative condenser plate, which is charge-compensated by cations (Fig. 3). The attrative force that a water dipole experiences depends on the distance to the clay surface. An electrical potential can arise due to repulsive

forces between the charged surface and cations under certain physicochemical conditions. Overlapping electrical potentials, e.g. when TOT layers are very close, can exist depending on the charge density, ionic composition (ionic strength) and dielectric permittivity of the pore solution. All these factores thus influence the thickness of the DDL. The water is interposed between the charged surface and counter ions like Ca^{2+} or Na^{+} in the diffuse layer with fixed distance from the clay surface (contrary to Cs) (Kosakowski *et al*., 2008). Cations like Cs^{+} (Sposito *et al*., 1999) are adsorbed on the Stern-Helmholtz layer and, hence, the water molecules from the hydration shell are missing at the contact plane.

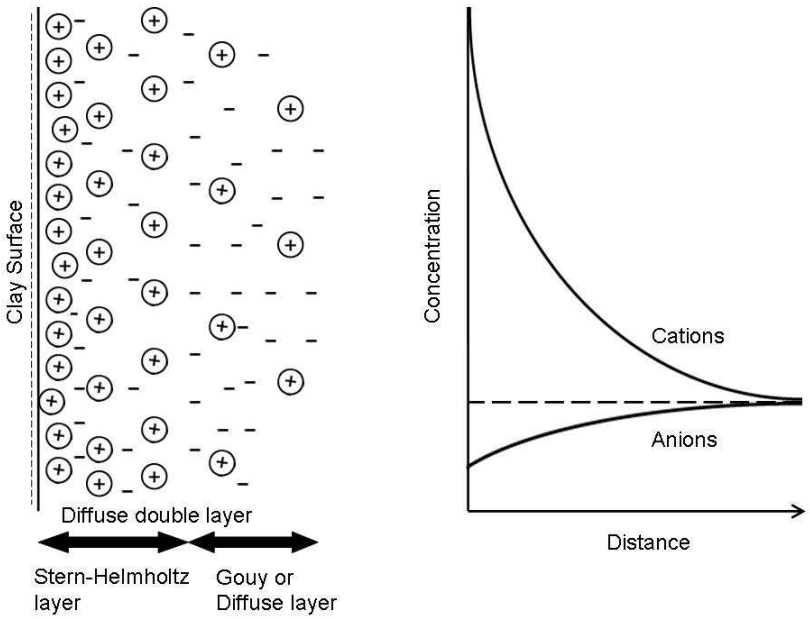

Figure 3. Schematic representation after Mitchell (2005). Left: Diffuse double layer consisting of a Stern-Helmholtz layer and Gouy or diffuse layer. Right: Distribution of ions adjacent to a negatively charged clay surface.

1.2.2 Literature review

Swelling clays, such as montmorillonite, have a large specific surface area when water is intercalated in the interlayer. The total specific surface area ($A_{s,\,tot}$, m^2/g) can be subdivided into external ($A_{s,\,ext}$, m^2/g) and internal ($A_{s,int} = A_{s,tot} - A_{s,ext}$) parts, e.g. for montmorillonite $A_{s,\,ext}$ = 28.0 m^2/g (González Sánchez et al., 2008a) and $A_{s,\,tot}$ = 807 m^2/g (Cases *et al.*, 1992). The surface area is relevant when obtaining the gravimetric interlayer water content w_{ILW} (g/g) through geometrical calculations: $w_{ILW} = 1/2 \cdot A_{s,int} \cdot (d - d_0) \cdot \rho_w \cdot 10^{12}$, where d (Å) is the measured d-spacing, d_0 (Å) the d-spacing of the dry clay given by the volume occupied by the TOT sheets and charge-compensating cations, and ρ_w (g/cm^3) the density of the adsorbed molecular water layer. Classical methods to determine w_{ILW} are based on quantifications of A_s from adsorption isotherms in combination with d-spacing from diffraction measurements (Bérend et al., 1995, Cases *et al.*, 1992, Cases *et al.*, 1997, Chiou and Rutherford, 1997, Michot *et al.*, 2006). The Brunauer-Emmett-Teller (BET) theory explains the adsorption of gas molecules on a solid surface and forms the basis for an important analytical technique for measuring the A_s of a solid. Common methods are nitrogen adsorption to determine $A_{s,\,ext}$, and water adsorption gravimetry or ethylene glycol methyl ether (EGME) adsorption to determine $A_{s,tot}$. Water adsorption gravimetry provides reasonable results for smectites with a high $A_{s,int,}$ (Madsen and Kahr, 1996). The total surface area is obtained using the assumption that the adsorbed water is present as one water layer. This method also gives information about the pore size distribution (structure and different porosities). However, there are high uncertainties in ρ_w. Martin (1960) determined ρ_w as a function of w (g/g) through pycnometric and X-ray diffraction measurements. For w corresponding to less than three molecular water layers (W), ρ_w is greater than that of normal water,

whereas at higher *w* it is less. This has an impact on the viscosity and mobility, as can be seen in diffusion properties (Martin, 1960). Anderson and Hoekstra (1965) used X-ray diffraction to investigate the difference in structure between surface water in the interlayers and free water in the interparticle pores of montmorillonite. The detected X-ray (001)-diffraction peaks for interlayer water correspond to a hexagonal ice structure exhibiting supercooling and a reduction in the usual freezing temperature of a liquid. The water in the interparticle pores has a bulk-like water structure (no supercooling, usual freezing temperature). The freezing behavior of the interlayer water in smectites could be also confirmed with Fixed Window Scans (FWS) on a neutron backscattering spectrometer (Gates *et al*., 2012, González Sánchez *et al*., 2008b).

Interactions on the atomic scale (ps, Å) from electrostatic constraints (q, -) are known to affect the local diffusion coefficient (D_l, m^2/s), defined as: $D_l = q \cdot D_0$ and the structure of the water (González Sánchez *et al.*, 2009). Bordallo *et al.*, (2008) and González Sánchez *et al*, (2008b) obtained D_l for Na-montmorillonite with low *w* from quasielastic neutron scattering (QENS) (Tab. I). González Sánchez *et al.* (2009) compared the water diffusion in compacted clays on two different scales with: (i) QENS at the observation scale of ps (Å), and (ii) tracer experiments at the observation scale of days (mm to cm). The obtained activation energies in swelling clays (Na- and Ca-montmorillonite) diverge notably due to differences in the diffusive processes on the different observation scales. Malikova *et al.* (2008) and Marry *et al.* (2011) performed QENS and nuclear spin echo (NSE) experiments on hectorite (smectite). The diffusion coefficients from NSE refer to temporal and spatial scales between those of QENS and tracer experiments. The complementary technique bridges the diffusion process of water in montmorillonite at different scales. Churakov and Gimmi (2011), Marry *et al.*, (2002, 2003), Marry and Turq (2003), Dufrêche *et al.* (2001), Malikova *et al.* (2003, 2004a, 2004b) and Ro-

tenberg *et al.*, (2007) successfully linked the different scales when modeling ion dynamics. Marry *et al.* (2002, 2003), Marry and Turq (2003), Dufrêche *et al.* (2001), Malikova *et al.* (2003, 2004a, 2004b) and Rotenberg *et al.* (2007) were able to determine the overall dynamic behavior of ions including the exchange properties between interlayer and interparticle pores. Different dynamic behavior was obtained for Na^+ and Cs^+ in the interlayer and near surfaces. The behavior of Na^+ is similar to that in bulk water, while Cs^+ partly dehydrates and diffuses by jumping from site to site (Malikova *et al.*, 2004).

Diffusion on the scale of days and mm-cm represents summation effects of (i) electrostatic constraints (q, -), e.g. the interaction forces between electrically charged surfaces, ions and water during clay hydration, and (ii) geometrical effects (G, -). The latter are determined by the tortuosity (τ, -) and constrictivity (δ, -) of the diffusion path according to $G = \tau / \delta$ (González Sánchez *et al.*, 2009). The diffusive transport of water and ions through smectites has been intensively studied with tracer experiments (Tab. I) to derive transport and retardation properties (D_e, D_p, α and D_a) for cations of different valences and sizes and water. Cations that undergo cation exchange due to sorption processes on the charged clay surfaces are significantly retarded compared to water tracers (Glaus *et al.*, 2007, Kozaki *et al.*, 1998 and Kozaki *et al.*, 2008). Combined reactions of ion exchange and surface complexation on the clay surface also take place (Bradbury and Baeyens, 2003). Surface diffusion enhances the diffusive rates for cations undergoing cation exchange. While such cations are found to diffuse preferentially in the interlayer and DDL (Glaus *et al.*, 2007), anions are excluded (Van Loon *et al.*, 2007). Contrary to the effective diffusion coefficient (D_e, m^2/s) of ionic species, which are dependent on the ionic strength of the pore solution and the bulk dry density (Glaus *et al.*, 2007, Kozaki *et al.*, 1998 and Kozaki *et al.*, 2008), D_e for neutral species depends only on the bulk dry density of the

sample (Nakazawa *et al.*, 1999; Sato *et al.*, 2003 and Suzuki *et al.*, 2004).

Table I. Effective, apparent and local diffusion coefficients (D_e, D_a, D_l) from tracer through- and in-diffusion (ID, TD), quasielastic neutron scattering (QENS) and neutron spin echo (NSE) experiments and molecular dynamic simulation (MDS) for montmorillonite (Mnt), smectites (Smc), bentonite (Bnt) and hectorite (Hct). Different Exchangeble cations (EC), bulk dry densities ρ_{bd}, (g/cm^3), gravimetric water contents w (g/g), molar concentrations A (mol/l) and temperatures T (°C) were used. The superscripts are a: $NaClO_4$, b: NaCl solution.

Reference		EC	ρ_{bd} and w	Tech-nique	Tracer	A		T
Glaus *et al.*, 2007	Mnt	Na^+	1.95	TD	Sr^{2+}, Na^+	1 / 0.1 [a]	D_e	25
Glaus *et al.*, 2010	Mnt	Na^+	1.90	TD	HTO, Na^+, Cl^-	1 / 0.1 [a]	D_e	25
Glaus *et al.*, 2013	Mnt	Na^+	1.3, 1.6	TD	Na^+, HTO	salt gradient [a]	D_e	25
González Sánchez *et. al.*, 2008a	Mnt	Na^+/ Ca^{2+}	1.90	TD	HTO	0.01, 1.0 [b]	D_e	0-60
Kozaki *et al.*, 1996	Mnt	Na^+	0.9-1.8	ID	Cs^+		D_a	5-50
Kozaki *et al.*, 2001	Mnt	Na^+	0.7-1.8	ID	Cl^-		D_a	5 - 50
Kozaki *et al.*, 2008	Mnt	Na^+	1.0	ID	Na^+	0.05 - 0.5 [b]	D_a	15-50
Nakazawa *et al.*, 1999	Mnt	Na^+	0.8-2.0	ID	Na^+, water		D_a	25-50
Sato *et al.*, 2002	Smc	Na^+	1.0, 1.5	TD	HTO		D_e	25
Sato *et al.*, 2007	Bnt		1.3, 1.6, 1.9			0.01-1.0 [b]	D_e	25
Suzuki *et al.*, 2004	Mnt	Na^+	0.9, 1.35	TD	HDO		D_e	25-50
Bordallo *et.al.*, 2008	Mnt	Na^+	only ILW	QENS, NSE			D_l	
Malikova *et.al.*, 2008	Hct		only ILW	QENS			D_l	25
Marry *et.al.*, 2011	Hct	Na^+	only ILW	QENS, NSE			D_l	25-75
González Sánchez *et. al.*, 2008b	Mnt	Na^+/ Ca^{2+}	only ILW	QENS	water		D_l	25-95

1.2.3 Diffusion in porous media (Macro diffusion)

Based on several ideas and concepts (e.g. Fick's first and second laws) the symbols for diffusive properties vary widely (Shackelford and Moore, 2013). The total diffusive flux (j_{tot}, $mol/m^2/s^1$) through the total sample volume, which is for instance obtained at steady state

(Fick's first law), is defined as (Fig. 4):

$$j_{tot} = -D_e \frac{dC}{dx} \quad (1)$$

where dC/dx (mol/m^4) is the pore water concentration gradient in the x-direction and D_e (m^2/s) the effective diffusion coefficient describing the molecular mobility:

$$D_e = \varepsilon \cdot D_p \quad (2)$$

with D_p (m^2/s) the pore diffusion coefficient:

$$D_p = D_0 \frac{\delta}{\tau} = D_0 \cdot G \quad (3)$$

where ε (-) is the diffusion-accessible porosity of the medium and D_0 (m^2/s) the diffusion coefficient in bulk water. The concentration change during the transient phase (Fick's second law) is given as:

$$\frac{dC}{dt} = \frac{D_e}{\alpha} \frac{d^2C}{dx^2} = D_a \frac{d^2C}{dx^2} \quad (4)$$

For sorbing cations undergoing cation exchange, the apparent diffusion coefficient D_a (m^2/s) and the rock capacity factor α (-) are the decisive values. The latter is defined as $\alpha = \varepsilon + \rho_{bd} \cdot K_d$, with K_d (cm^3/g) the equilibrium distribution coefficient and ρ_{bd} (g/cm^3) the bulk dry density. As mentioned, adsorption on the clay surface may lead to enhanced diffusive rates and are therefore a broadly discussed topic in the literature (Glaus et al. 2007, 2013; Birgersson and Karnland, 2009; Gimmi and Kosakowski, 2011). The difference between interlayer

and interparticle pores from geometrical calculations is considered as a transport-relevant property in the case of dual porosity models for diffusion (e.g. Bourg *et al.*, 2006, Bourg *et al.*, 2007, Gimmi and Kosakowski, 2011). The distribution of pore water between different pore compartments, different transport-accessible porosities for ions compared to neutral species and the specific interactions of ions with the charged surfaces (e.g. sorption) are taken into account in those models. The total flux (j_{tot}, mol/m^2/s) is viewed as the sum of two parallel fluxes through the interlayer pores (j_{IL}, mol/m^2/s) and any larger pores (j_{IP}, mol/m^2/s), such as the interparticle pores.

1.3 Objectives

1.3.1 Determination of geometrical properties of clays

In this study, neutron spectroscopy was applied and fractions of pore water with slightly different properties were obtained and compared with fractions obtained from adsorption of liquids and neutron diffraction. The fractions in montmorillonite samples were specifically compared with regard to:

• Different hydration and saturation paths from vapor or water phase under free or confined swelling conditions. In the literature the fractions of pore water were frequently investigated under confined swelling conditions and data are presented as a function of the bulk dry density (Van Loon *et al.*, 2007).

• Water distribution in Na-montmorillonite with high gravimetric water contents. Hitherto, only samples with low gravimetric water content had been characterized by neutron spectroscopy. In the present study we present and compare for the first time a complete hydration curve (w_{SW} /

w_{BLW} and w_{ILW} / w_{IPW} versus w and d-spacing) obtained by both methods.

• Cs and Na as counter cations. The aim was to reveal the effect of cation hydration, which contributes to the concept of microstructure qualitatively described in Melkior *et al*. (2009).

1.3.2 Tracer diffusion in clays

The aim of the tracer diffusion experiments was to investigate the diffusive transport of HTO and ^{22}Na and its dependence on the bulk dry density and ionic strength under conditions under which a measurable contribution of both fluxes (j_{IL} and j_{IP}) can be expected.

• The variation of the ionic strength shall give information on the validity of the various porosity models (single, dual). For this purpose and for obtaining internally consistent results, the diffusive fluxes of HTO and ^{22}Na through medium- to weakly compacted Na-montmorillonite samples were simultaneously measured and effective diffusion coefficients were derived.

• The temperature of the diffusive flux was varied in order to see the effects of the bulk dry density on the deduced activation energy.

1.3.3 Quasielastic neutron scattering in clays

A further aim of this study was to quantify the amount of surface water (SW) in interlayer pores and bulk-like water (BLW) in larger (e.g. interparticle) pores with Fixed Window Scans (FWS) on a neutron backscattering spectrometer (Chapter 2). It was assumed that FWS would yield more precise values than the derived fractions from d-spacing and surface area measurements (Chapter 2). However, it turned out that, during the FWS measurements, water most likely redistributes and therefore the obtained fraction is relevant only below about -10 °C (Anderson, 1967). This conclusion is not yet verified and for this reason the data analysis using

these values is also presented. The aim was to obtain D_l from QENS for Na-montmorillonite with 1 to 4 *W*. For the first time in the literature, the fractions of molecular water layers (n_W), surface water (n_{SW}) and bulk-like water (n_{BLW}) were taken into account in order to obtain D_l.

1.4 Material and Methods

1.4.1 Techniques applied

Macroscopic diffusion can be measured in a tracer through-diffusion setup according to Figure 4 (modified after Van Loon *et al.*, 2005). The sample of interest, a cylindrical clay pellet with both radius and thickness of $1.00 \cdot 10^{-2}$ m, and low (0.80, 1.07), intermediate (1.32, 1.33, 1.35) and high (1.56, 1.63, 1.68, 1.70) bulk dry densities (g/cm^3), was located between reservoirs of high and low concentrations of the tracer. A solution of $NaClO_4$ at various concentrations (0.1, 1 and 5 mol/l) in both reservoirs circulated at a flow rate of 0.1 ml/min, thereby maintaining an almost homogeneous tracer concentration for one month until the sample was saturated. Afterwards, the tracer through-diffusion experiment of HTO and ^{22}Na was started. The flux of the steady state was evaluated and D_e obtained (Fig. 5) analogously to Van Loon *et al.* (2005).

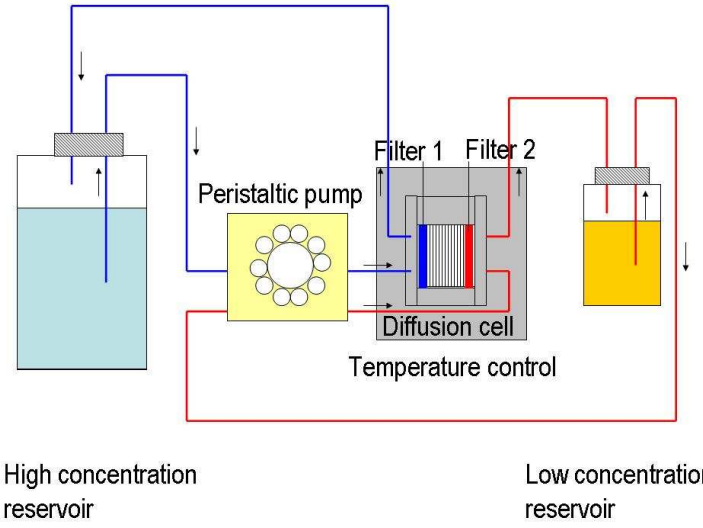

Figure 4. Sketch of the tracer through-diffusion experiment (modified after Van Loon *et al.*, 2005). The sample is located between two reservoirs and stainless steel filters. The arrows present the directions of the flow from the high concentration reservoir to filter 1 (blue) and from the low concentration reservoir to filter 2 (red). The temperature was maintained with a thermostat.

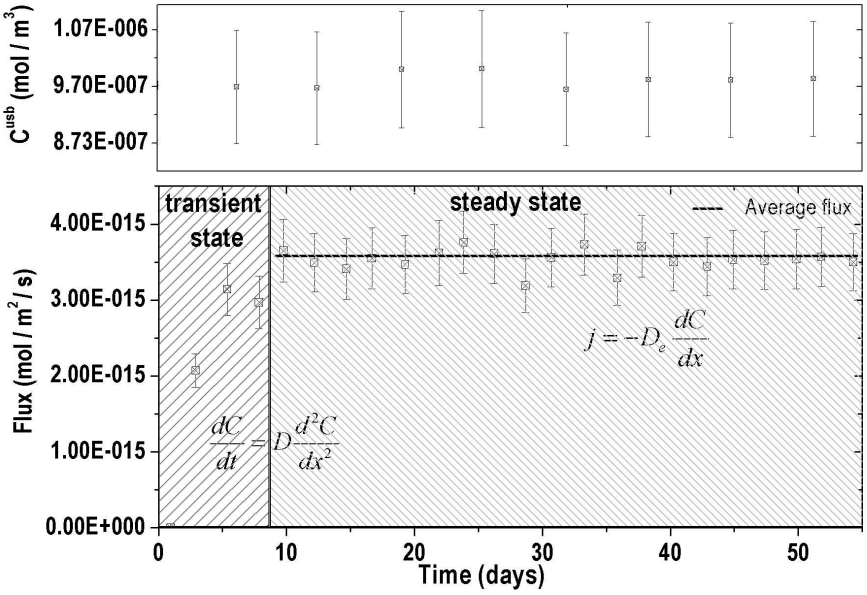

Figure 5. Tracer concentration in the high tracer concentration reservoir (top) and the diffusive flux to the low tracer concentration reservoir (bottom) as a function of time. The values in the dark gray shaded area correspond to the transient state (Fick's second law) and the values in the light gray shaded area correspond to the steady state (Fick's first law).

Methods using neutrons are complementary to those using X-ray because bulk matter is transparent for neutrons. Neutrons are uncharged particles, carry a magnetic moment and have wavelengths (λ, Å) similar to atomic scales (Pynn, 2009). The energy resolution *ΔE*, which is in the order of μeV, is very high. Neutrons interact with the atomic nuclei in a material through inelastic, quasielastic or elastic scattering processes (Fig. 6). During an inelastic scattering process, the neutron with mass $m_n = 1.675 \cdot 10^{-27}$ kg can lose or gain energy *E* (meV):

$$\Delta E = \hbar^2 \frac{\vec{k}_i^{\,2} - \vec{k}_f^{\,2}}{2 \cdot m_n} \quad (5)$$

where $\hbar = 6.68 \cdot 10^{-16}$ eV·s is the Planck constant and $\vec{k}_i$ the incident and $\vec{k}_f$ the final wave vectors in real space. Transfer of energy and momentum can occur within the sample, e.g. in the case of diffusion resulting in quasielastic neutron scattering (QENS). The momentum transfer (Δp) is the product of $\hbar$ and the scattered wave vector in reciprocal space *Q* (Å^{-1}):

$$\Delta p = \hbar \cdot Q \quad (6).$$

Neutron scattering allows the study of materials that contain light elements such as hydrogen (^{1}H) with a large total neutron scattering cross section compared to other elements (http://www.ncnr.nist.gov/resources/n-lengths/). Incoherent scattering takes place mainly where the incident neutron wave interacts independently with each hydrogen nucleus in the sample; the scattered waves from different nuclei cannot interfere with each other (Hippert *et al.,* 2006). The higher coherent scattering for the chemically equivalent deuterium (^{2}H) arises from a periodicity of the atomic lattice (Hippert *et al.,* 2006). The scattered wave from an equilibrium

position of an atom is elastic giving information about the structure. Bragg's law (Eq. 7) can be applied to characterize the structure:

$$n \cdot \lambda = 2 \cdot d \sin\theta \quad (7)$$

with n (-) an integer, λ (Å) the incident wavelength, d (Å) the d-spacing between the planes in the atomic lattice, and θ (º) the angle between the incident and the scattered beam. The wave vectors in equation 5 can change in direction but the absolute values are identical: $\left|\vec{k}_i\right| = \left|\vec{k}_f\right|$ and there is no energy transfer (E = 0 meV). The elastic incoherent scattering is isotropic and usually seen as background.

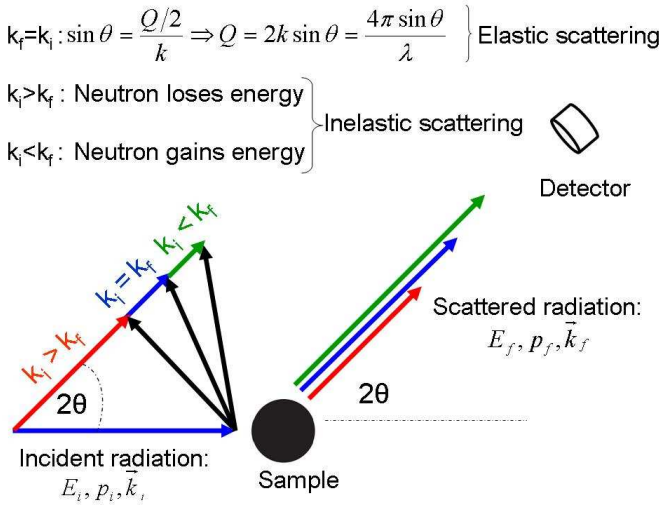

Figure 6. Representation of the elastic and inelastic scattering process with the incident energy (E_i), momentum (p_i) and wave-vectors ($\vec{k}_i$) and scattered final energy (E_f), momentum (p_f) with and wave vectors ($\vec{k}_f$). *Q* is the scattering wave vector in the reciprocal space.

The total scattering of a hydrated Na-montmorillonite sample is predominantly incoherent. The total scattering is heavily dominated by hydrogen belonging to the water in the interlayer or in-

terparticle voids and hydroxyl groups. Depending on the technique and experimental set up of the instrument (e.g. λ, ΔE, Q) the scattering process can give information about the position and motion of the hydrogen. The energy spectra of scattered neutrons interacting (i) with dry clay has an elastic peak at $E = 0$ only (ii) with hydrated clay has a quasielastic broadening centered around the elastic peak due to dynamics of water (Fig. 7). Local diffusion coefficients D_l (m^2/s) can be obtained e.g. from quasielastic neutron scattering (QENS). The obtained scattering signal of the localized diffusion process with a scattered intensity *S(Q,E)* is proportional to the sum of the elastic intensity $A(Q)\cdot\delta(E)$ and the long-range diffusion $[1-A(Q)]\ L(\Gamma^T, E)$ (Bee, 1988):

$$S(Q,E) \propto A(Q)\cdot\delta(E) + [1-A(Q)]\cdot L(\Gamma^T, E) \quad (8)$$

The functions of the long-range diffusion are Lorentzians (*L*) with a line width Γ^T (meV) from translational diffusion. Different length scales and geometries are accessible through the *Q*-dependence. The local diffusion coefficient D_l (m^2/s) is determined from the probability that a particle at time t=0 was at origin r=0 and the same particle is found at time t and position r in a volume element dr: $G_s(r, t=0) = \delta(r)$ (Bee, 1988):

$$\frac{d}{dt}G_s(r,t) = D_l\nabla^2 G_s(r,t)\,. \quad (9)$$

The solution of the equation is (Bee, 1988):

$$G_s(r,t) = (4\cdot\pi\cdot D_l\cdot t)^{-3/2}\exp\left(-\frac{r^2}{4\cdot D_l\cdot t}\right). \quad (10)$$

The local diffusion coefficient D_l can be obtained from the dominating translational diffusion to

the rotational diffusion at small *Q* through a double Fourier transformation from the real space of position and time (r, t) to the reciprocal space (Q, ω) (Bee, 1988):

$$S(Q,\omega) = \frac{1}{\pi\hbar}\frac{D_l Q^2}{\omega^2 + D_l Q^2} \quad (11)$$

representing Fick's law. At high *Q* the approximation is not valid anymore and the line widths Γ^T can be described by the jump diffusion model (Singwi and Sjölander, 1960):

$$\Gamma^T(Q) = \frac{\hbar \cdot D_l \cdot Q^2}{1 + D_l \cdot Q^2 \cdot \tau_t} \quad (12)$$

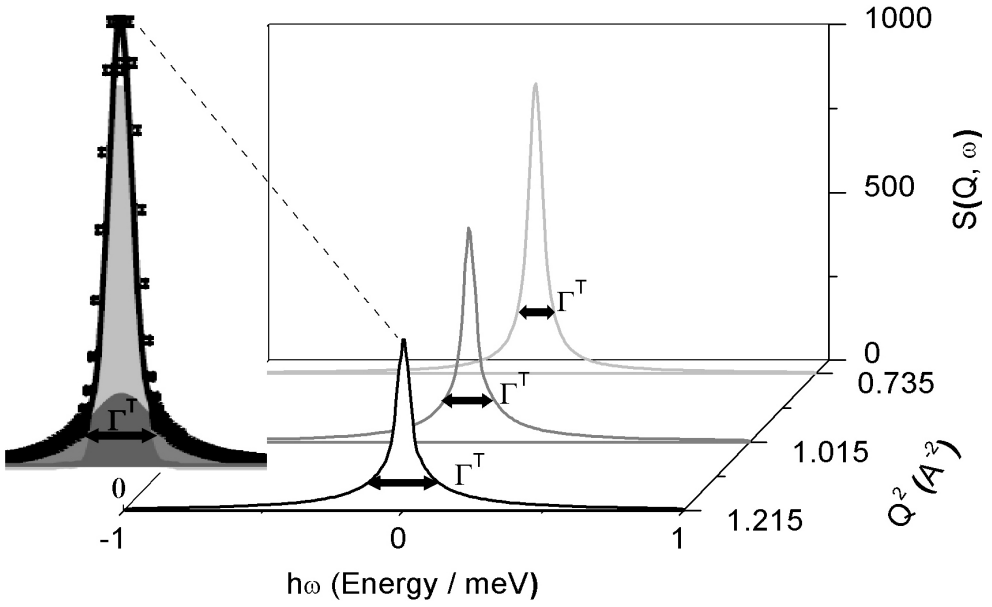

Figure 7. The scattered intensity ($S(Q,\omega)$) as a function of energy transfer ($\hbar\omega$) for different scattering wave vector (Q) values. The QENS spectra were fitted with Lorentzians of different translational line width (Γ^T, meV). The inserted figure shows the total scattering intensity, the localized diffusion with an elastic peak at *ΔE* = 0 (light grey) and long-range diffusion with a quasielastic broadening (dark grey) (Bee, 1988).

QENS experiments were performed on FOCUS (SINQ, PSI, Villigen, Switzerland), a time and space focusing time-of-flight (tof) spectrometer for cold neutrons (Fig. 8) (Mesot *et. al.*, 1995). The neutrons are monochromized and pulsed. The number of neutrons scattered in a sample are measured as a function of intensity *I (2θ, tof)*. The results from geometrical properties (adsorption of liquids, neutron diffraction) were compared with results from the Fixed Window Scan (FWS) measurements on a neutron backscattering spectrometer SPHERES (FRM II, Garching, Germany). The technique allows fixed incident and final wavevectors (Fig. 8) (Wuttke *et. al.*, 2012). The energies of the neutrons are filtered through Bragg reflection from monochromator and analyzer crystals under an angle Θ close to 90°. Dynamic processes on a time scale slower than the instrument resolution in the order of µeV are not resolved and counted within the scan. Elastic scans were performed in this study as a function of temperature. The method can give an overview of the various dynamics of a system.

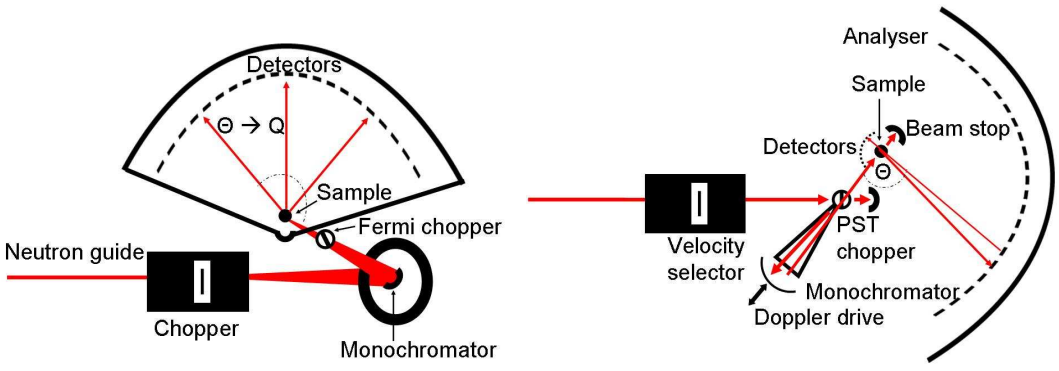

Figure 8. Left) Schematic drawing of FOCUS (SINQ, PSI, Villigen, Switzerland) and the main components (modified after Mesot *et al.*, 1995). Right) Schematic drawing of SPHERES (FRM II, Garching, Germany) and the main components (modified after Wuttke *et al.*, 2012).

1.4.2 Samples used

Montmorillonite from Milos Island (Greece) was equilibrated with CsCl and NaCl and converted into a homoionic Cs- and Na-montmorillonite (Chapter 2). A final powdery product was obtained by freeze drying. For the experiments, the homoionic clay powder was desiccated at 110 °C for one day and the amount of dry clay (m_s, g) was subsequently hydrated. The sample preparation was an important part of this work because the sample had to be homogeneous in order to compare results from QENS and tracer experiments performed on different splits. For the tracer experiments, the samples were saturated under volume-constrained conditions. In contrast, the samples for neutron scattering experiments were hydrated through (i) vapor phase in a desiccator and (ii) liquid phase in volume-constrained conditions. Thereafter, the sample was compacted to a bulk dry density (g/cm^3) defined as $\rho_{bd} = m_s / V_{sample}$ and filled into hermetic aluminium sample cans. The saturation (S,-) is defined as the volume of water per volume of total pores (ε, -), with $\varepsilon = 1 - \rho_{bd}/\rho_s$:

$$S = \frac{w \cdot \rho_{bd}}{\varepsilon \cdot \rho_w} \quad (13)$$

where w is the gravimetric water content defined as mass of total water (g) per dry clay mass (g) and $\varepsilon \cdot \rho_w / \rho_{bd}$ equals the gravimetric water content at full saturation (w_{sat}) (or analogously $w \cdot \rho_{bd} / \rho_w$ equals the volumetric water content) for the measured ρ_{bd} and the solid density (ρ_s, g/cm^3). We aimed to obtain a high degree of saturation to allow comparison of the results from QENS and tracer experiments. However, when compacting the hydrated powder to a corresponding bulk dry density a significant amount of interparticle pores remained unsaturated. The samples for the neutron scattering experiments were, for this reason, characterized through w.

Inhomogeneities of the bulk dry density and in the water distribution were observed, e.g. different amounts of water are distributed in the interlayer and interparticle pores. This makes the comparison between QENS and tracer experiments difficult. The samples for the tracer experiments were characterized through ρ_{bd}.

1.5 References

Anderson, D.M., Hoekstra, P., 1965. Crystallization of clay-adsorbed water. Science 149, 318-319.

Anderson, D.M., 1967. Interface between ice and silicate surfaces. Journal of Colloid and Interface Science 25, 174-191.

Archie, G.E., 1942. The electrical resistivity log as an aid in determining some reservoir characteristics. Trans. AIME 146, 54-62

Bée M., 1988. Quasielastic Neutron Scattering: Principles and Applications in Solid State Chemistry, Biology and Material Science In: Institute of Physics Publishing. ISBN 0852743718

Berend, I., Cases, J.M., Francois, M., Uriot, J.P., Michot, L., Masion, A., Thomas, F., 1995. Mechanism of adsorption and desorption of water-vapor by homoionic montmorillonites. 2. The Li^+, Na^+, K^+, Rb^+ and Cs^+-exchanged forms. Clays and Clay Minerals 43, 324-336.

Birgersson, M., Karnland, O., 2009. Ion equilibrium between montmorillonite interlayer space and an external solution-Consequences for diffusional transport. Geochimica et Cosmochimica Acta 73, 1908-1923.

Bordallo, H.N., Aldridge, L.P., Churchman, G.J., Gates, W.P., Telling, M.T.F., Kiefer, K., Fouquet, P., Seydel, T., Kimber, S.A.J., 2008. Quasi-elastic neutron scattering studies on clay interlayer-space highlighting the effect of the cation in confined water dynamics. Journal of Physical Chemistry C 112, 13982-13991.

Bourg, I.C., Sposito, G., Bourg, A.C.M., 2006. Tracer diffusion in compacted, water-saturated bentonite. Clays and Clay Minerals 54, 363-374.

Bradbury, M.H., Baeyens, B., 2003. Porewater chemistry in compacted re-saturated MX-80 bentonite. Journal of Contaminant Hydrology 61, 329-338.

Cases, J.M., Berend, I., Besson, G., Francois, M., Uriot, J.P., Thomas, F., Poirier, J.E., 1992. Mechanism of adsorption and desorption of water-vapor by homoionic montmorillonites. 1. The sodium-exchanged form. Langmuir 8, 2730-2739.

Cases, J.M., Berend, I., Francois, M., Uriot, J.P., Michot, L.J., Thomas, F., 1997. Mechanism of

adsorption and desorption of water vapor by homoionic montmorillonite. 3. The Mg^{2+}, Ca^{2+}, Sr^{2+} and Ba^{2+} exchanged forms. Clays and Clay Minerals 45, 8-22.

Center for Neutron Research (NIST), http://www.ncnr.nist.gov/resources/n-lengths/

Chapman, D.L., 1913. A Contribution to the Theory of Electrocapillarity. Philosophical Magazine 25, 475-481.

Chiou, C.T., Rutherford, D.W., 1997. Effects of exchanged cation and layer charge on the sorption of water and EGME vapors on montmorillonite clays. Clays and Clay Minerals 45, 867-880.

Churakov, S.V., Gimmi, T., 2011. Up-Scaling of Molecular Diffusion Coefficients in Clays: A Two-Step Approach. Journal of Physical Chemistry C 115, 6703-6714.

Dufrêche, J.F., Marry, V., Bernard, O., Turq, P., 2001. Models for electrokinetic phenomena in montmorillonite. Colloids and Surfaces A: Physicochemical and Engineering Aspects 195, 171-180.

Fleury, M., Kohler, E., Norrant, F., Gautier, S., M'Hamdi, J., Barre, L., 2013. Characterization and Quantification of Water in Smectites with Low-Field NMR. Journal of Physical Chemistry C 117, 4551-4560.

Gates, W.P., Bordallo, H.N., Aldridge, L.P., Seydel, T., Jacobsen, H., Marry, V., Churchman, G.J., 2012. Neutron Time-of-Flight Quantification of Water Desorption Isotherms of Montmorillonite. Journal of Physical Chemistry C 116, 5558-5570.

Gimmi, T., Kosakowski, G., 2011. How Mobile Are Sorbed Cations in Clays and Clay Rocks? Environmental Science & Technology 45, 1443-1449.

Glaus, M.A., Baeyens, B., Bradbury, M.H., Jakob, A., Van Loon, L.R., Yaroshchuk, A., 2007. Diffusion of Na-22 and Sr-85 in montmorillonite: Evidence of interlayer diffusion being the dominant pathway at high compaction. Environmental Science & Technology 41, 478-485.

Glaus, M.A., Frick, S., Rosse, R., Van Loon, L.R., 2010. Comparative study of tracer diffusion of HTO, Na-22(+) and Cl-36(-) in compacted kaolinite, illite and montmorillonite. Geochimica et Cosmochimica Acta 74, 1999-2010.

Glaus, M.A., Frick, S., Rosse, R., Van Loon, L.R., 2011. Consistent interpretation of the results of through-, out-diffusion and tracer profile analysis for trace anion diffusion in compacted montmorillonite. Journal of Contaminant Hydrology 123, 1-10.

Glaus, M.A., Birgersson, M., Karnland, O., Van Loon, L.R., 2013. Seeming Steady-State Uphill Diffusion of Na-22(+) in Compacted Montmorillonite. Environmental Science & Technology 47, 11522-11527.

Gouy, G., 1910. Sur la constitution de la charge électrique à la surface d'un electrolyte, Annales de Physique (Paris). Série 4 (Vol. 9), 457– 468.

González Sánchez, F., Van Loon, L.R., Gimmi, T., Jakob, A., Glaus, M.A., L.W., D., 2008a. Self-diffusion of water and its dependence on temperature and ionic strength in highly com-

pacted monmorillonite, illite and kaolinite. Applied Geochemistry 23, 3840-3851.

González Sanchez, F., Juranyi, F., Gimmi, T., Van Loon, L., Unruh, T., Diamond, L.W., 2008b. Translational diffusion of water and its dependence on temperature in charged and uncharged clays: A neutron scattering study. The Journal of Chemical Physics 129, 174706-174706.

González Sánchez, F., Jurányi, F., Gimmi, T., Van Loon, L., Seydel, T. and Unruh, T. 2008c. Dynamics- of supercooled water in highly compacted clays studied by neutrons scattering, Journal of Physics: Condensed Matter, 20, 415102.

González Sánchez, F., Gimmi, T., Jurányi, F., Van Loon, L., Diamond, L.W., 2009. Linking the diffusion of water in compacted clays at two different time scales: tracer through-diffusion and quasielastic neutron scattering. Environmental Science & Technology, 43, 3487–3493

Graham, J., West, G.W., Walker, G.F., 1964. Nuclear magnetic resonance study of interlayer water in hydrated silicated. Journal of Chemical Physics 40, 540-550.

Hensen, E.J.M., Smit, B., 2002. Why clays swell. Journal of Physical Chemistry B 106, 12664-12667.

Hippert, F., Geissler, E., Hodeau, J.L., Lelièvre-Berna, E., Regnard, J.R., 2006. Neutron and X-ray spectroscopy. Springer.

Holmboe, M., Wold, S., Jonsson, M., 2012. Porosity investigation of compacted bentonite using XRD profile modeling. Journal of Contaminant Hydrology 128, 19-32.

Jurányi, F., Bestel, M., Wattson, M., Schneider, G., Garcia, C., to be submitted. Quantitative separation of nano- and interparticle pore water in swelling clays by means of neutron scattering. Physical Review.

Keeling, P.S., Kirby, E.C., Robertson, R.H.S., 1980. Moisture adsorption and specific surface-area. Transactions and Journal of the British Ceramic Society 79, 36-40.

Kosakowski, G., Churakov, S.V., Thoenen, T., 2008. Diffusion of Na and Cs in montmorillonite. Clays and Clay Minerals 56, 190-206.

Kozaki, T., Inada, K., Sato, S., Ohashi, H., 2001. Diffusion mechanism of chloride ions in sodium montmorillonite. Journal of Contaminant Hydrology 47, 159-170.

Kozaki, T., Fujishima, A., Sato, S., Ohashi, H., 1998. Self-diffusion of sodium ions in compacted sodium montmorillonite. Nuclear Technology 123, 120-120.

Kozaki, T., Sato, H., Fujishima, A., Sato, S., Ohashi, H., 1996. Activation energy for diffusion of cesium in compacted sodium montmorillonite. Journal of Nuclear Science and Technology 33, 522-524.

Kuila, U., Prasad, M., 2013. Specific surface area and pore-size distribution in clays and shales. Geophysical Prospecting 61, 341-362.

Martin, T. (1960) Adsorbed water on clay: A review.Natl. Clay Conf., Purdue University.

Madsen, F.T., Kahr, G., 1996. Wasserdampfadsorption und spezifische Oberfläche von Tonen. Nagra Technical Report NTB, 93-17, Nagra, Wettingen, Switzerland.

Malikova, N., Marry, V., Dufreche, J.F., Simon, C., Turq, P., Giffaut, E., 2004. Temperature effect in a montmorillonite clay at low hydration-microscopic simulation. Molecular Physics 102, 1965-1977.

Malikova, N., Marry, V., Dufreche, J.F., Turq, P., 2004. Na/Cs montmorillonite: temperature activation of diffusion by simulation. Current Opinion in Colloid & Interface Science 9, 124-127.

Marry, V., Turq, P., Cartailler, T., Levesque, D., 2002. Microscopic simulation of structure and dynamics of water and counterions in a monohydrated montmorillonite. Journal of Chemical Physics 117, 3454-3463.

Marry, V., Turq, P., 2003. Microscopic simulations of interlayer structure and dynamics in bi-hydrated heteroionic montmorillonites. Journal of Physical Chemistry B 107, 1832-1839.

Marry, V., Dubois, E., Malikova, N., Durand-Vidal, S., Longeville, S., Breu, J., 2011. Water Dynamics in Hectorite Clays: Infuence of Temperature Studied by Coupling Neutron Spin Echo and Molecular Dynamics. Environmental Science & Technology 45, 2850-2855.

Mesot, J., Janssen, S., Holitzner, L. and Hempelmann, R. (1995) Focus: Project of a space and time focusing time-of-flight spectrometer for cold neutrons at the spallation source SINQ of the Paul Scherrer Institute. Journal of Neutron Research, 3, 293-310

Michot, L.J., Bihannic, I., Maddi, S., Funari, S.S., Baravian, C., Levitz, P., Davidson, P., 2006. Liquid-crystalline aqueous clay suspensions. Proceedings of the National Academy of Sciences of the United States of America 103, 16101-16104.

Mitchell, J.K., Soga, K., 2005. Fundamentals of soil behavior. 3rd Edition

Muurinen, A., Karnland, O., Lehikoinen, J., 2004. Ion concentration caused by an external solution into the porewater of compacted bentonite. Physics and Chemistry of the Earth 29, 119-127.

Nagra, 2009. The Nagra Research, Development and Demonstration (RD&D) Plan for the Disposal of Radioactive Waste in Switzerland. Nagra Technischer Bericht. NTB 09-06. Nagra, Wettingen, Switzerland.

Nakazawa, T., Takano, M., Nobuhara, A., Torikai, Y., S., S., H., O., 1999. Activation energies of diffusion of tritium and electrical conduction in water-saturated compacted sodium montmorillonite. Radioactive Waste Management and Environment Remediation - ASME

Norrish, K., 1954. The swelling of montmorillonite. Discuss. Faraday Soc, 18, 120-134.

Pynn R., 2009. An Introduction to Neutron and X-Ray Scattering, Indiana University and Oak Ridge National Lab: http://neutrons.ornl.gov/conf/nxs2009/pdf/IntroductoryLecturesPynn.pdf

Pusch, R., 1999. Microstructural evolution of buffers. Engineering Geology 54, 33-41.

Rotenberg, B., Marry, V., Dufreche, J.-F., Giffaut, E., Turq, P., 2007. A multiscale approach to ion diffusion in clays: Building a two-state diffusion-reaction scheme from microscopic dynamics. Journal of Colloid and Interface Science 309, 289-295.

Rouquerol, J., Avnir, D., Fairbridge, C.W., Everett, D.H., Haynes, J.H., Pernicone, N., Ramsay, J.D.F., Sing, K.S.W., Unger, K.K., 1994. Recommendations for the characterization of porous solids. Pure and Applied Chemistry 66, 1739-1758.

Saiyouri, N., Tessier, D., Hicher, P.Y., 2004. Experimental study of swelling in unsaturated compacted clays. Clay Minerals 39, 469-479.

Salles, F., Bildstein, O., Douillard, J.M., Jullien, M., Raynal, J., Van Damme, H., 2010. On the Cation Dependence of Interlamellar and Interparticular Water and Swelling in Smectite Clays. Langmuir 26, 5028-5037.

Sato, H., Suzuki, S., 2003. Fundamental study on the effect of an orientation of clay particles on diffusion pathway in compacted bentonite. Applied Clay Science 23, 51-60.

Shackelford, C.D., Moore, S.M., 2013. Fickian diffusion of radionuclides for engineered containment barriers: Diffusion coefficients, porosities, and complicating issues. Engineering Geology 152, 133-147.

Sing, K.S.W., Everett, D.H., Haul, R.A.W., Moscou, L., Pierotti, R.A., Rouquerol, J., Siemieniewska, T., 1995. Pure and Applied Chemistry, 57(4), 603-619

Singwi, K.S., Sjolander, A., 1960. Diffusive motions in water and cold neutron scattering. Physical Review 119, 863-871.

Sposito, G., Skipper, N.T., Sutton, R., Park, S.H., Soper, A.K., Greathouse, J.A., 1999. Surface geochemistry of the clay minerals. Proceedings of the National Academy of Sciences of the United States of America 96, 3358-3364.

Sterling, 1940. Base exchange of the clay mineral montmorillonite for organic cations and its dependence upon adsorption due to van der Waals forces.

Suhr, N.H., Ingamell.Co, 1966. Solution technique for analysis of silicates. Analytical Chemistry 38, 730-734.

Van Loon, L.R. and Soler, J.M., 2003. Diffusion of HTO, $^{36}Cl^-$, $^{125}I^-$ and $^{22}Na^+$ in Opalinus Clay: Effect of confining pressure, sample orientation, sample depth and temperature. Nagra Technical Report NTB 03-07, Nagra, Wettingen, Switzerland.

Van Loon, L.R., Muller, W., Iijima, K., 2005. Activation energies of the self-diffusion of HTO, $^{22}Na^+$ and $^{36}Cl^-$ in a highly compacted argillaceous rock (Opalinus Clay).
Applied Geochemistry 20, 961-972.

Van Loon, L.R., Glaus, M.A., Mueller, W., 2007. Anion exclusion effects in compacted bentonites: Towards a better understanding of anion diffusion. Applied Geochemistry 22, 2536-2552.

Wuttke, J., Budwig, A., Drochner, M., Kaemmerling, H., Kayser, F.-J., Kleines, H., Ossovyi,

V., Carlos Pardo, L., Prager, M., Richter, D., Schneider, G.J., Schneider, H., Staringer, S., 2012. SPHERES, Julich's high-flux neutron backscattering spectrometer at FRM II. Review of Scientific Instruments 83.

2 Chapter 2: Water distribution in Na- and Cs-montmorillonite

Martina BESTEL[*1,4], Thomas GIMMI[2,4], Martin A. GLAUS[2], Luc R. VAN LOON[2], Michaela ZAMPONI[3], Larryn W. DIAMOND[4] and Fanni JURÁNYI[1]

[1]Laboratory for Neutron Scattering, Paul Scherrer Institut, 5232 Villigen PSI, Switzerland
[2]Laboratory for Waste Management, Paul Scherrer Institut, 5232 Villigen PSI, Switzerland
[3]Forschungszentrum Jülich, Centre for Neutron Science at FRM II, 85747 Garching, Germany

[4]Institute of Geological Sciences, University of Bern, 3012 Bern, Switzerland

[*]*Corresponding author: mbestel@gmx.de*

Abstract - Smectite-rich porous media, like montmorillonite, are considered as barrier material in nuclear waste management. In this context the diffusion of water and ions is an important topic. It is known that diffusion properties strongly depend on the geometry (the structure) of the pores, and notably on the distribution of pore water between different pore compartments. At high bulk densities of the smectites, the pore water is present virtually only in interlayers (or interlamellar regions). At low densities water with slightly different properties exists in interlayers and in interparticle pores (or extralamellar regions). In the present study the distribution of water in Na- and Cs-montmorillonite between these two pore environments was deciphered based on molecular motions of water on a nanosecond time scale and neutron diffraction data. Interlayer water or generally water near surfaces can be significantly supercooled, whereas water in larger (e.g., interparticle) pores cannot. Thus the ratio of surface wa-

ter with respect to bulk-like water in larger pores could be obtained from neutron backscattering spectroscopy of samples exposed to temperatures below zero. This technique was applied to Na- and Cs-montmorillonite samples with different bulk densities and gravimetric water contents. Exposing samples to T < 0°C may, unfortunately, modify the pore structure, i.e., the distribution of water between the different compartments. The number of water layers in interlayers calculated from geometrical conisderations based on surface area and neutron diffraction (d-spacing) at room temperature are similar to those obtained from neutron backscattering spectroscopy for low total water contents. For larger water contents, some deviations occur. The discrepancy can be attributed to the change of pore structure of the spectroscopy samples for T < 0°C. In the water content range from 0 to 0.7 g/g the fraction of bulk-like water in Na-montmorillonite increased monotonically, but not linearly from 0 to 64%. The number of water layers in interlayers increased similarly. Only little swelling occurs in Cs-montmorillonite; the water was predominantly attributed to the interparticle pore environment. Our findings help to interpret experimental results, for instance on macroscopic diffusive transport through montmorillonites, which is related to the proportions of water in the different pore environments.

Key words - Swelling clays, neutron spectroscopy, neutron diffraction, surface water, bulk-like water, interlayer, interparticle porosity

Introduction

Na-montmorillonite is a major component of bentonite considered to be used for engi-

neered barriers in nuclear waste repository systems. The low hydraulic permeability of compacted bentonite originates from the very small sizes of the water-filled pores, which typically are in the order of nanometers. The complexity of the network of the small pores leads also to large tortuosities or geometrical factors (González-Sánchez *et al.*, 2009) and thus to comparably small diffusion coefficients for water and solutes through such material. Assessing the safety function of bentonite barriers requires a thorough knowledge of the structure and the properties of the clay pore space. Microstructural modeling shows that in montmorillonite at low water contents most water molecules are located in interlayer (or interlamellar) pores (Pusch, 1999), and that the microstructural evolution during water uptake is first dominated by swelling of the interlayers. Pores not directly attributed to interlayers may be denoted as extralamellar pores or interparticle pores. Lowly compacted swelling clays (with high water content) consist – depending on the type of exchangeable cations and the water content – of slightly disordered platelets, tactoids and/or particles (Segad *et al.*, 2012). Pores between these platelets can be denoted as extralamellar pores or interparticle pores.

Structure of Cs- and Na-montmorillonite

Montmorillonite is composed of negatively charged layers of octahedral (O) alumina mineral sheets which are sandwiched between two tetrahedral (T) silica mineral sheets to form TOT layers (Figure 9). The negative charge in the octahedral sheet is compensated by counter cations (like Na^+ or Cs^+) that are located nearby the surface area of the tetrahedral sheet and are exchangeable. Different TOT layers are hold together by these cations to form stacks of clay platelets or tactoids, which may again be grouped to particles or aggregates. The space between the TOT layers forms the so-called interlayer where interlayer water and the counter ions are

located. The interlayer and the counterions can be hydrated to various degrees. The type of counter cations influences the hydration of the interlayer pores and thus the clay microstructure (Sposito *et al.*, 1999). Cs counterions tend to weakly hydrate (G_h = -258 kJ/mol) and form inner-sphere surface complexes (Sposito *et al.*, 1999; Kosakowski *et al.*, 2008). Accordingly, Cs-montmorillonite has a small swelling capacity and typically the average number of molecular water layers (*W*) in the interlayer remains small (~1, Bérend *et al.*, 1995, Salles *et al.*, 2010). Contrary to that, Na counterions have a larger affinity for water (G_h = -375 kJ/mol) and can form outer-sphere complexes on the charged mineral surface (Sposito *et al.*, 1999). A more or less stepwise swelling up to maximum 4 water layers in the interlayers has been observed by X-ray diffraction (XRD) during an increase of the total water content to about 0.41 g/g (Norrish, 1954; Kozaki *et al*., 1998; Muurinen *et al.*, 2004; Saiyouri *et al.*, 2004; Holmboe *et al.*, 2012). Norrish *et al.* (1954) and Kozaki *et al*. (1998) investigated the nature of swelling in water and different electrolyte contact solutions by X-ray diffraction and categorized regions of crystalline (d-spacing up to about 20 Å) and macroscopic (osmotic) swelling (d-spacing larger than 30 Å). The microstructure, that is, the number of TOT layers per stack and the tactoid or particle sizes, of compacted Na- and Cs-bentonite (1.6 g/cm^3) depends also on the ionic strength of the contacting NaCl solutions (Melkior *et al.*, 2009). The Cs-form has stacks of more than 200 TOT layers (Figure 9) and forms particles with diameters up to 2.0 µm (Melkior *et al.*, 2009). No gel phase was observed, whereas the Na-form with 3 *W* clearly shows such a gel phase for a water content of 0.44 g/g (ρ_{bd}=1.25 g/cm^3) (Melkior *et al.*, 2009). Na-montmorillonite stacks consist typically of only 3-5 TOT layers (Pusch *et al.*, 2001) resulting in smaller (up to 0.5 µm) particles (González Sánchez *et al.*, 2008a), but stacks and tactoids may also form larger aggregates. At water contents where crystalline swelling occurs, unfortunately not much is known about

water distribution between the different pore environments. Also, the properties of water within the different pores are not well known.

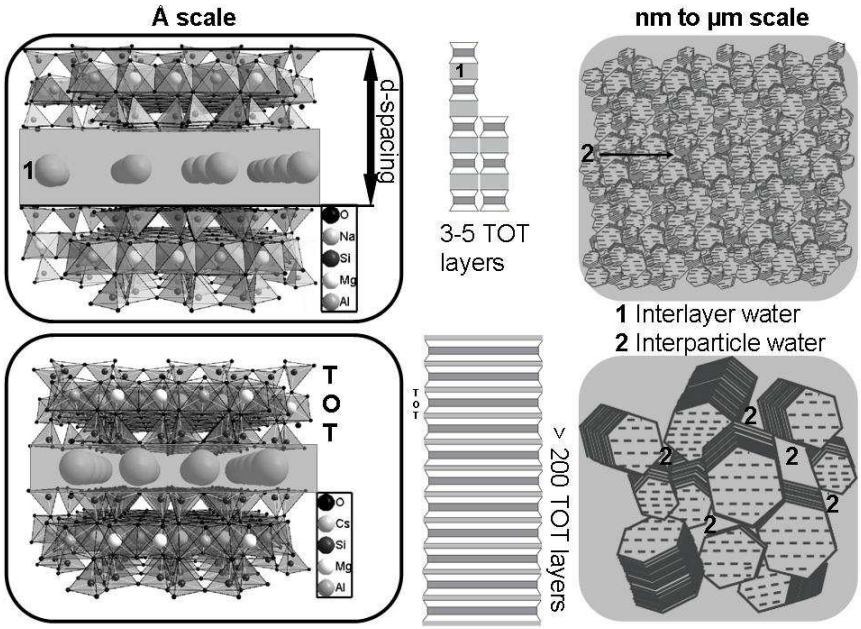

Figure 9. Left: schematic representation at the atomic scale of arrangements of tetrahedral (T) - octahedral (O) - tetrahedral (T) aluminosilicate sheets. The aggregates are stacked together (center) to form the particles by 3-5 TOT layers for Na-montmorillonite (Pusch *et al.*, 2001) and more than 200 TOT layers for Cs-montmorillonite (Melkior *et al.*, 2009). Right: schematic representation shows the clay particles with surrounded interparticle pores at the microscopic scale. Note the different structure for Na-montmorillonite (top) and Cs-montmorillonite (bottom).

From geometrical considerations, a smectite can schematically be devided into three parts: the first one is the "solid" part which consists of the TOT clay sheets, the second one is the interlayer space in between the TOT layers occupied by variable amount of water, and the third one is the interparticle pore compartment in between the clay platelets. Charge-compensating cations may be considered to belong to any of these compartments. Values for the porosities in different pore compartments can be derived from surface area determinations, as obtained from

adsorption isotherms, and from d-spacings as obtained from diffraction measurements. Adsorption is strongly depending on the fluid and the nature of the counter cation (Chiou and Rutherford, 1997). From nitrogen vapor adsorption measurements external surface areas ($A_{s,ext}$ in m^2/g) for Na-montmorillonites are comparably small (e.g., 28.0 m^2/g, González Sánchez *et al.*, 2008a) but somewhat larger for Cs-montmorillonite (64.0-79.0 m^2/g, De Boer *et al.*, 1966; Bérend *et al.*, 1995). The difference seems to be odd with the typically smaller particle sizes reported for Na-montmorillonite. Possibly, Na-montmorillonite forms larger aggregates of particles, especially at high densities or under the measurements conditions of the adsorption isotherms, resulting in lower external surface areas. The total specific surface area ($A_{s,tot}$ in m^2/g) including the interlayer surfaces can be obtained by water adsorption gravimetry (Keeling *et al.*, 1980) through a single adsorbed water layer in smectites with high internal surface area ($A_{s,int}$ in m^2/g) (Madsen and Kahr, 1996). Values for $A_{s,tot}$ for montmorillonite are around 807 m^2/g (Cases *et al.*, 1992).

Spectroscopic consideration: local properties of pore water

The properties of water in clay pores can be influenced by i) the interaction between water and clay surfaces, ii) the interaction between water and counter cations (here Na^+ or Cs^+) and iii) the geometrical confinement (i.e. volume restriction). Especially water in the narrow interlayers is affected. There, both the structure (e.g. forming of water layers) and the dynamics (e.g. slower diffusion (González Sánchez *et al.*, 2008b)) are different from the bulk. Neutron scattering is an ideal method to study such alterations of water properties due to several reasons: (i) hydrogen has a huge neutron scattering cross-section, (ii) observation time and length scales are well suited, (iii) the relatively weak interaction between neutrons and samples allows study

average properties of large (mm-cm) samples, even in a complicated sample environment. Nevertheless, only few examples can be found in the literature where water molecules in clays are distinguished based on molecular properties. Gates *et al*. (2012) used neutron spectroscopy, but they measured only samples with negligible amount of interparticle water. Fleury *et al.* (2013) determined the amount of interlayer water using NMR spectroscopy on samples with only interlayer water.

Aim of this study

In this work neutron spectroscopy was applied to distinguish and quantify fractions of pore water with slightly different properties. The fractions were compared with fractions calculated from the surface area and d-spacings obtained through adsorption of liquids and neutron diffraction. Neutron diffraction was chosen to obtain a d-spacing representative for the whole sample volume, which is advantageous compared to X-ray diffraction which is mostly representing properties near the sample surface. Identical montmorillonite samples were used for neutron spectroscopy and neutron diffraction. The following sample properties were varied:

• Type of counter ion (Cs or Na), to check the effect of the cation hydration on the microstructure, as qualitatively described in Melkior *et al*. (2009).

• Specific water contents (variable bulk dry densities) of Na-montmorillonite. In the literature sample properties were frequently investigated under confined swelling conditions and data are presented as a function of the bulk dry density (Van Loon *et al*., 2007). Here, the samples were hydrated from vapor or water phase under free or confined swelling conditions, which partly led to incomplete water saturation.

• Ionic strength of the equilibrium solution (distilled water or 5 M $NaClO_4$), to check the effect

on swelling and pore microstructure of Na-montmorillonite.

In a further work, the obtained values were used to derive local diffusion coefficients in confined pore compartments of clays from quasielastic neutron scattering measurements.

Material and methods

The source material, a montmorillonite powder from Milos (Greece), was conditioned to a homoionic form with either Na or Cs as exchangeable counter ions. After conditioning, the composition of the clay was analysed. To this end, the material was digested by fusion with $LiBO_2$ and dissolving the melt in HNO_3 (Suhr and Ingamells, 1966). Major elements were measured by inductively coupled plasma atomic emission spectroscopy (ICP-AES). All other elements were measured by inductively coupled plasma mass spectrometry (ICP-MS) (Tab. II). The remaining Ca was assumed to occur rather as a separate contamination and not on the cation-exchange sites (Glaus *et al.*, 2010).

For the experiments, most samples were hydrated via the vapor phase in a dessiccator under free swelling conditions. After the clay powder took up the desired amount of water the samples were compacted to the desired bulk dry density ($\rho_{bd} = m_s / V_{sample}$) and placed in a sample holder. Some samples with high water content were hydrated via the liquid phase in a confined geometry (V_{sample}). To this end the dry clay powder was compacted to the desired bulk dry density and placed between two stainless steel plates and a porous filter. An external solution (water or, in one case, 5 M $NaClO_4$) circulated through the porous filter in the samples. After hydration the samples were placed in a hermetically sealed aluminum sample holder for performing the neutron scattering measurements. The total gravimetric water content was determined after the experiment by drying the samples at 110°C. The water content in the sample

hydrated with 5 M $NaClO_4$ was obtained through desiccation. The amount of the $NaClO_4$ remaining in the pores after evaporation was calculated from $\varepsilon \cdot V_{sample} \cdot I \cdot 10^{-3}$ where $I=A \cdot M$ with M=122.44 g/mol and A=5 mol/l - was subtracted from the $m_{s+5NaClO4}$. Neutron and X-ray imaging showed that a more complete saturation and a more homogeneous distribution of the water was reached when saturating via the liquid phase rather than via the gas phase.

In the following, the samples are characterized through the gravimetric water content w (g/g) defined as mass of total water per dry clay mass. The total porosity of a sample (ε) is given as $\varepsilon = 1 - \rho_{bd} / \rho_s$, where ρ_s is the solid density which was measured by pycnometry for Na-montmorillonite (Tab. II). The same solid density was taken for the Cs-form. The saturation of a sample (S) is defined as volume of water per volume of pores (-) and can be calculated as:

$$S = \frac{w \rho_{bd}}{\varepsilon \rho_w} \quad (14)$$

where $w_{sat} = \varepsilon \rho_w / \rho_{bd}$ equals the gravimetric water content at full saturation for the measured ρ_{bd} and ρ_s (or analogous $w \rho_{bd} / \rho_w$ equals the volumetric water content of the sample). When the compaction was done after hydration it was often not possible to achieve the desired bulk dry density, especially for samples with low w. The relevant ρ_{bd} was determined from the sample mass and from the sample volume V_{sample} obtained from length (5 cm), width (1.5 cm) and thickness t. The thickness (t) varied over the sample on average by 12 %.

Table II. Chemical composition and calculated structural formula of Na and Cs-montmorillonite. Results are given as percent fraction on weight basis.

	Na-montmorillonite		Cs-montmorillonte	
SiO_2	60.16	$[Si_{3.86}O_{10}(OH)_2]$	55.84	$[Si_{3.91}O_{10}(OH)_2]$
Al_2O_3	18.91		17.60	
Fe_2O_3	1.91	$(Al_{1.43}Fe_{0.09}Mg_{0.34})$	1.67	$(Al_{1.45}Fe_{0.09}Mg_{0.37})$
MnO	0.01		0.01	
MgO	3.55		3.15	
CaO	0.41		0.22	
Na_2O	2.39		0.24	
K_2O	0.52	$(Na_{0.3}K_{0.04})$	0.49	$(Cs_{0.29}\ K_{0.04}Na_{0.03})$
Cs_2O	0.00		9.61	
TiO_2	0.17		0.20	
$A_s(m^2/g)$				
$A_{s,\ ext}$	16±2		64±6	
$A_{s,\ tot}$	710		693	
ρ_s (g/cm^3)	2.8		2.8	

Assessing the amount of interlayer water (ILW) from geometrical properties

One relevant parameter to obtain the amount of interlayer water (w_{ILW}) is the d-spacing giving information about the swelling and the corresponding number of water layers in interlayers. In this study, neutron diffraction instead of the more common X-ray diffraction (e.g. Kozaki *et al.*, 1998) was used. The d-spacing obtained from neutron diffraction analysis represents an average value over the whole sample volume. Furthermore, subsequently fixed window scan measurements could be done on identical samples. The same water content was assured by keeping the samples hermetically sealed in the sample holders. The diffraction patterns were studied as a function of *w*. The measurements were performed on the 2-axis diffractometer MORPHEUS at SINQ, PSI, Switzerland. The sample was positioned in reflexion or transmission mode. The diffraction peak was fitted by one or two Gaussians. When using two Gaussians, the relative abundance of the number of water layers (1*W*, 2*W*, 3*W*, 4*W*) was determined from the ratio of the peak areas; furthermore an average d-spacing value was calculated. These d-

spacing values are not as precise as the ones obtained by profile fitting (Holmboe *et. al.*, 2012), however the deviation is negligible in comparison to the uncertainties in A_s, sample volume and d-spacing of the dry clay. Based on the d-spacing and the number of water layers, samples were selected to quantify the amount of water in the different pore environments with Fixed Window Scans.

Adsorption of nitrogen and water was used to obtain A_s. The external specific surface area was obtained by nitrogen adsorption volumetry (BET) and $A_{s,tot}$ through water adsorption gravimetry at a relative humidity of 75 % (Keeling *et al.*, 1980). The specific interlayer (internal) surface area is $A_{S,int} = A_{S,tot} - A_{S,ext}$ (Tab. II). Holmboe *et al.* (2012) calculated the surface area from the lattice parameters, which might be more precise. However obtaining the lattice parameters would have required a much larger range of the diffractogram than what was measured in our case. The amount of interlayer water (w_{ILW}) was then estimated from the geometry parameters as:

$$w_{ILW} = 1/2 \cdot A_{s,int} \cdot (d - d_0) \cdot \rho_w \cdot 10^{12} \quad (15)$$

with d the measured d-spacing, d_0 the d-spacing of the dry clay, which equals the spacings of TOT sheets and compensating cations, and thus d-d_0 the effective thickness of the water in the interlayer. Note that d_0 from molecular modeling (Na-form 10.4 Å, Cs-form 10.8 Å, Kosakowski *et al.*, 2008) has to be somewhat larger than the thickness of the TOT sheets. A water density ρ_w of 1.00 g/cm^3 was assumed in general, except for the sample saturated with 5 M $NaClO_4$, where a value of 1.37 g/cm^3 was used.

Assessing the amount of surface water (SW) from dynamic water properties: Fixed Window Scan on a neutron backscattering spectrometer

Neutron backscattering spectroscopy is a proven technique to study the freezing behavior of the supercooled water state in highly compacted clays (Bordallo *et al.*, 2008; González Sánchez *et al.*, 2008c). Fixed Window Scan (FWS) is a widely used method, where the intensity of the elastically scattered neutrons is measured as a function of temperature. Elastic scattering occurs on those units which are seen as immobile within the given observation time of the instrument. Such contributions arise from the clay crystals and bound, frozen or very slowly moving water molecules and compensating cations. However - as mentioned before - beside the hydrogen (both in water molecules and in hydroxyl groups of the clay crystals) all other elements can be neglected. Units which are diffusing fast enough cause quasielastic scattering, and therefore do not contribute to the elastic intensity. The observation time is given by the energy resolution of the instrument.

The amount of water in different pore geometries was derived from the Fixed Window Scans obtained on SPHERES (FRM II, Garching, Germany) (Wuttke *et al.*, 2012). The set up of the instrument is described in table III. Vanadium was used to calibrate the detector efficiency and to determine the energy resolution. Measurements for the empty sample holder and the dry clay were used as background. Two water populations in montmorillonite were discriminated (Fig. 10 left & right). Because strongly confined surface water (SW) can be significantly supercooled and remains partly mobile at temperatures below 273 K, it can be discriminated from the bulk-like water (BLW) which freezes and loses its molecular mobility at around 273 K. The presence of freezing BLW in a Na-montmorillonite with two water populations when decreasing

the temperature from 300K to 255K was verified through the appearance of hexagonal ice peaks between 300K and 255K in the neutron diffraction pattern (see appendix). Such peaks can be attributed to the crystallization of bulk-like water (Juranyi *et al.,* (to be submitted)). The difference in intensity between the plateaus at the highest and lowest temperature is proportional to the total amount of water. From freezing curves of samples with different *w* (g/g) the amount of SW and BLW was quantified as seen in figure 10 left for Na-montmorillonite and figure 10 right for Cs-montmorillonite. The temperature to discriminate the two water populations (255K) was selected by eye which contributes to the error of the results (Jurányi *et al.*, (to be submitted). The surface water content (w_{SW} in g/g) was calculated from *w* (g/g) and the obtained fraction SW (wt %):

$$w_{SW} = SW \cdot w \quad (16)$$

Table III. Experimental set up of the neutron diffractometer and the neutron backscattering instument.

Instrument	MORPHEUS	SPHERES
technique	diffraction	FWS
λ (Å)	5.00	6.27
ΔE (μeV)		0.65
Q (A^{-1})	0.22-0.42	0.60-1.80

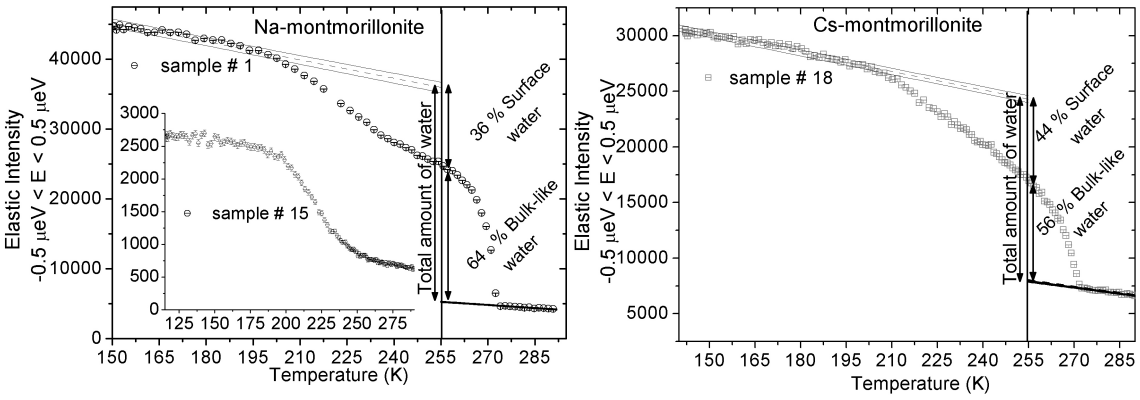

Figure 10. Left) Fixed Window Scans for Na-montmorillonite. Elastically scattered neutrons are shown as a function of temperature for samples with high (sample # 1) and low (sample # 15) total water content. The jump in intensity below 270 K (sample # 1) is proportional to the amount of bulk-like water (64 %) in the interparticle pores. The difference in intensity between the plateaus at the highest and lowest temperatures is proportional to the total amount of water. Right) Fixed Window Scans for Cs-montmorillonite. Elastically scattered neutrons are shown as a function of temperature for a sample with low total water content (sample # 18).

Results

Geometrical characteristics of samples

Figure 11 displays typical neutron diffraction patterns obtained for Na and Cs montmorillonite at different water contents. Clear peaks corresponding to numbers of water layers between 1 and 4 (d-spacing of ~12.5 to 22 Å) are seen for gravimetric water contents up to ~0.7 g/g. All results are given in Tab. IV. At certain water contents, a single peak only was observed, whereas at other water contents two peaks could be discriminated, meaning that some interstratification in terms of number of water layers in interlayers occurs. The d-spacings and number of molecular water layers are similar to those of Norrish (1954), Kozaki *et al*. (1998) and Saiyouri *et al.* (2004). The observed range of d-spacings belongs to the so-called crystalline swelling. No peaks corresponding to so-called osmotic swelling, i.e. d-spacings larger than

~30Å, were observed, even at the highest water contents, consistent with earlier results (Norrish *et al.*, 1954, Kozaki *et al.*, 1998, Holmboe *et al.*, 2012)

For Cs montmorillonite, d-spacings of only 12.5 Å and 12.7 Å (corresponding to 1-2 *W*) were obtained for water contents up to 0.24 g/g. This corroborates the low swelling capacity of this clay.

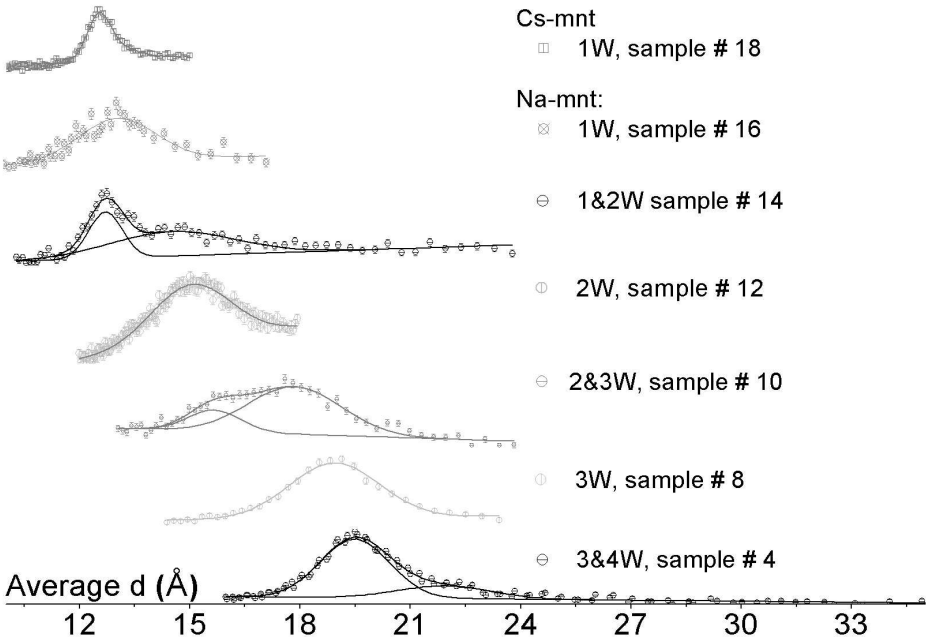

Figure 11. Neutron diffraction patterns of water and 5 M $NaClO_4$ (sample #10) saturated Na- and Cs-montmorillonite samples. Note the lack of reflexions allocated to osmotic swelling at high d-spacings.

The total specific surface areas of 710 m^2/g and 693 m^2/g (Tab.II) for the Na and Cs forms of montmorillonite, respectively, are similar; $A_{s,ext}$ is somewhat larger for Cs montomorillonite (64 m^2/g) than for Na mont (16 m^2/g). These values are about consistent with literature data (e.g. Bérend *et al*., 1995). The comparably low $A_{s,\,ext}$ for Na-montmorillonite may be affected by the typical pre-treatment (drying) of the sample, as mentioned in the introduction. The

internal surface areas (without considering edge surfaces separately) are thus 694 m^2/g (Na form) and 629 m^2/g (Ca form). The average d-spacing as a function of the water content *w* is shown in figure 12 (top).

Fraction of interlayer water as a function of total water content (w) from geometrical calculations

The amount of ILW (w_{ILW}) was geometrically obtained through equation 15 with the reported geometrical parameters for Na-montmorillonite and Cs-montmorillonite (Fig. 12 bottom, Tab. IV). The data look of course similar as those in Fig. 12 top, because w_{ILW} is linearly related to d for each clay form. The linear part at low *w* ($w < 0.32$ g/g) of the curve for Na-montmorillonite can be interpreted as interlayer swelling leading to an increasing amount of interlayer water. The observed maximum d-spacing leads of course to a maximum value of interlayer water ($w \approx 0.32$ g/g). The deviation from the linear behavior at high *w* ($w > 0.32$ g/g) is interpreted as occurrence of interparticle (or extralamellar) pore water. Because of the much lower swelling capacity of Cs montmorillonite (up to 1 well defined water layer, with a narrow FWHM), only a comparably small amount of interlayer water exists and already at low water contents (> ~0.15 g/g) deviations from the linear part occur. Cs-montmorillonite intercalates at most 1 *W* in the interlayers.

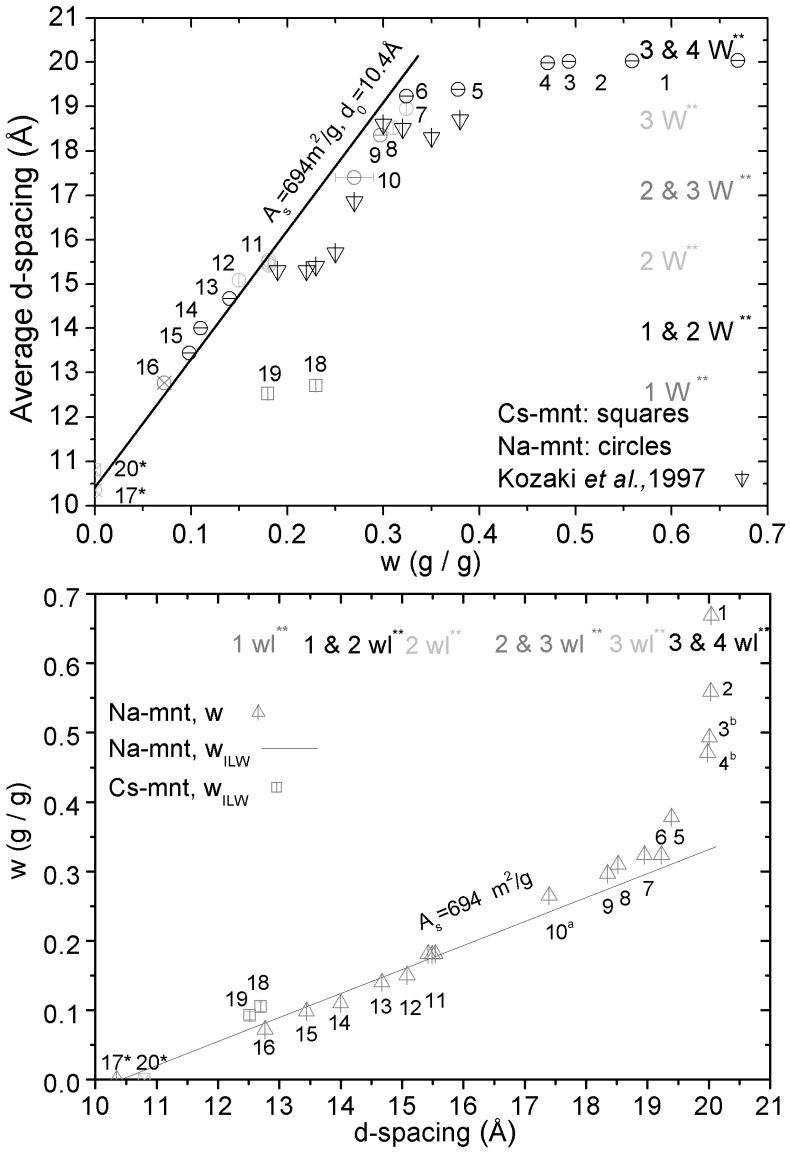

Figure 12. Top) c) Average d-spacing and number of molecular water layers (*W*) calculated from neutron-diffraction measurements as a function of total water content (*w*). The numbers correspond to the samples in table IV. The solid line represents the calculated amount of interlayer water for Na-montmorillonite from the d-spacing (value for the dry clay was taken from Kosakowski *et al.*, 2008) and from the specific surface area (A_s, Tab. II) using eq. 15. The total amount of water is increasing up to 0.3 g/g and 3 *W* linearly with the d-spacing for Na-montmorillonite. Bottom) The total amount of water (*w*) and the amount of interlayer water (w_{ILW}) from neutron diffraction and surface area measurements as a function of d-spacing.

Fraction of surface water as a function of total water content (w) from spectroscopic measurements

The obtained gravimetric surface water content (w_{SW}) is shown in table IV and Figure 13 with the number of molecular water layer (W) derived from neutron diffraction. The gravimetric surface water content (w_{SW}) was obtained for Na-montmorillonite samples with different sample parameters (w, ρ_{bd} and S). The degree of saturation S of the samples was found to be irrelevant; all obtained values for different S plot along a common relation with w when considering their uncertainties. The water content w was found to be the determining parameter. Similar to the geometrical results the obtained w_{SW} is increasing linearly with w, however up to a low w ($w<$ 0.18 g/g) for Na-montmorillonite. For higher w values ($w>$ 0.18 g/g) w_{SW} does increase only slightly further and the pores start to contain BLW. The amount of surface water remains about constant at ~0.24 g/g for $w >$ 0.5 g/g.

In Cs-montmorillonite the obtained gravimetric surface water content (w_{SW}) remains rather low (w_{SW} ~0.1 g/g) and thus bulk-like water starts to dominate at much lower w compared to Na-montmorillonite.

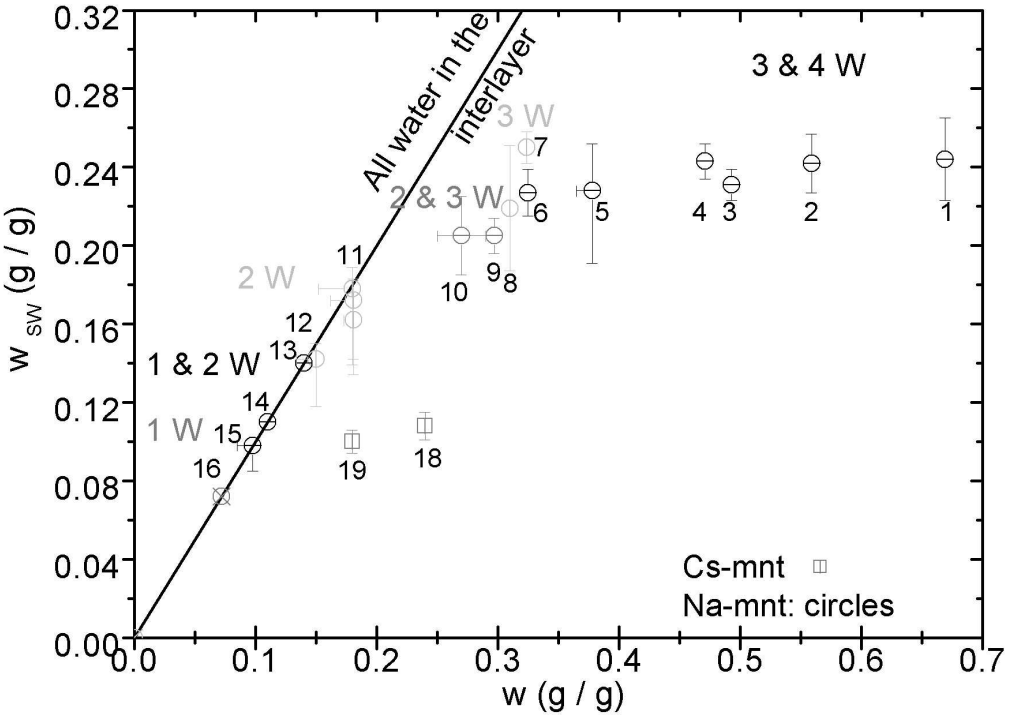

Figure 13. Amount of surface water (SW) from Fixed Window Scans and the number of molecular water layer (*W*) from neutron-diffraction measurements as a function of the total amount of water. The numbers correspond to the samples in table IV. The solid line represents the calculated amount of interlayer water for Na-montmorillonite from the d-spacing (value for the dry clay was taken from Kosakowski *et al.*, 2008) and from the specific surface area (A_s, table II) using eq. 15. The total amount of water is increasing up to 0.2 g/g and 2 *W* linearly with the d-spacing for Na-montmorillonite.

Discussion

Uncertainties of w_{SW} and w_{BLW}

The temperature describing the transition from BLW to SW freezing properties is one of the important parameters when distinguishing SW from BLW. The temperature was estimated to be 255K (Jurányi *et al.*, (to be submitted)); any mathematical evaluation of this transition-temperature (as a reversal point) was not successful. The instrument resolution is high enough to identify the transition temperature and separate different water populations in Na-

montmorillonite. For the Cs-form the reversal point is however less pronounced and the discrimination between SW and BLW less clear. The transition shows a dependency on counter cation, sample density and the composition of the saturating solution. The transition-temperature of the Na-montmorillonite sample saturated with 5 M $NaClO_4$ is weakly pronounced; a clearly different freezing temperature of the SW compared to the BLW was not evident. The freezing temperature of a saline solution should be lower compared to pure water and the transition temperature lower than 255K. The instrument resolution should thus be adapted in order to separate the SW from BLW in a sample saturated with highly saline solution.

The way of hydration (through liquid or vapour phase) has a slight influence on the observed amount of SW and BLW. Similar to the conclusion from neutron diffraction from Devineau et al. (2006) samples with same w show higher amount of SW when the hydration is from liquid compared to vapour phase (Fig. 14).

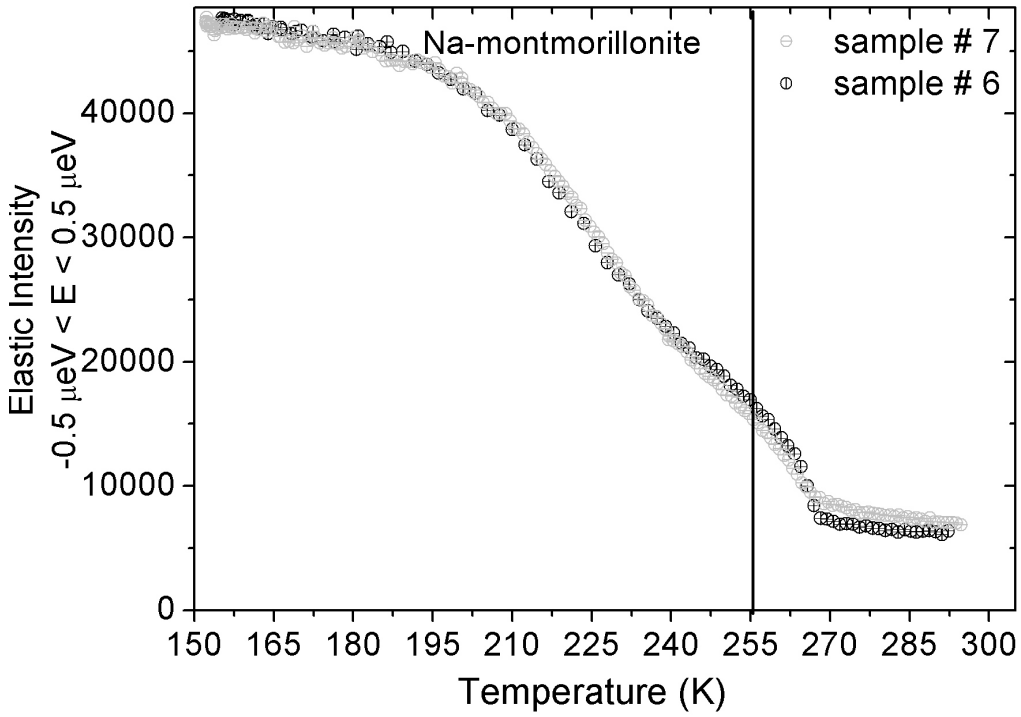

Figure 14. Fixed Window scans for samples 7 and 6 with same total water content. The jump in intensity below 270 K is proportional to the amount of bulk-like water in the interparticle pores. Note the slightly higher amount of bulk-like water for the sample hydrated via gas phase (sample 6) compared to the sample hydrated via constant volume conditions from liquid phase.

Uncertainties of w_{ILW} and w_{IPW}

The total specific surface area is an important parameter when calculating w_{ILW}. The following assumptions were used to derive A_s: (i) the density of water ρ_w is 1 g/cm^3 and (ii) 1 g of water on the surfaces covers 3310 m^2 (Keeling *et al.*, 1980). For low *w* the water density may be higher and the covered area of 1 g lower, for high w contrariwise, even though results of density measurements are conflicting (e.g. Anderson, 1967). The specific surface area was derived from a sample with w = 0.2 g/g containing 2*W* in the interlayer for Na-montmorillonite and 1 *W* in the interlayer for Cs-montmorillonite. Specific configurations of water molecules with varying mo-

lecular cross sections (2.82 ± 0.14) Å (Mackenzie, 1958) and a higher ρ_w than 1 g/cm^3 can contribute to the error of the calculations. For Cs-montmorillonite the surface area was calculated taking into account that only a single water layer is present in interlayers at the used relative humidity of 0.75. The uncertainties for $A_{s,tot}$ for this clay are mainly due to the uncertain water density in the interlayers because max. 1 *W* can be intercalated. The same source material was used, suggesting similar total surface areas for both, Cs- and Na-montmorillonite, as was obtained from the measurements.

The obtained $A_{s,ext}$ is lower than the value from González Sánchez *et al.* (2008a) for Na-montmorillonite, and similar to values of De Boer *et al.* (1966) and Bérend *et al.* (1995) for Cs-montmorillonite. It is higher for the Cs- compared to the Na-form, similar as reported by Bérend *et al,* (1995). The external surface areas are comparably small, anyway, so that $A_{s,int}$ are dominated by the total surface areas.

The average d-spacing (17.40 Å, ~2-3 *W*) of the single Na-montmorillonite sample saturated with 5 M $NaClO_4$ solution plots about in line with the values obtained for samples saturated with water (Figure 12 top). It has only a slightly lower average d-spacing compared to a water-hydrated sample with similar water content *w* (18.35 Å, ~2-3 W). Thus, the lower extent of the diffuse double layer and the lower swelling pressure expected for a clay sample in contact with a higher ionic strength solution does not clearly affect the sample microstructure at this water content or bulk density. It would be interesting to check whether this is also true for samples having larger water contents, or whether there the high ionic strength of the saturation solution would lead to a smaller d-spacing and possibly a larger amount of interparticle (or extralamellar) water.

Fractions of interlayer / interparticle versus surface / bulk-like water

The obtained fraction of (i) SW and calculated (ii) ILW decreases linearly (Tab. IV): in Na-montmorillonite (i) from 100 to 36% and (ii) from 114 to 51 %. The fractions of SW and BLW were compared with the fractions of ILW and IPW as seen in fig. 15. For Na-montmorillonite the amount of SW is increasing linearly up to w = 0.18 g/g with 2W and the ILW is increasing linearly up to w = 0.32 g/g with 3 *W* in the interlayers. At first glance, this could be interpreted as presence of some water with bulk-like properties in interlayers with 3 and 4 *W*. This would be consistent with calculated diffusion coefficients approaching those of bulk water for interlayers with more than 4 *W* (Kosakowski *et al*. 2008). This interpretation, however, seems unlikely in view of the X-ray diffraction results of Andersen (1967). He investigated the d-spacing of Na-montmorillonite during freezing and thawing and reports a decrease from larger values to 19 Å (3 *W*) at about –2°C and to 16 Å (2 *W*) at about –10°C. Svensson and Hansen (2010) obtained similar conclusions from time-resolved synchrotron X-ray diffraction data, with a first collapse to a 3 *W* state, a mixed 2-3 *W* state at –15°C, and a 2 *W* state at –50°C. It appears thus likely that during the FWS the microstructure of the samples with higher water contents (initially 3 and 4 *W*) changed and the number of water layer was reduced to only 2 *W*. In this sense, our data can be considered as a confirmation of the above mentioned results. A distinction of SW and BLW for samples with comparably high water contents and large numbers of molecular water layer in interlayers by the FWS technique appears thus impossible.

Interestingly, the situation is different for Cs-montmorillonite. A higher amount of SW compared to the ILW was obtained, with a decrease to 43% (SW) compared to 29 % (ILW). There a maximum of 1 *W* in the interlayers is observed, and the obtained w_{SW} is similar to w_{ILW}. It appears thus that the (low) interlayer spacing of Cs-montmorillonite was not affected by the

freezing. In fact, the water content for SW is even higher (w_{SW}=0.11 g/g) compared to the one for ILW (w_{ILW}=0.07 g/g). The higher fraction of SW could be due to the higher amount of SW on the $A_{s,ext}$ compared to Na-montmorillonite, or due to an opposite change of the microstructure upon freezing.

The observations favor the microstructural concept of fewer but larger platelets in Cs- whereas in the Na-form significantly less and smaller platelets are stacked parallel to each other (Melkior *et al*., 2009; Pusch, 2001).

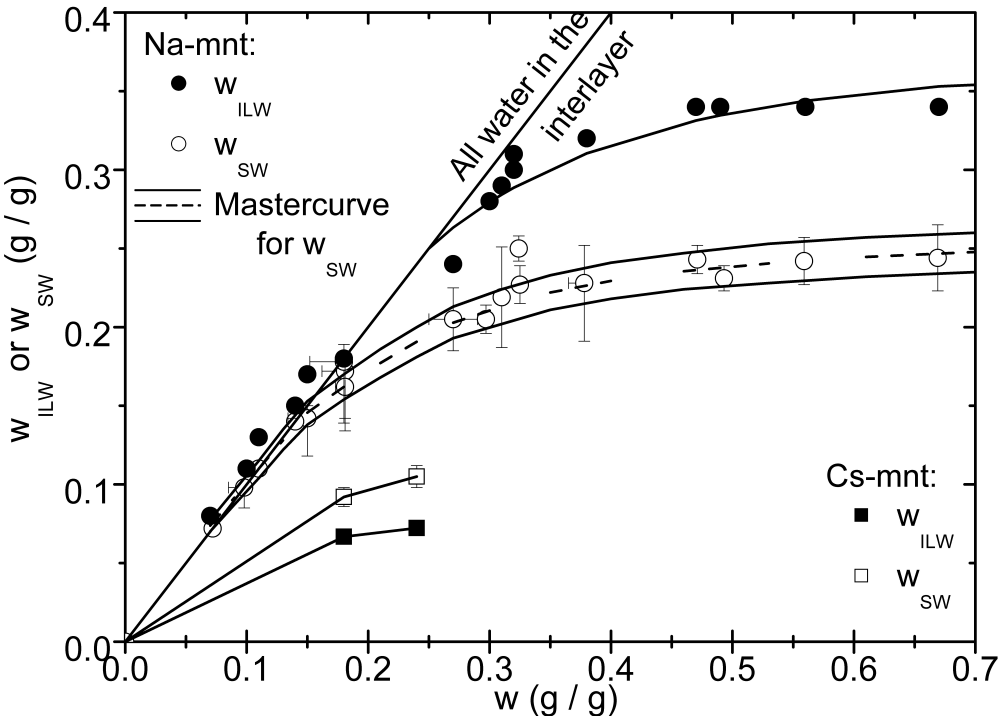

Figure 15. Amount of interlayer water (w_{ILW}) from neutron diffraction and surface area measurements, and the amount of surface water (w_{SW}) from fixed window scans as a function of total water content (w) for Na- and Cs-montmorillonite. The black dashed line is the fit (eq. 21) to w_{SW} and the black solid line is the fit to w_{ILW}.

Interlayer and interparticle porosity

Models describing the diffusive transport are based on different concepts regarding the accessible porosity. Birgersson and Karnland (2009) envisage the whole clay porosity as a single environment, whereas others (e.g., Bradbury and Baeyens, 2003) distinguish different pore environments. Experimentally, different transport-accessible porosities were derived for ions and neutral species (Van Loon *et al.*, 2007; Glaus *et al.*, 2010). Due to anion-exclusion from the interlayer, diffusion of anions is envisaged to take place mainly through the interparticle porosity (Van Loon *et al.*, 2007).

To quantify the porosity in different pore environments from neutron spectroscopy it is necessary that these environments have different scattering properties. The scattering of the hydrogen can be attributed to water on external surfaces, in interlayers, or in interparticle pores. It is likely that external surfaces and narrow interlayer pores have similar properties and contribute both to SW. Internal surfaces dominate especially for Na-montmorillonite, such that SW mainly represents interlayer water. BLW, on the other hand, mainly represents interparticle water. Because of the possible change of the Na-montmorillonite microstructure for samples with higher w (w > ~0.25 g/g), during the FWS measurements, the originally present interparticle porosity is probably overestimated by the BLW, and the interlayer water under estimated by the SW for these samples. The ILW directly estimated through the d-spacing represents the interlayer porosity. Accordingly, the IPW can be attributed to the interparticle porosity, for all water contents.

The water filled porosity $\varepsilon_W = w \cdot \rho_{\mathrm{bd}} / \rho_{\mathrm{w}}$ is in all cases lower than the porosity $\varepsilon = 1 - \rho_{\mathrm{bd}} / \rho_{\mathrm{s}}$. Accordingly, water saturations S are all <1. This fact has to be taken into account when attributing porosities to the different pore compartments. The difference between

ε_W and ε can in principle be explained in three different ways: (1), air-filled void space exists as external, comparably large pores that are not a part of the actual clay microstructure; (2), inter-particle pores are only partially saturated; and (3), interlayer pores are only partially saturated. A combination of all these effects may occur, but case (3) appears very unlikely. Thus, we proceed by considering just cases (1) and (2) and full saturation for the interlayer pores in all samples. Then the interlayer porosity equals:

$$\varepsilon_{\mathrm{IL}} = \mathrm{V}_{\mathrm{ILW}} / \mathrm{V}_{\mathrm{sample}} = w_{\mathrm{ILW}} \frac{\rho_{\mathrm{bd}}}{\rho_{\mathrm{w}}} \quad (17)$$

The interparticle pores occurring at higher water contents, however, may be partly filled with air. The interparticle porosity ε_{IP}, defined as interparticle pore volume per sample volume, is then

$$\varepsilon_{\mathrm{IP}} = (\mathrm{V}_{\mathrm{IPW}} + \mathrm{V}_{\mathrm{IP\,air}}) / \mathrm{V}_{\mathrm{sample}} \quad (18)$$

where V_{IPair} (cm^3) is any volume of air in the interparticle pores. Two extreme cases are distinguished in the following. Either all unsaturated pores are external pores (case 1 above), or all unsaturated pores belong to the interparticle pore space (case 2 above). In the first case, V_{IPair} is zero and the interparticle porosity from the geometrically obtained w_{IPW} is thus:

$$\varepsilon_{IP}^{\min} = \varepsilon_{IPW} = w_{IPW} \frac{\rho_{bd}}{\rho_w} \quad (19)$$

In the second case V_{IPair} is the total pore volume minus the volume occupied by water, such that the interparticle porosity equals the total porosity minus the interlayer porosity:

$$\varepsilon_{IP}^{\max} = \varepsilon - \varepsilon_{ILW} = \varepsilon - w_{ILW}\frac{\rho_{bd}}{\rho_w} \quad (20)$$

The same calculation can be made for the SW and BLW fractions obtained from neutron spectroscopy:

$$\varepsilon_{IP}^{\min} = \varepsilon_{BLW} = w_{BLW}\frac{\rho_{bd}}{\rho_w} \quad (21)$$

and

$$\varepsilon_{IP}^{\max} = \varepsilon - \varepsilon_{SW} = \varepsilon - w_{SW}\frac{\rho_{bd}}{\rho_w} \quad (22)$$

A further complication arises from the fact that the distribution between SW and BLW (or, correspondingly ILW and IPW) depends on the water content *w*. A saturation of the air-filled pores in the samples would lead to an increased water content *w* and thus very likely to a slight change of the microstructure, i.e., the distribution between SW and BLW (or ILW and IPW). We proceeded by assuming that our observed relation for w_{SW} versus *w* represents the master curve that can be used to estimate these microstructural shifts during an increase of *w*. The master curve with an error of ±5%, shown in Fig. 15 is given by

$$\mathrm{w} = (\mathrm{w} + 13.91 \cdot \mathrm{w}^{2.3}) / (1 + 3.89 \cdot (\mathrm{w} + 13.91 \cdot \mathrm{w}^{2.3})) \quad (23)$$

From these master curves relations for the dependence of the interparticle porosity on the water content *w* at saturation (or on bulk dry density) can be derived by inserting w_{SW} from Eq. (23) into Eq. 22. This relation is also shown in Fig. 16, together with the calculated $\varepsilon_{IP}^{\min}$ and $\varepsilon_{IP}^{\max}$ represented by the bars. Deviations in the values from eq. 19, 20 and eq. 21, 22 are due to the saturation in samples for high ρ_{bd}. The interparticle porosity obtained from the master curve (Eq.

23) is for low ρ_{bd} higher and for high ρ_{bd} similar compared to the average values of Eq. 19, 20 or 21, 22. When comparing the values from diffraction (eq. 19, 20) with values from spectroscopy (eq. 21, 22), ε_{IP} is similar at high ρ_{bd} and different at low ρ_{bd}. This is just a consequence of the differences between w_{SW} and w_{ILW} at high w. Note that the degree of saturation for Cs-montmorillonite is higher compared to Na-montmorillonite with similar ρ_{bd}. The deviation in the values between partly and fully saturated pores is thus less pronounced. The interparticle porosity is generally for Cs-montmorillonite higher when comparing with the values for Na-montmorillonite.

The view of Birgersson and Karnland (2009) appears to be supported by the observations of Holmboe *et al.* (2012). According to the measurements of Holmboe *et al.* (2012), most of the pore water should be considered as interlayer water, even at low ρ_{bd}. Contrary to the fitting results of Holmboe *et al.* (2012), reflexions allocated to osmotic swelling were absent in the XRD measurements of Kozaki *et al*. (1998) and Muurinen et al. (2004) resulting in a higher interparticle porosity with decreasing bulk dry density. Contrary to Holmboe *et al*. (2012) and consistent with Kozaki *et al*. (1998, 2001) and Van Loon *et al*. (2007) the interparticle porosity of this study increases with decreasing ρ_{bd}. Similar to Pusch (1999) most water molecules are located in interlayers at high ρ_{bd} for Na montmorillonite. The calculated interparticle porosity for full saturation is for Na-montmorillonite very similar to modeling results from Van Loon *et al.* (2007) for a bentonite with 71% smectite where anion-accessible interparticle pores were calculated. The present study shows additionally an increasing interparticle porosity at low ρ_{bd} in average from 0 to 36 % from geometric results and from 0 to 50 % from spectroscopic results.

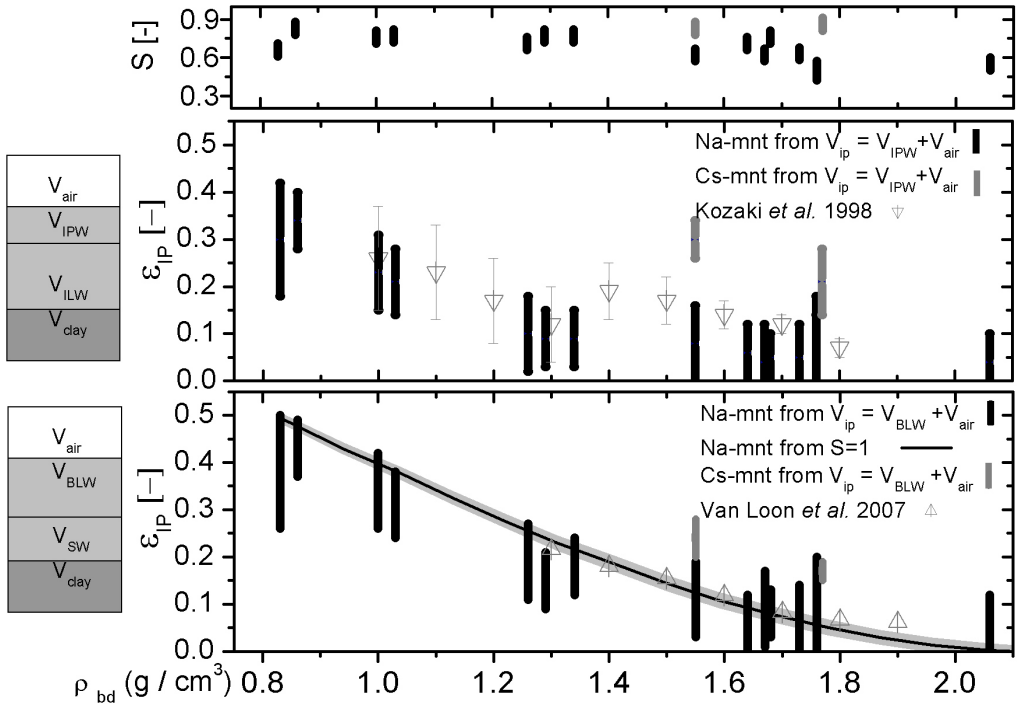

Figure 16. Saturation, *S* (top), interparticle porosity, ε_{IP} from neutron diffraction and surface area measurements (center) and from fixed window scans (down) as a function of bulk dry density (ρ_{bd}) for Na- and Cs-montmorillonite. The saturation was calculated from eq. 14. The interparticle porosity from the estimated interlayer / interparticle water (w_{ILW}, w_{IPW}) are the bars with the low value calculated from eq. 19 and the high value from eq. 20. The interparticle porosity from the estimated surface / bulk-like water (w_{SW}, w_{BLW}) are the bars with the low value from equation 21 and the high value from eq. 22. The gray shaded, black solid line corresponds to the fully saturation from the master curve eq. 23.

Table IV. Sample properties and results for Na-montmorillonite (black font) and Cs-montmorillonite (grey font). The Sample number (#) corresponds to the ones in the figures. The samples with the superscript d were hydrated in a set-up under confined conditions: # 10 in a 5M $NaClO_4$ solution and # 2, 4 & 7 in a water bath. The hydration of the other samples was in a desiccator; the samples with the superscript e are powder samples. The d-spacings for the dry clay (d_0) for Na-mnt (10.4 Å) and Cs-mnt (10.8 Å) were taken from Kosakowski *et al*. (2008).

Sample properties				Geometric calculation								Spectroscopic calculation					
#	ρ_{bd} (g/cm^3)	w (g/g)	S (-)	d (Å)	n_W (%) 1	2	3	4	w_{ILW} (g/g)	n_{ILW} (%)	ε_{IP} (-)	n_{SW} (%)	n_{BLW} (%)	w_{SW} (g/g)	w_{BLW} (g/g)	ε_{IP} (-)	$\varepsilon_{IP, S=1}$ (-)
19	1.77	0.18	0.86	12.5	100				0.07	39	0.22±0.02	56.2	43.8	0.10	0.08	0.17±0.02	
18	1.55	0.24	0.83	12.7	100				0.07	29	0.30±0.04	43.5	56.5	0.11	0.13	0.24±0.04	
16	2.06	0.07	0.55	12.77	100				0.08	114	0.04±0.06	100	0	0.07	0.00	0.06±0.06	0.00
15	1.76	0.10	0.47	13.44	41	59			0.11	110	0.08±0.10	100	0	0.10	0.00	0.10±0.10	0.05
14	1.76	0.11	0.52	14.00	34	66			0.13	118	0.05±0.09	100	0	0.11	0.00	0.09±0.09	0.05
13	1.73	0.14	0.63	14.67	11	89			0.15	107	0.05±0.07	100	0	0.14	0.00	0.07±0.07	0.06
12	1.67	0.15	0.62	15.08		100			0.17	113	0.04±0.08	93.3	6.7	0.14	0.01	0.09±0.08	0.08
11a	1.68	0.18	0.76	15.42		100			0.18	100	0.05±0.05	88.9	11.1	0.16	0.02	0.08±0.05	0.08
11b	1.64	0.18	0.71	15.49		100			0.18	100	0.06±0.06	100	0	0.18	0.00	0.06±0.06	0.09
11c	1.55	0.18	0.62	15.54		100			0.18	100	0.08±0.08	88.9	11.1	0.16	0.02	0.11±0.08	0.12
10 [d]	1.19	0.27	0.56	17.40		36	64		0.24	89	0.16±0.13	76.72	23.28	0.21	0.06	0.20±0.13	
9	1.34	0.30	0.77	18.35		33	67		0.28	93	0.09±0.06	70.00	30	0.21	0.09	0.18±0.06	0.22
8	1.26	0.31	0.71	18.52			100		0.29	94	0.10±0.08	71.0	29	0.22	0.09	0.19±0.08	0.25
7 [d]	1.29	0.32	0.77	18.95			100		0.30	94	0.09±0.06	79.29	20.71	0.25	0.07	0.15±0.06	0.24
6 [e]		0.32		19.23			93	7	0.31	97		71.9	28.1	0.23	0.09		
5 [e]		0.38		19.39			88	12	0.32	84		60.5	39.5	0.23	0.15		
4 [d]	1.00	0.49	0.76	19.98			83	17	0.34	69	0.23±0.08	46.9	53.1	0.23	0.26	0.34±0.08	0.40
3	0.83	0.56	0.66	20.01			83	17	0.34	61	0.30±0.12	42.9	57.1	0.24	0.32	0.38±0.12	0.50
2 [d]	1.03	0.47	0.77	20.03			77	23	0.34	72	0.21±0.07	51.1	48.9	0.24	0.23	0.31±0.07	0.38
1	0.86	0.67	0.83	20.04			83	17	0.34	51	0.34±0.06	35.8	64.2	0.24	0.43	0.43±0.06	0.48

Conclusions

The relative fractions of surface and bulk-like water in different pore environments of Na- and Cs-montmorillonite were obtained directly from neutron backscattering measurements. The results were compared with calculated fractions of interlayer and interparticle water obtained from neutron diffraction and adsorption measurements.

The obtained fractions of surface and bulk-like water are independent on the degree of saturation; the decisive parameter was rather found to be the water content. Depending on the characterization method different fractions of surface water in the interlayer and interlayer water were obtained. For Na-montmorillonite with low water content only surface and interlayer water exists. The amount of (i) surface water is increasing linearly up to two molecular water layers and (ii) interlayer water up to three molecular water layers. At high water content subsequently bulk-like water and interparticle water exist. The amount is increasing monotonically, but not linearly for bulk-like water from 0 to 64% and for interparticle water from 0 to 49 %. The obtained fractions of (i) surface and interlayer water were attributed to the interlayer pores and (ii) bulk-like water and interparticle water were attributed to the interparticle pores. The derived values are increasing for bulk-like water from 0 % to 50 % and for interparticle water from 0 to 36 %. Our samples were only partially saturated, which creates some uncertainty regarding the total volume of interparticle pores. The additional air-filled pore space belongs very likely also to the interparticle pores.

Cs-montmorillonite however can intercalate maximal one molecular water layer and an initial linear increase of surface and interlayer water (like in Na-montmorillonite) was not observed. The obtained surface water is higher with predominantly bulk-like water compared to Na-montmorillonite with similar d-spacing. The calculated interlayer/interparticle and measured

surface/bulk-like water show furthermore contrary results to Na-montmorillonite. The amount of (i) bulk-like is lower compared to the (ii) interparticle water increasing for (i) from 0 to 57% and for (ii) from 0 to 71 %. The derived interparticle porosity from bulk-like water is increasing from 0 % to 25 % and from interparticle water from 0 to 31 %.

Acknowledgment

This work is based on experiments performed at the Swiss spallation neutron source SINQ, Paul Scherrer Institute, Villigen, Switzerland and the Forschungs-Neutronenquelle Heinz Maier-Leibnitz, FRM II, Garching, Germany. The first author acknowledges the financial support of the Swiss National Science Foundation (SNF). We thank S.A.R.M. (Nancy, France) for the ICP-MS and Michael Plötze for the water adsorption measurements. The authors are grateful for the support from Sabrina Frick in the laboratory, Matthew Watson for preparing some samples and Enzo Curti for the help with a figure.

References

Anderson, D.M., 1967. Interface between ice and silicate surfaces. Journal of Colloid and Interface Science 25, 174-191.

Berend, I., Cases, J.M., Francois, M., Uriot, J.P., Michot, L., Masion, A., Thomas, F., 1995. Mechanism of adsorption and desorption of water–vapor by homoionic montmorillonites. 2. The Li^+, Na^+, K^+, Rb^+ and Cs^+-exchanged forms. Clays and Clay Minerals 43, 324-336.

Birgersson, M., Karnland, O., 2009. Ion equilibrium between montmorillonite interlayer space and an external solution-Consequences for diffusional transport. Geochimica et Cosmochimica Acta 73, 1908-1923.

Bordallo, H.N., Aldridge, L.P., Churchman, G.J., Gates, W.P., Telling, M.T.F., Kiefer, K., Fouquet, P., Seydel, T., Kimber, S.A.J., 2008. Quasi-elastic neutron scattering studies on clay interlayer-space highlighting the effect of the cation in confined water dynamics. Journal of Physical Chemistry C 112, 13982-13991.

Bradbury, M.H., Baeyens, B., 2003. Porewater chemistry in compacted re-saturated MX-80 bentonite. Journal of Contaminant Hydrology 61, 329-338.

Chiou, C.T., Rutherford, D.W., 1997. Effects of exchanged cation and layer charge on the sorption of water and EGME vapors on montmorillonite clays. Clays and Clay Minerals 45, 867-880.

Devineau, K., Bihannic, I., Michot, L., Villieras, F., Masrouri, F., Cuisinier, O., Fragneto, G., Michau, N., 2006. In situ neutron diffraction analysis of the influence of geometric confinement on crystalline swelling of montmorillonite. Applied Clay Science 31, 76-84.

Fleury, M., Kohler, E., Norrant, F., Gautier, S., M'Hamdi, J., Barre, L., 2013. Characterization and Quantification of Water in Smectites with Low-Field NMR. Journal of Physical Chemistry C 117, 4551-4560.

Gates, W.P., Bordallo, H.N., Aldridge, L.P., Seydel, T., Jacobsen, H., Marry, V., Churchman, G.J., 2012. Neutron Time-of-Flight Quantification of Water Desorption Isotherms of Montmorillonite. Journal of Physical Chemistry C 116, 5558-5570.

Glaus, M.A., Frick, S., Rosse, R., Van Loon, L.R., 2010. Comparative study of tracer diffusion of HTO, $^{22}Na^{+}$ and $^{36}Cl^{-}$ in compacted kaolinite, illite and montmorillonite. Geochimica et Cosmochimica Acta 74, 1999-2010.

González Sánchez, F., Van Loon, L.R., Gimmi, T., Jakob, A., Glaus, M.A., L.W., D., 2008a. Self-diffusion of water and its dependence on temperature and ionic strength in highly compacted monmorillonite, illite and kaolinite. Applied Geochemistry 23, 3840-3851.

González Sanchez, F., Juranyi, F., Gimmi, T., Van Loon, L., Unruh, T., Diamond, L.W., 2008b. Translational diffusion of water and its dependence on temperature in charged and uncharged clays: A neutron scattering study. The Journal of Chemical Physics 129, 174706-174706.

González Sánchez, F., Jurányi, F., Gimmi, T., Van Loon, L., Seydel, T. and Unruh, T., 2008c. Dynamics- of supercooled water in highly compacted clays studied by neutrons scattering, Journal of Physics: Condensed Matter, 20, 415102.

De Boer, J. H., Lippens, B.C., Linsen, B.G., Broekhoff, J.C.P., van den Heuval, A., Osinga, T.J., 1966. The t-curve of multimolecular N2-adsorption. Journal of Colloid and Interface Science 21, 405-414.

Holmboe, M., Wold, S., Jonsson, M., 2012. Porosity investigation of compacted bentonite using XRD profile modeling. Journal of Contaminant Hydrology 128, 19-32.

Jurányi, F., Bestel, M., Wattson, M., Schneider, G., Garcia, C., to be submitted. Quantitative separation of nano- and interparticle pore water in swelling clays by means of neutron scattering. Physical Review.

Keeling, P.S., Kirby, E.C., Robertson, R.H.S., 1980. Moisture adsorption and specific surface-area. Transactions and Journal of the British Ceramic Society 79, 36-40.

Kosakowski, G., Churakov, S.V., Thoenen, T., 2008. Diffusion of Na and Cs in montmorillonite. Clays and Clay Minerals 56, 190-206.

Kozaki, T., Fujishima, A., Sato, S., Ohashi, H., 1998. Self-diffusion of sodium ions in compacted sodium montmorillonite (vol 121, pg 63, 1998). Nuclear Technology 123, 120-120.

Kuila, U., Prasad, M., 2013. Specific surface area and pore-size distribution in clays and shales. Geophysical Prospecting 61, 341-362.

Melkior, T., Gaucher, E.C., Brouard, C., Yahiaoui, S., Thoby, D., Clinard, C., Ferrage, E., Guyonnet, D., Tournassat, C., Coelho, D., 2009. Na^+ and HTO diffusion in compacted bentonite: Effect of surface chemistry and related texture. Journal of Hydrology 370, 9-20.

Mackenzie, R.C., 1958. Density of water sorbed on montmorillonite. Nature 181, 334-334.

Madsen, F.T., Kahr, G., 1996. Wasserdampfadsorption und spezifische Oberfläche von Tonen. Nagra Technical Report NTB, 93-17, Nagra, Wettingen, Switzerland.

Muurinen, A., Karnland, O., Lehikoinen, J., 2004. Ion concentration caused by an external solution into the porewater of compacted bentonite. Physics and Chemistry of the Earth 29, 119-127.

Norrish, K., 1954. The swelling of montmorillonite. Discussions of the Faraday Society, 120-134.

Pusch, R., 1999. Microstructural evolution of buffers. Engineering Geology 54, 33-41.

Pusch, R., 2001. The microstructure of MX-80 clay with respect to its bulk physical properties under different enviromental conditions., Swedish Nuclear Fuel and Waste Management Co. (SKB), ISSN 1404-0344.

Saiyouri, N., Tessier, D., Hicher, P.Y., 2004. Experimental study of swelling in unsaturated compacted clays. Clay Minerals 39, 469-479.

Salles, F., Bildstein, O., Douillard, J.M., Jullien, M., Raynal, J., Van Damme, H., 2010. On the Cation Dependence of Interlamellar and Interparticular Water and Swelling in Smectite Clays. Langmuir 26, 5028-5037.

Segad, M., Jonsson, B., Cabane, B., 2012. Tactoid Formation in Montmorillonite. Journal of Physical Chemistry C 116, 25425-25433.

Sposito, G., Skipper, N.T., Sutton, R., Park, S.H., Soper, A.K., Greathouse, J.A., 1999. Surface geochemistry of the clay minerals. Proceedings of the National Academy of Sciences of the United States of America 96, 3358-3364.

Suhr, N.H., Ingamell.Co, 1966. Solution technique for analysis of silicates. Analytical Chemistry 38, 730-734.

Svensson, P.D., Hansen, S., 2010. Freezing and thawing of montmorillonite - A time-resolved synchrotron X-ray diffraction study. Applied Clay Science 49, 127-134.

Van Loon, L.R., Glaus, M.A., Mueller, W., 2007. Anion exclusion effects in compacted bentonites: Towards a better understanding of anion diffusion. Applied Geochemistry 22, 2536-2552.

Wuttke, J., Budwig, A., Drochner, M., Kaemmerling, H., Kayser, F.-J., Kleines, H., Ossovyi, V., Carlos Pardo, L., Prager, M., Richter, D., Schneider, G.J., Schneider, H., Staringer, S., 2012.

SPHERES, Julich's high-flux neutron backscattering spectrometer at FRM II. Review of Scientific Instruments 83.

Appendix 1

The neutron diffraction patterns for a Na-montmorillonite sample compacted to ρ_{bd}=0.88 g/cm3 and saturated with D_2O to S=0.83 were recorded at different temperatures (Fig. 17). The d-spacing of 19.8 Å was calculated from Braggs law. Three hexagonal ice peaks are appearing from 300 to 255 K due to the crystallization of water. From this we concluded that the water in the interparticle pores freezes like bulk water (BLW).

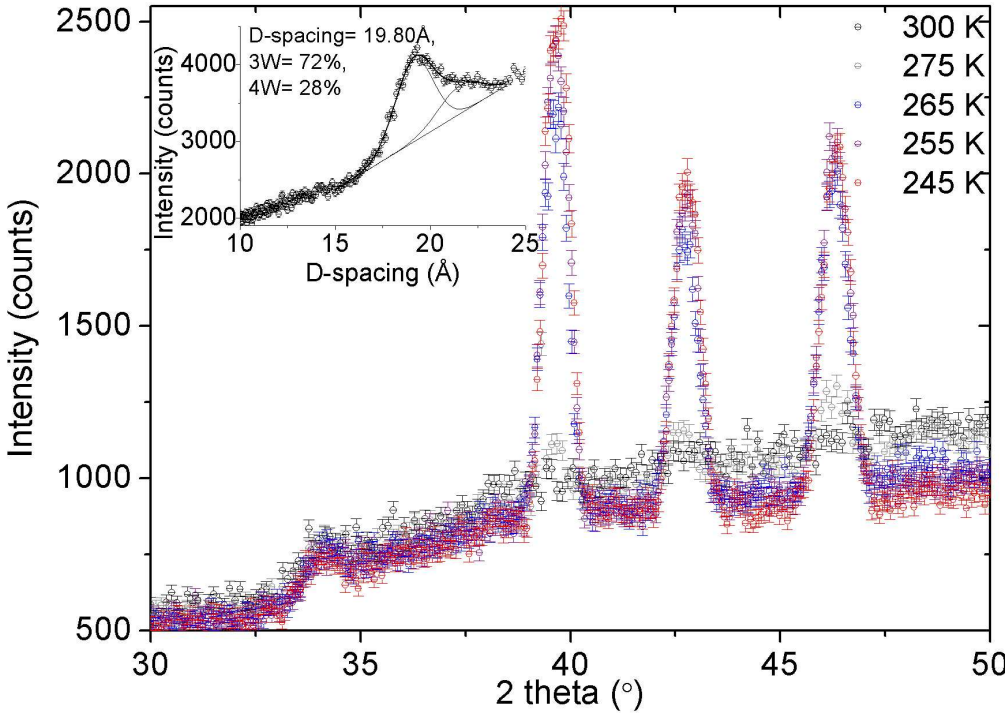

Figure 17. Neutron diffraction pattern for a deuterium saturated Na-montmorillonite sample. The intensity is shown as function of a 2 theta scan for different temperatures. In the inserted diagram shows the d-spacing range (Å) at 25ºC corresponding to 2 theta between 6º and 15º with the Gaussian fit corresponding to 3 and 4 D_2O layers (the solid line).

3 Chapter 3: Combined tracer through-diffusion of HTO and ^{22}Na through Na-montmorillonite with different bulk dry densities

Martina BESTEL[*1,3], Sabrina FRICK[2], Martin A. GLAUS[2], Thomas GIMMI[2,3] , Luc R. VAN LOON[2] and Larryn W. DIAMOND[3]

[1]Laboratory for Neutron Scattering, Paul Scherrer Institut, 5232 Villigen PSI, Switzerland
[2]Laboratory for Waste Management, Paul Scherrer Institut, 5232 Villigen PSI, Switzerland
[3]Institute of Geological Sciences, University of Bern, 3012 Bern, Switzerland

[*]*Corresponding author: mbestel@gmx.de*

Abstract - The suitability of swelling clays as a barrier to isolate nuclear waste repositories is based on their microstructure, characterized by pore sizes down to atomic scale, and by their physicochemical properties such as favourable hydraulic and transport retarding properties. In this study, the effect of bulk dry density and ionic strength (0.1, 1 and 5 M $NaClO_4$) in the external contact solution on the diffusion of HTO and $^{22}Na^+$ through Na-montmorillonite was studied. Both parameters affect the microstructure of clay and the molecular properties of pore water such as its mobility and the degree of ordering. While the diffusion of neutral species, such as water, depends on the bulk dry density only, the diffusive fluxes of Na^+ were additionally shown to be a function of the ionic strength. In a plot of logarithmic effective diffusion coefficients versus the logarithmic external salt concentrations slopes of less than unity were observed for low bulk dry densities. This is an indication that the diffusive flux of $^{22}Na^+$ is affected by more than one transport pathway which is in agreement with the inter-

pretation of e.g. a dual porosity model or dual compartment. Additionally, the diffusive behaviour of both tracers were investigated here as a function of the temperature (between 0 and 80 °C). The activation energy was calculated from the Arrhenius equation. It was found that for samples with high bulk dry density the activation energy values were slightly higher and for low bulk dry density smaller compared to bulk water (17 kJ/mol), and similar for low and medium ionic strength. Coupled diffusion of HTO and $^{22}Na^{+}$ is a possible interpretation of the observation that the values of the activation energies were almost the same for both tracers under all conditions.

Key words – Swelling clays, tracer diffusion, activation energy, dual porosity concept, dual compartment concept, surface diffusion

Introduction

Due to the low hydraulic conductivity and its favourable sorption properties bentonite is considered in many countries as a sealing material to isolate nuclear waste repositories from the environment. The main component of bentonite is montmorillonite, which consists of two-dimensional octahedral (O) alumina sheets sandwiched between tetrahedral (T) silica sheets to form a so-called TOT layer. The layers are negatively charged because of isomorphic substitutions of some central cations mainly in the octahedral sheet, for cations of lower charge. Between these TOT layers are interlayer pores where charge-compensating cations, like Na^{+}, and water molecules are intercalated. Stacks of multiple TOT layers form larger clay platelets. Depending on the bulk dry density, interparticle pores may occur in various amounts near the external surfaces of the hydrated clay platelets. Water is thus located in different pore environments and may have different properties originating from the physicochemical interaction with the ions in solution, with the excess cations near the surfaces, and with the charged surfaces.

Different nomenclatures exist in the literature to characterize the different water types (e.g. Gates *et al.*, 2012). In the following we simply discriminate between water present in the interlayer pores and the very near surface of clay platelets (ILW) and water in the interparticle pores (IPW). Bestel *et al*. (to be submitted) measured the ratio of surface water in interlayer pores to bulk-like water in larger (e.g. interparticle) pores using neutron backscattering spectroscopy. The results from geometrical calculations based on neutron diffraction and surface area measurements were similar to those from neutron backscattering spectroscopy for low total water contents (high bulk dry density). This confirms the finding from Pusch *et al*. (2001) that most water molecules are located in the interlayers as surface water at low water contents. At high water contents (low bulk dry densities) water with bulk-like properties is present in the interparticle pores.

Molecular diffusion is the main transport process through bentonites at high bulk dry densities or in natural claystones and clay minerals (e.g. Boving and Grathwohl, 2001; Gimmi *et. al.*, 2007; Mazurek et. al., 2011). To predict the diffusive mass transport for saturated clays of the engineered barrier system the influence of pore geometry has to be taken into account. This is typically done by introducing empirical factors such as the tortuosity (τ, -) and constrictivity (δ, -) in the definition of the pore diffusion coefficient (D_p, m^2/s):

$$D_p = D_0 \frac{\delta}{\tau} = D_0 \cdot G \quad (24)$$

D_0 (m^2/s) is the self diffusion coefficient in bulk water and G (-) the geometrical factor is lumping together τ and δ (Shackelford, 1991; González Sánchez *et al.*, 2008; Shackelford and Moore, 2013). Note that these quantities cannot be determined independently of each other. Diffusion coefficients for tritiated and deuterated synthetic porewater were experimentally obtained

and are increasing with decreasing compaction (González Sánchez *et al.*, 2008; Nakazawa *et al.*, 1999, Sato, 2002, Suzuki *et al.*, 2004).

For charged species, however, the effect of fixed surface charges is in addition important. Different concepts exist for the implementation of such effects. In the single porosity concept, a homogeneous pore space made up of interlayer water only is considered (Birgersson and Karnland, 2009). Cations of the alkaline and earth alkaline series equilibrate between the external solution and the montmorillonite pore space by cation exchange. All species in the montmorillonite pore space are viewed as being mobile. A certain amount of anions enters the interlayer pores according to the Donnan equilibrium. Birgersson and Karnland (2009) were able to model literature data for $^{22}Na^{+}$ (Glaus *et al.*, 2007) and $^{36}Cl^{-}$ (Van Loon *et al.*, 2007) in a consistent manner using the calculated tracer concentrations in the montmorillonite pore space as the driving force for Fickian diffusion.

The difference in geometrical respect between interlayer and interparticle pores is considered as a transport-relevant property in the case of dual porosity models for diffusion (e.g. Bourg *et al.*, 2006/2007). The distribution of pore water between different pore compartments, different transport-accessible porosities for ions compared to neutral species and the specific interactions of ions with the charged surfaces (e.g. sorption) are taken into account in those models. On a microscopic scale, the total flux j_{tot} (mol/m^2/s) is viewed as the sum of two parallel fluxes through the interlayer j_{IL} (mol/m^2/s) and larger pores j_{IP} (mol/m^2/s), like the interparticle pores. When assuming Fickian diffusion the total flux is driven by the local concentration gradients in x, y and z direction in these porosities (∇C_{IL} and ∇C_{IP}, mol/m^4):

$$j_{tot} = j_{IL} + j_{IP} = D_{e,IL} \cdot \nabla C_{IL} + D_{e,IP} \cdot \nabla C_{IP} \quad (25)$$

$D_{e,IL}$ and $D_{e,IP}$ (m^2/s) are the respective effective diffusion coefficients for the interlayer and the larger pores. They can be represented as $\varepsilon_{IL} \cdot D_{p,IL}$, $\varepsilon_{IP} \cdot D_{p,IP}$ where ε (-) and D_p (m^2/s) denote the corresponding porosity and pore diffusion coefficient. Depending on the species under consideration C_{IL} is directly related to C_{IP} by a thermodynamic equilibrium condition (such as cation exchange or a Donnan two-phase equilibrium). C_{IP} is mostly assumed to be equal to the concentration of the diffusing species in the external bulk solution. If all interlayer cations are considered as sorbed and all interparticle cations as being in solution, eq. (25) is equal to a surface diffusion model for parallel transport of sorbed cations on the surfaces and cations in solution (e.g., Oscarson, 1994; Gimmi and Kosakowski, 2011). Such a surface diffusion model should be denoted more generally as a dual compartment model, rather than as a dual porosity model. Gimmi and Kosakowski (2011) proposed a scaling procedure in which the effective diffusion coefficient of a cationic species is normalised by its bulk water diffusion coefficient and by the tortuosity obtained from a water tracer. The relative contribution to diffusion from the sorbed cations is expressed by a relative surface mobility (μ_s, –) and the capacity ratio (κ, –). The resulting normalised relative effective diffusion coefficient (D_{erw}, –) is related to these quantities in the following manner (where *w* refers to the water molecule, respectively):

$$D_{erw} = \frac{D_e D_0^w}{D_0 D_e^w} = 1 + \kappa\mu_s \quad (26)$$

The capacity ratio is defined as the amount of sorbed cations per amount of cations in pore solution (or the amount of interlayer cations per amount of interparticle cations, if interlayer cations represent the sorbed cations):

$$\kappa = \frac{\rho_{bd} \cdot S}{\varepsilon \cdot C} = \frac{\varepsilon_{IL} \cdot C_{IL}}{\varepsilon_{IP} \cdot C_{IP}} \quad (27)$$

where S (mol/g solid) is the sorbed concentration. Using a sorption distribution coefficient K_d (cm^3/g)=S/C·10^6 and the bulk dry density ρ_{bd} (g/cm^3), the capacity ratio can be given as:

$$\kappa = \frac{\rho_{bd} \cdot K_d}{\varepsilon} \quad (28)$$

For identical G for diffusion through the two compartments κ directly controls the individual contributions to the overal cation flux because the ratio of concentration gradients in these compartments are related to κ. Finally, μ_s is defined as the ratio of an intrinsic surface diffusion coefficient on a flat surface ($D_{s0,}$ m^2/s) and D_0

$$\mu_s = \frac{D_{s0}}{D_0} \quad (29)$$

Summarising eq. 24-29, the diffusive fluxes relative to those of water tracers may thus mainly be governed by (i) the relative surface diffusion coefficients μ_s and by (ii) the sorption processes on internal or external surface of the TOT layers characterised by the parameter κ.

From the dependence of κ on the salinity of the solution in contact with the clay, the diffusion of ^{22}Na is expected to correlate with the ionic strength, the diffusion increases for ^{22}Na with decreasing ionic strength of the background solution (NaCl, $NaClO_4$) (Glaus *et al.*, 2007, 2010, 2013 and Melkior *et al.*, 2009). From the inverse dependency of the steady-state tracer flux on the salinity of the external solution, Glaus *et al.* (2007) concluded that for cationic species like $^{22}Na^+$ the transport in the interlayers dominated the overall flux j_{tot}, meaning that the contribution of j_{IP} (equation 25) was negligible in those cases. Upon correcting for the dependency of these gradients for salinity effects, Glaus *et al.* (2007) ended with a single diffusion coefficient

valid for diffusion in the interlayer pores for all conditions tested. Norrish *et al.* (1954) and Amorim *et al.* (2007) studied the swelling of montmorillonite under contact with different electrolyte solutions using X-ray diffraction and interpreted the basal spacing beween 20 to 40 Å with formation of diffuse double layers (DDL). The thickness of the DDL in Na-montmorillonite decreases with increasing ionic strength affecting the volume of the transport-accessible porosity. It leads to a different concentration distribution of species in surface and bulk-like water. It can thus be expected that at sufficiently low degrees of compaction or at large external salinities the contribution from the interparticle pore space has an increasing importance and that the simple relationships observed by Glaus *et al.* (2007) may be no longer valid.

Aim of this work

The aim of this work was to investigate the diffusive transport of HTO and ^{22}Na and its dependence on the bulk dry density and ionic strength under conditions under which a measurable contribution of both fluxes (j_{IL} and j_{IP}) can be expected. The variation of the ionic strength shall give information on the validity of the various porosity models (single, dual). For this purpose and for obtaining internally consistent results, the diffusive flux of HTO and ^{22}Na through medium to lowly compacted Na-montmorillonite samples was simultaneously measured and effective diffusion coefficients were derived. The temperature of the diffusive flux was varied in order to see effects of the deduced activation energy on the bulk dry density. Further there is a general interest in the temperature dependence of diffusion in view of the high initial temperatures of high-level radioactive wastes, for which bentonite is foreseen as the buffer and/or backfill material.

Material and Methods

A homoionic Na-montmorillonite with identical chemical composition as in Bestel *et al.* (to be submitted) was investigated. Because humid samples were easier to compact, the powder samples were partially hydrated from the vapor phase in a first step to gravimetric water contents (*w* defined as the ratio of mass of water to mass of dry clay) varying between 0.2 and 0.6 g/g. After compaction of the wetted clay samples these were placed between porous filters and subsequently saturated under constant volume conditions using $NaClO_4$ solutions present at various concentrations (0.1, 1 and 5 mol/l). Diffusion cells with an appropriate sealing system enabling a continuous flow of the contacting solutions through the confining filters were used to minimise concentration gradients in the filters (Glaus *et al.*, 2013). The cylindrical clay pellets had a radius of $1.00 \cdot 10^{-2}$ m and a thickness (d_c) of $1.00 \cdot 10^{-2}$ m. The thickness of the confining filters (d_f) was $1.65 \cdot 10^{-3}$ m. Samples of low (0.80, 1.07), intermediate (1.32, 1.33, 1.35) and high (1.56, 1.63, 1.68, 1.70) bulk dry densities (g/cm^3) were investigated (Tab. V). The background electrolyte solution circulated through the porous filters at flow rates of 0.1 ml/min maintaining thereby an almost homogeneous tracer concentration. The compacted sample took up 1-2 g background electrolyte solution (corresponding to a change in water content of up to 0.33 g/g) within one month of saturation time. The obtained *w* (g/g) and the degree of saturation *S* (-) were determined after the tracer through-diffusion experiment by desiccation at 110°C (Tab. V). The degree of saturation *S* is defined as the volume of water per volume of pores (-): $S = {w\rho_{bd}}/{\varepsilon\rho_w}$ where $\varepsilon\rho_w / \rho_{bd}$ equals the gravimetric water content at full saturation (w_{sat}). The total porosity of a sample (ε) was calculated from $\varepsilon = 1 - {\rho_{bd}}/{\rho_s}$ with the solid density (ρ_s

= 2.8 g/cm^3) measured by pycnometry. The amount of $NaClO_4$ backlog from evaporation was calculated from the porosity of the sample.

Table V. Sample properties for Na-montmorillonite

Sample	1	2	3	4	5	6	7	8	9	10	11
[M] $NaClO_4$	0.1	0.1	0.1	0.1	0.1	0.1	1	1	1	1	5
ρ_{bd} (g/cm^3)	0.80	1.07	1.07	1.33	1.56	1.63	1.32	1.33	1.68	1.70	1.35
ε (-)	0.71	0.62	0.62	0.53	0.44	0.42	0.53	0.53	0.40	0.39	0.52
w (g/g)	0.86	0.59	0.55	0.39	0.24	0.27	0.33	0.40	0.26	0.25	0.38
S (-)	0.97	1.02	0.95	0.98	0.85	1.05	0.82	1.00	1.09	1.08	0.99

After saturation the experiment was started with an identical setup for the tracer through-diffusion experiment as described in Van Loon *et al.* (2005). Owing to the long duration of the experiment involving several temperature steps, the tracer reservoir volumina have been chosen relatively large in order to avoid drastic changes in the tracer concentration. For HTO, the reservoir concentration remained virtually unchanged, while a measurable decrease could be noticed for ^{22}Na. This led to a diffusive flux that slightly decrease with time. The solution at the low concentration side was changed three times a week against tracer free solutions to keep the tracer concentrations as low as reasonably possible. The tracer fluxes at the downstream filter boundary were calculated from the activities $A_{dif}^{\Delta t_i}$ (Bq) accumulated during each time intervall Δt_i (s), the cross section area S (m^2) of the clay plug and the specific activity of the tracer A_{sp} (Bq/mol):

$$j_{tot} = \frac{A_{dif}^{\Delta t_i}}{S \Delta t_i A_{sp}} \quad (30)$$

The activities of HTO and ^{22}Na (half lives of 12.3 and 2.6 years, respectively) were detected through liquid scintillation counting. $\beta - \beta$ discrimination using two energy windows was

used to determine the activities of HTO and $^{22}Na^{+}$ separately. The two windows were 0 to 20 keV for the combined contribution of HTO and $^{22}Na^{+}$ and 20 to 600 keV for the contribution of $^{22}Na^{+}$ only. All values for $A_{dif}^{\Delta t_i}$ were corrected for radioactive decay using a unique reference date for all samples.

We applied the continuous method of temperature variation (Van Loon *et al.*, 2005) in which the temperature is changed as soon as a sufficiently long steady-state phase has been observed for a given temperature. Temperatures between 0 and 80 ° were applied by keeping the diffusion cells in a thermostate laboratory incubator (Friocell 111, IG Instrumentengesellschaft, Zürich, Switzerland). Two different flux phases built up: (i) a short transient state for the initial temperature only and (ii) quasi steady-state phases during which the flux remains almost constant, viz. decreasing only as the result of decrease in concentration in the source reservoir. Data at 25 ºC were measured at the beginning and at the end of the temperature cycle in order to verify that the properties for diffusion such as the clay structure remained unchanged during the entire experiment.

The effective diffusion coefficient D_e (m^2/s) was calculated from Fick's first law for each set of the measured flux data. Despite the advective flushing of the filters, some heterogeneities in solution concentrations are to be expected due to an inhomogeneous flow in the filters. For simplicity these inhomogeneities are treated as a diffusive resistance of an isotropic medium in the flushed filters. A virtual diffusion coefficient for the filter D_f (m^2/s) was estimated to be $1.50 \cdot 10^{-9}$ m^2/s at 25 ºC. Its value for other temperatures was estimated through the Arrhenius relation assuming an activation energy E_a of 17 kJ/mol (Low, 1962). According to the serial arrangement of filter-clay-filter, D_e was calculated from the one-dimensional steady state flux (j_{tot})

at time *t* and the respective tracer concentration in the upstream reservoir C_t^{usb} (Glaus *et al.*, 2008):

$$D_e = \frac{j_{tot} \cdot d_c \cdot D_f}{C_t^{usb} \cdot D_f - 2 \cdot j_{tot} \cdot d_f} \quad (31)$$

Average values for a given temperature were calculated from groups of data (j_{tot}) with near-constant flux values and the respective groups of C_t^{usb} values. Equation 31 is strictly valid for constant boundary concentration conditions only. Variable boundary conditions from the experiment were however acceptable in our experiments because the changes in C_t^{usb} within a time interval used to derive diffusion coefficients were insignificant compared to the allocated error bars. According to equation 31 the effective diffusion coefficient was calculated assuming a zero tracer concentration in the downstream boundary reservoir.

The capacity ratio κ was calculated (eq. 28) from K_d values determined from the break-through curves during the transient phase of the experiments carried out at 25 °C. For linear sorption K_d (defined as the per-dry weight amount of solute adsorbed onto the solid phase divided by its solution concentration) is calculated from the rock capacity factor (α, –) by the following relation:

$$K_d = \frac{\alpha - \varepsilon}{\rho_{bd}} \quad (32)$$

The break-through time t_{bt} (s) (Van Loon *et al.*, 2005) was determined from the intercept of the abscissa by the extension of the linear part of the plot of $\sum_{i=1}^{n} A_{dif}^{\Delta t_i}$ versus time for the purpose of calculating α according to the following equation which again takes into account the diffusive resistance of the filters (Yaroshchuk *et al.*, 2008, Glaus et al., 2008):

$$\alpha = \frac{6 j_{tot} t_{bt} C_t^{usb} (D_f)^2}{d_c (C_t^{usb})^2 (D_f)^2 + 2 d_f d_c C_t^{usb} D_f j_{tot} - 2 d_c (d_f)^2 (j_{tot})^2} \quad (33)$$

α is also used to calculate the apparent diffusion coefficient D_a (m^2/s) according to Fick's second law (given in a one-dimensional representation):

$$\frac{dC}{dt} = \frac{D_e}{\alpha} \frac{d^2C}{dx^2} = D_a \frac{d^2C}{dx^2} \quad (34)$$

Alternatively κ may also be calculated from the cation exchange capacity *CEC* (mmol/g) according to:

$$\kappa = \frac{CEC \cdot \rho_{bd}}{\varepsilon \cdot A} \quad (35)$$

where *A* is the molar concentration of the background electrolyte in the contacting solution.

Table VI. Average HTO concentrations in the upstream boundary reservoir (C_t^{usb}) and estimated flux (j_{tot}) at 25ºC. A typical bunching of data for average formation is shown in Fig. 18.

Sample	1	2	3	4	5	6	7	8	9	10	11
$C_t^{usb} \cdot 10^7$ (mol/m^3)	4.03	4.09	4.05	9.64	9.79	9.83	5.13	5.18	5.24	5.28	3.86
$j^i_{tot} \cdot 10^{14}$ ($mol/m^2/s$)	1.12	0.73	1.16	0.69	0.38	0.35	0.47	0.44	0.19	0.17	0.40

Table VII. Average ^{22}Na concentrations in the upstream boundary reservoir (C_t^{usb}) and estimated flux (j_{tot}) for at 25ºC. A typical bunching of data for average formation is shown in Fig. 19.

Sample	1	2	3	4	5	6	7	8	9	10	11
$C_t^{usb} \cdot 10^7$ (mol/m^3)	0.21	0.22	0.21	0.057	0.11	0.12	0.81	0.51	0.51	0.52	0.20
$j^i_{tot} \cdot 10^{14}$ ($mol/m^2/s$)	0.15	0.14	0.15	0.025	0.038	0.040	0.084	0.061	0.027	0.026	0.012

Activation energy

The dependence of the effective diffusion coefficient on temperature *T* (K) was evaluated from the Arrhenius equation (Gonzalez *et al.*, 2008):

$$D_e = A \cdot \exp \frac{E_a}{RT} \quad (36)$$

where *A* is the preexponential factor and *R*=8.314 J/K/mol is the molar gas constant. The activation energy was estimated from the linear regression of the plotted logarithmic effective diffusion coefficients versus reciprocal temperature.

Neutron diffraction

Neutron diffraction measurements were carried out on the 2-axis diffractometer MORPHEUS (SINQ, PSI, Switzerland) with the same setup as given in Bestel *et al.* (to be submitted). The converted d-spacing peak was fitted by two Gaussian functions. The relative abundance of 3 *W* (3 water layer) and 4 *W* (4 water layer) in the interlayer were determined from the ratio of the peak areas and the average d-spacing value.

Results & Discussions

As can be seen from Table V the investigated samples were fully saturated (90-100%), and the obtained diffusion coefficients are thus directly comparable as a function of ρ_{bd} or ε (Table VI, VII). The effective diffusion coefficients for the different temperatures, α, K_d, κ and E_a are listed in Tab. VIII and IX (Appendix). Representative examples of the dependence of the diffusive flux on temperature are shown in Fig. 18 for HTO and Fig. 19 for ^{22}Na. Also shown in

these Figures is the evolution of the tracer concentration in the source reservoir which acts as a concentration boundary condition for the diffusive process. As expected j_{tot} increases with increasing temperature. For HTO, the quasi-steady-state flux and the diffusion coefficients at 25 ºC are equal within the error bars at the beginning and at the end of the experiment indicating that no major structural changes occurred over the entire duration of the temperature cycle. The respective values for ^{22}Na are however significantly higher at the beginning than at the end of the experiment. This is explained by the decrease of C_t^{usb} during the temperature cycle; the diffusion coefficients remain equal within the error bars (with one exception). The flux values for ^{22}Na show somewhat larger scatter than the HTO data. This can be explained by the fact that the tracer concentration in the downstream-boundary reservoir increases until the reservoir flask gets exchanged. It can be shown that this increase leads to a rather significant change in the tracer concentration gradients near the clay interface at the downstream boundary. As a result the variance of the time dependent flux values in the quasi steady-state phase of ^{22}Na is larger than those of HTO. Note that D_e is systematically underestimated for the assumption of $C_t^{dsb} = 0$ (Eq. 31). The arising bias is rather in the range of statistical uncertainties, even for $^{22}Na^+$, and thus not taken into account in the data evaluation.

Large uncertainties are inherently associated with the α values for HTO because of the very short break-through times. The values are similar to ε which can be expected for a non-sorbing diffusing species. For ^{22}Na, α is higher than ε for all samples except of the sample saturated with 5 M $NaClO_4$, for which α is similar to ε. Note the good consistency between κ values calculated from α and values calculated from *CEC* (Tab. IX, Appendix).

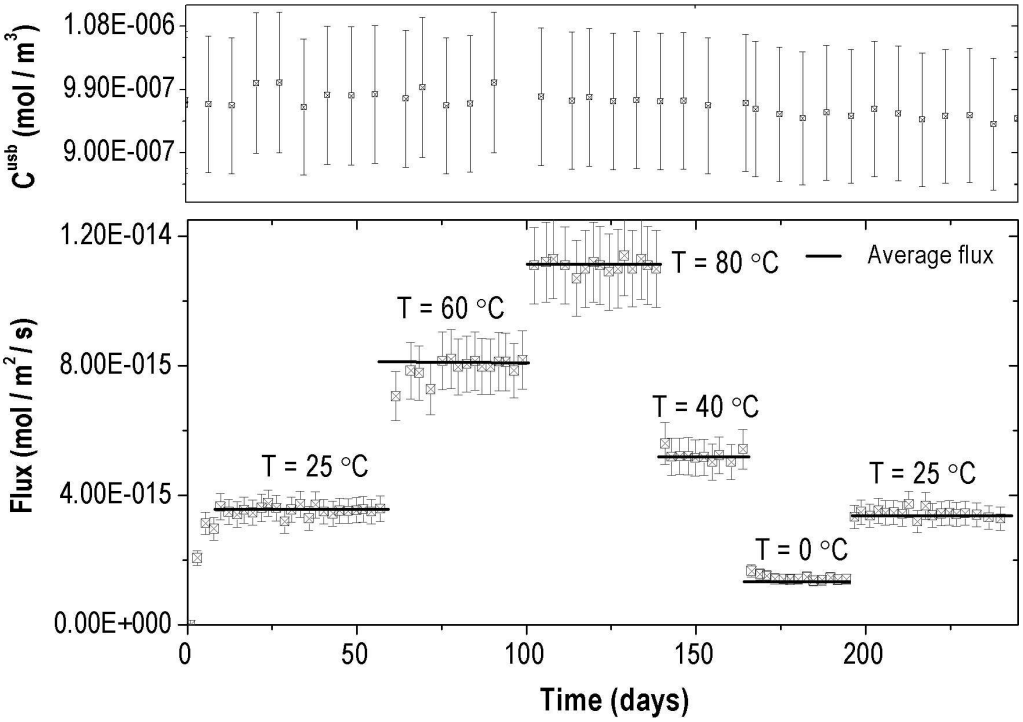

Figure 18. Diffusion of HTO through a compacted Na-montmorillonite (1.63 g/cm3) at 0.1 M Na-ClO_4 (sample 6) for different temperatures. The tracer concentration in the high tracer concentration reservoir (top) and the diffusive flux into the low tracer concentration reservoir (bottom) are shown as a function of time. The bars indicate groups of data used for average formations for the steady state (cf. Tab. VI) to estimate the effective diffusion coefficients (Tab. VIII, Appendix).

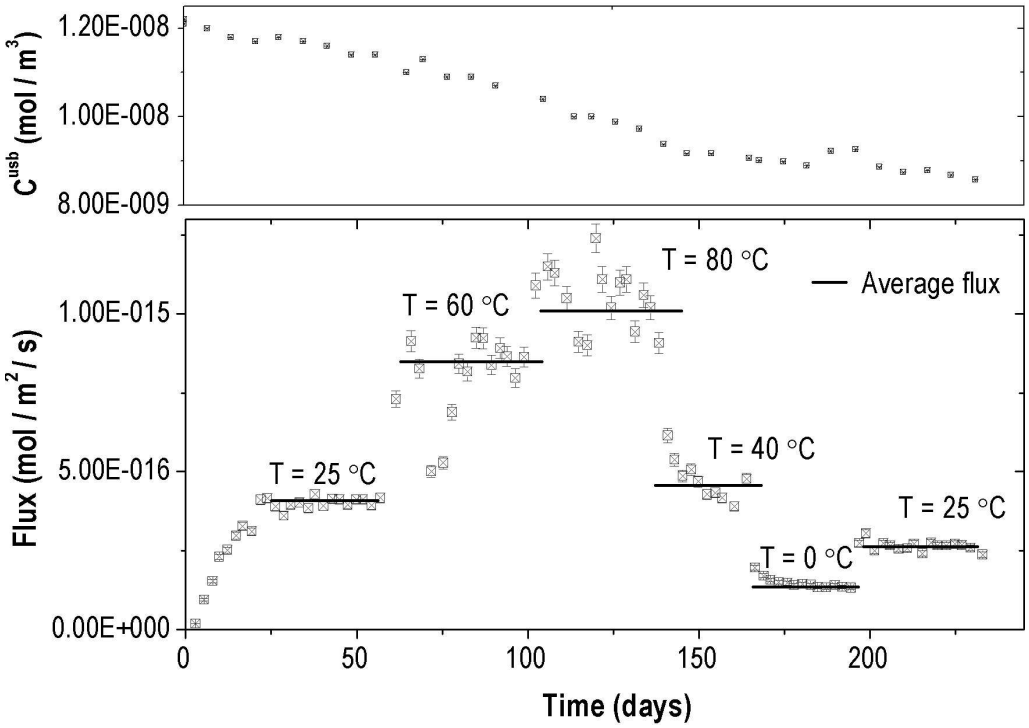

Figure 19. Diffusion of ^{22}Na through a compacted Na-montmorillonite (1.63 g/cm^3) at 0.1 M $NaClO_4$ (sample 6) for different temperatures: The tracer concentration in the high tracer concentration reservoir (top) and the diffusive flux into the low tracer concentration reservoir (bottom) are shown as a function of time. The bars indicate groups of data used for average formations for the steady state (cf. Tab. VII) to estimate the effective diffusion coefficients (Tab. IX, Appendix).

Dependence of D_e on salinity and bulk dry density

The dependency of D_e values for HTO at 25 ºC on the ionic strength A is illustrated in a logarithmic representation in Fig. 20. For samples with similar bulk dry densities D_e for HTO is independent on A. As evidenced by the identity of α and ε, the whole porosity is accessible for HTO, diffusing through the interlayer and interparticle porosity. This means that the existence of different quantities of the interlayer and interparticle porosity have no significant influence on j_{tot} in a dual porosity model, from which it can in turn be concluded that the geo-

metrical factors (equation 24) for the interlayer or interparticle porosity are approximately identical. This is somewhat surprising from the nanoscopic point of view of molecular diffusion. As indicated by neutron spectroscopy (Bestel *et al.*, to be submitted; González *et al.*, 2008) the molecular movement of a water molecule in the surface water is lower than in bulk-like water by a factor of 2–3. It appears that such differences are outplayed when considering the diffusion process on a macroscopic scale taking into account geometric effects originating from the porous network in the clays.

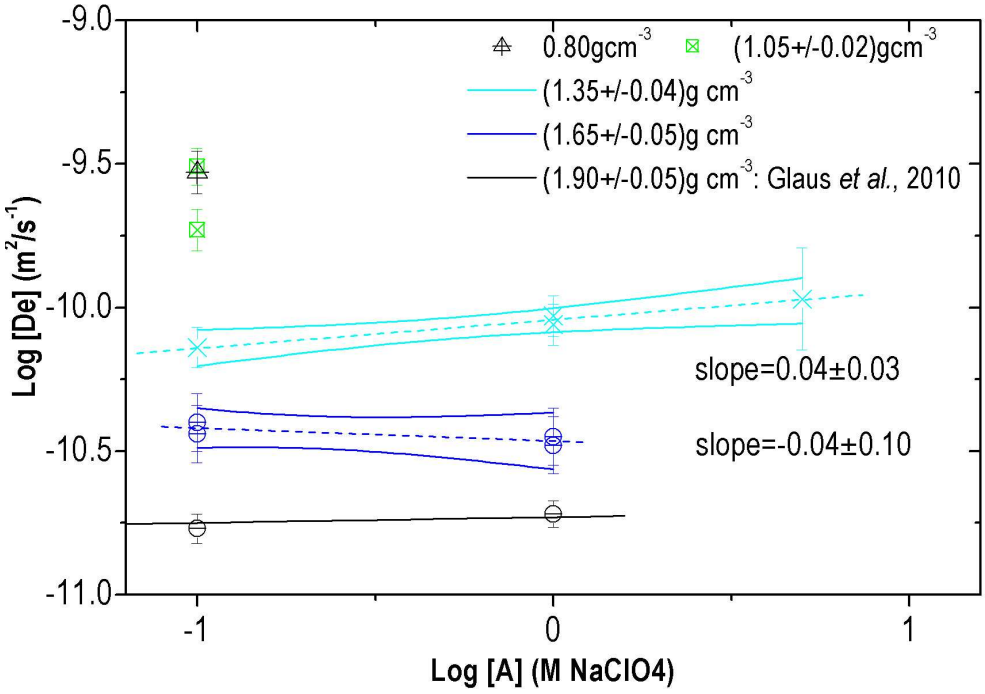

Figure 20. Dependence of the effective diffusion coefficients (D_e) for HTO on the ionic strength at 25 ºC on logarithmic scales.

In order to relate D_e or D_p values measured at different bulk dry densities, empirical relationships such as Archie's law (Archie, 1942) are useful (Van Loon *et al.*, 2007):

$$\log D_p = \log D_0' + (m-1)\log \varepsilon \quad (37)$$

with $D_0^{'}$ (m^2/s) the diffusion coefficient at ε=1 (supposed to be the diffusion coefficient in water, D_0 (m^2/s)), m (-) an empirical exponent often denoted as the cementation factor. Figure 21 shows such a relation for the HTO data. The factor m is influenced by the type and degree of consolidation (Archie, 1942), pore geometry (Thompson, 1987), rock texture and particle geometry like preferred orientation (Sen *et al*., 1984). Similarly to literature data from Nakazawa *et al.* (1999), Suzuki *et al.* (2004), Sato (2002), González Sánchez *et al.* (2008) and Glaus *et al.* (2010, 2013), the D_p values for HTO are increasing monotonously with increasing porosity. This shows that our data give an internally consistent picture in agreement with literature data.

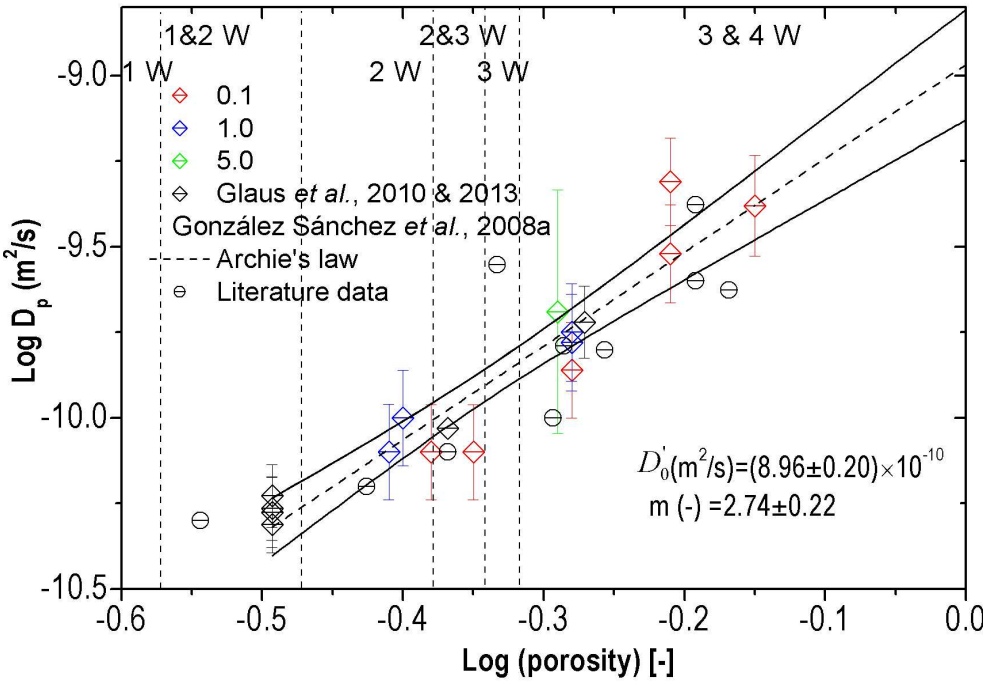

Figure 21. Dependence of the pore diffusion coefficients (D_p) for HTO on the porosity at a temperature of 25 °C on logarithmic scales. The black lines are the fit with Archie's law to data measured and data from González Sánchez *et al.* (2008) and Glaus *et al.* (2010, 2013). The number of water layer (*W*) for these porosities from neutron diffraction measurements was taken from Bestel *et al.* (to be submitted). Literature data are from Nakazawa *et al.* (1999), Suzuki *et al.* (2004) and Sato (2002).

A completely different situation for the dependence on ionic strength is observed for the diffusion of the ^{22}Na tracer. The D_e values obviously depend on the ionic strength and in most cases, D_e values for $^{22}Na^+$ are larger than those of HTO. Only in the case of the experiment carried out using 5 M $NaClO_4$ an opposite ratio was measured. A slope of 0.64 and 0.85 in a plot of logarithmic effective diffusion coefficients versus logarithmic values of salinity was obtained for the lower density of 1.35 g/cm^3 and 1.65 g/cm^3, respectively (Fig. 22).

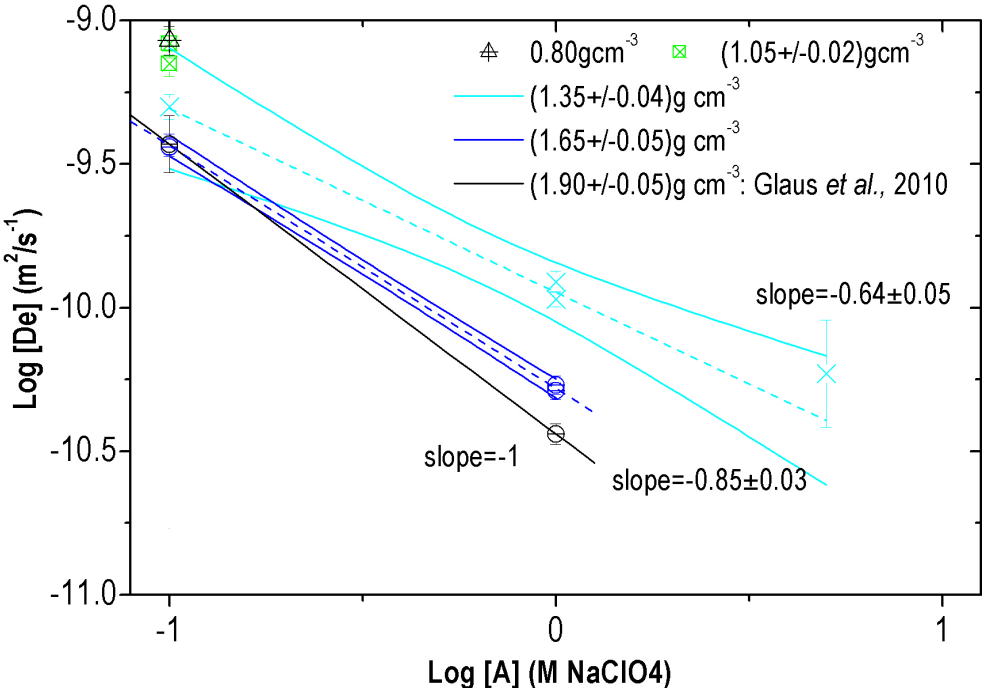

Figure 22. Dependence of the effective diffusion coefficients (D_e) for ^{22}Na on the ionic strength *A* at 25 °C on logarithmic scales.

Glaus *et al.* (2007) showed that, for the limiting case of interlayer diffusion being the dominant diffusion pathway ($D_{e,IP} \cdot \nabla C_{IP}$ of eq. 25 can thus be neglected), the slope in such a plot is expected to be the reciprocal root of the charge of a cation undergoing cation-exchange on the clay. For the case of diffusion of $^{22}Na^+$ a limiting slope of 1 can thus be expected. This expectation was confirmed in experiments using Milos montmorillonite compacted to dry densities of

1.9 g/cm^3 (Glaus *et al.*, 2007). If the slope is > 1, a considerable part of j_{tot} for ^{22}Na is attributed to $D_{e,IP}$, which is – for the present consideration – independent of the charge of the tracer or of the ionic strength of the pore solution. It can thus be concluded that, under compaction of ρ_{bd}=1.3 g/cm^3 the j_{IP} contributes significantly to the overall flux and that these data cannot be represented by a simple model as proposed by Glaus *et al* (2007) for highly compacted smectites. Consequently the model applied to these data needs refinement.

In a first step we plot the $^{22}Na^+$ data given as normalized D_a values as a function of porosity which is in essence the same representation as given by Bourg *et al*. (2007). The apparent diffusion coefficients slightly increase with increasing porosity (Fig. 23). Whether this dependence can be used for model discrimination is questionable.

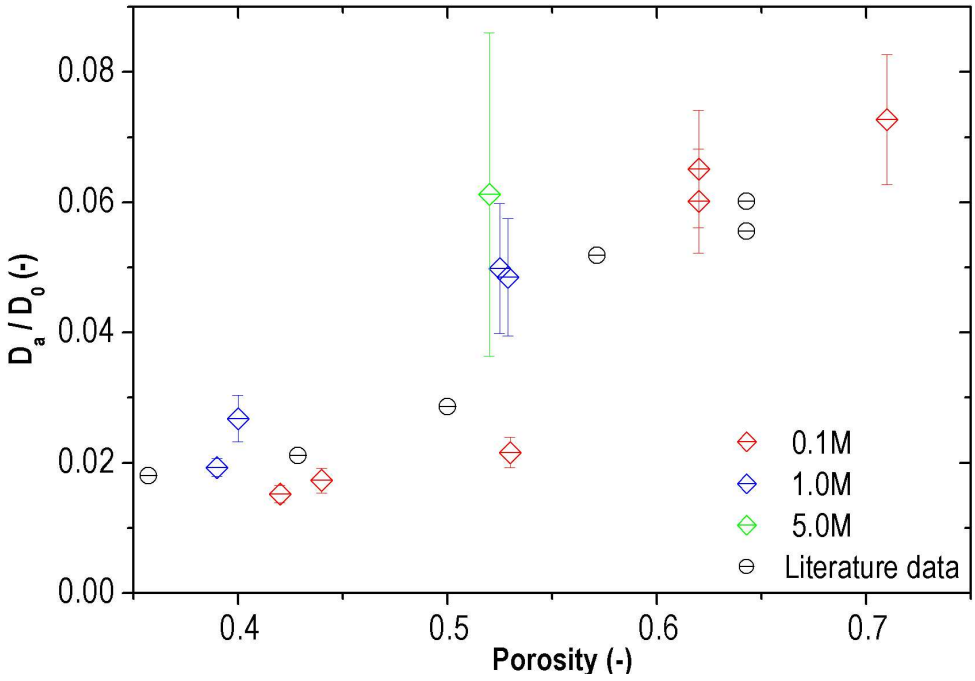

Figure 23. Apparent diffusion coefficient (D_a) normalized to the diffusion coefficient in bulk water (D_0) for ^{22}Na versus porosity at 25 °C. Literature data are from Kozaki *et al.* (1998) (water saturated samples) and Glaus *et al.* (2007) (1.95 g/cm^3 compacted samples saturated with 0.1 and 1.0 M $NaClO_4$).

We use the scaling procedure proposed by Gimmi and Kosakowski (2011) as a next step. This formalism is also based on a dual-flux concept comprising a surface and pore diffusion component (equation 26). The resulting picture is given in Fig. 24. In agreement with the data compilation of Gimmi and Kosakowski (2011) the scaled diffusion coefficients are around 1 for low κ and increase with increasing κ values. The obtained surface mobility (μ_s=0.40±0.02) is similar to the value (μ_s=0.52) from Gimmi and Kosakowski (2011). The good quality of the fit curve given in Fig. 24 is thus a confirmation that the data measured in the present work comprise conditions, for which a dual-flux model is required for an adequate description of the experimental data.

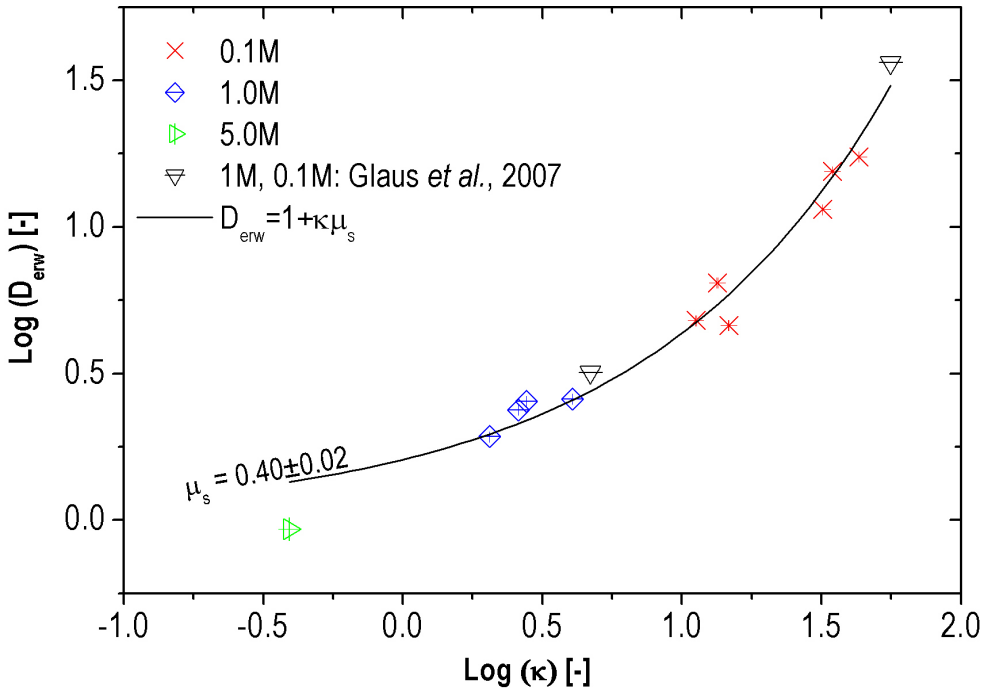

Figure 24. Scaled diffusion coefficients (D_{erw}) for ^{22}Na as a function of the capacity ratio for sorption κ. The dashed line represents the surface diffusion model from Gimmi and Kosakowski (2011) fitted to the measured data. Literature data from Glaus *et al.* (2007) are for samples compacted to 1.95 g/cm^3 and saturated with 0.1 and 1.0 M $NaClO_4$.

For the κ (Na^+) values smaller than unity, D_e for cations was found to be smaller than for water. This observation is in agreement with the interpretation from calculated d-spacings from neutron diffraction measurements (Fig. 25). The d-spacing for lowly compacted samples (1.0 g/cm^3) and the thickness of the DDL are smaller (Norrish *et al.*, 1954; Amorim *et al.*, 2007) suggesting a lower volume of the transport-accessible porosity for the 5 M $NaClO_4$ compared to the water saturated sample.

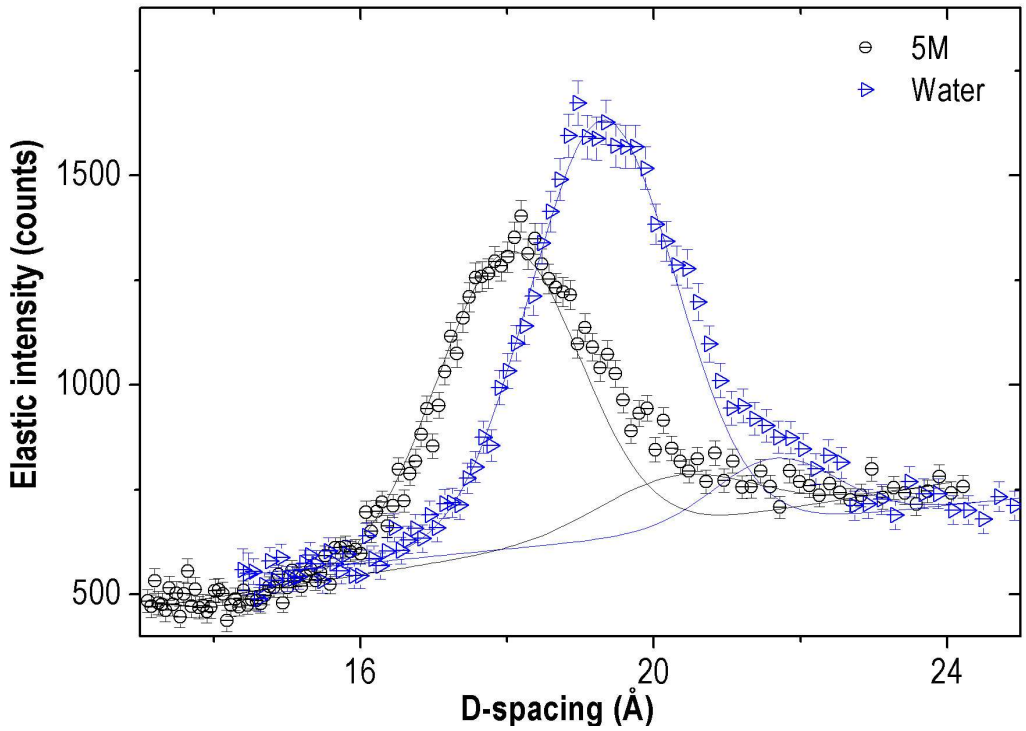

Figure 25. Neutron diffractogram for a Na-montmorillonite sample compacted to 1.00 g/cm^3 and saturated with (i) water and (ii) 5 M $NaClO_4$. The solid lines are Gaussian fits to the experimental data resulting in (i) 85 % of 3 molecular water layer (W) and 15 % of 4 W with mean d-spacing of 19.57 Å, and for (ii) 89 % of 3 W and 11 % 4 W with mean d-spacing of 18.46 Å.

Activation energy versus bulk dry density

The activation energy (E_a, kJ/mol) for diffusion is the minimum amount of energy required to reach a transition state for molecular displacement, viz. for breaking intermolecular forces. It is seen as an indicator for the state of confinement of water in compacted clay systems (Kozaki *et al.*, 1996/1998; Liu *et al*., 2003; Suzuki *et al*., 2004, Van Loon *et al.,* 2005). The activation energy for HTO and ^{22}Na through lowly compacted clay is lower compared to bulk water with (17±1) kJ/mol (Low, 1962) and for highly compacted Na-montmorillonite increases with increasing bulk dry density to a value higher than bulk water (Kozaki *et al.*, 1996/1998). The diffusion of cations is further influenced by sorption processes. Thus, the activation energy for diffusion of sorbing cations can differ from that of water. Except for Cs with predominantly larger E_a at high compaction, it is for most cations and anions similar.

The dependence of E_a on ρ_{bd} for HTO and ^{22}Na is shown in Fig. 26, Fig. 27-34 (Appendix). The derived E_a values are similar for ^{22}Na to the ones of Kozaki *et al.* (1998) and for HTO to the ones of González Sánchez *et al.* (2008) and Suzuki *et al.* (2004). The values for E_a are similar for both species for all samples. This indicates a dynamic coupling between HTO and ^{22}Na meaning that both species move together, e.g. HTO in hydration shells around Na^+ provided that the residence time of water in the hydration shell is exceeding the time scales of diffusion at the molecular scale. The activation energy slightly increases with increasing bulk dry density. For low consolidation the activation energy is slightly lower than for bulk water. For intermediate consolidation E_a is higher than for bulk water. The predominantly larger E_a for ^{134}Cs (Kozaki *et al.*, 1996) compared to HTO indicates a non-coupled diffusive transport.

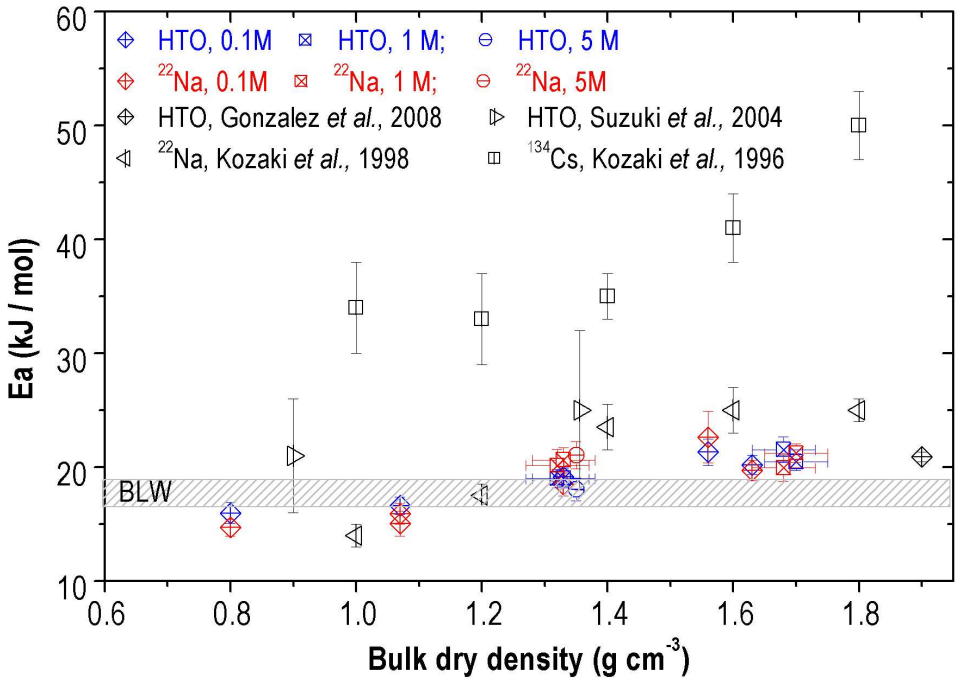

Figure 26. Activation energies derived from effective diffusion coefficients for ^{22}Na and HTO as a function of bulk dry density. The band represents the activation energy for bulk like water (BLW) of 17±1 kJmol^{-1} (Low, 1962). The values of González Sánchez *et al.* (2008) and Suzuki *et al.* (2004) are derived from effective diffusion coefficients and of Kozaki *et al.* (1996/1998) from apparent diffusion coefficient of water saturated samples.

Conclusion

The diffusive flux for HTO and ^{22}Na through compacted Na-montmorillonite was simultaneously measured and effective diffusion coefficients for different temperatures and bulk dry densities were obtained. The diffusion of HTO is independent of the ionic strength of the external solution with which it has been equilibrated. The diffusion is rather dependent on the bulk dry density, which confirms the observations made in the literature. The diffusion of ^{22}Na was found to be dependent on the ionic strength of the pore (background) solution and the bulk dry density. The dependence of ^{22}Na diffusion through samples with intermediate compaction (1.33±0.01 g cm^{-3}) on the ionic strength of the pore solution is weaker (slope of –0.64 in a log-

log plot) as compared to the dependence reported earlier for highly compacted samples (slope of –1). This can be explained by the weaker contribution by trend (depending on the ionic strength) of interlayer or surface diffusion to the overall flux at the lower density. Diffusion in the interlayers (surfaces) only would lead to a limiting slope of –1 for Na^+. The combined dependence of the ^{22}Na diffusion coefficients on the bulk density and the ionic strength of the equilibrium solution can be captured by considering the capacity ratio κ for sorption. Scaled ^{22}Na diffusion coefficients follow the pattern for Na^+ reported by Gimmi and Kosakowski (2011) with a similar estimated surface mobiliy of 0.40±0.02. The activation energies of ^{22}Na and HTO are similar for all samples indicative of a dynamic coupling between water and cations.

Acknowledgment

This work is partly based on experiments performed at the Swiss spallation neutron source SINQ, Paul Scherrer Institute, Villigen, Switzerland. The first author acknowledges the financial support of the Swiss National Science Foundation (SNF).

References

Amorim, C.L.G., Lopes, R.T., Barroso, R.C., Queiroz, J.C., Alves, D.B., Perez, C.A., Schelin, H.R., 2007. Effect of clay-water interactions on clay swelling by X-ray diffraction. Nuclear Instruments & Methods in Physics Research Section a-Accelerators Spectrometers Detectors and Associated Equipment. 580, 768-770.

Archie, G.E., 1942. The electrical resistivity log as an aid in determining some reservoir characteristics. Trans. AIME 146, 54-62.

Baeyens, B., Bradbury, M.H., 1997. A mechanistic description of Ni and Zn sorption on Na-montmorillonite .1. Titration and sorption measurements. Journal of Contaminant Hydrology 27, 199-222.

Bestel, M., Gimmi, T., Glaus, M.A., Van Loon L.R., Zamponi, M., Diamond, L.W., Jurányi, F., to be submitted. Water distribution in Na- and Cs-montmorillonite. Clays and Clay Mineralogy.

Birgersson, M., Karnland, O., 2009. Ion equilibrium between montmorillonite interlayer space and an external solution-Consequences for diffusional transport. Geochimica et Cosmochimica Acta 73, 1908-1923.

Boving, T. B.; Grathwohl, P., 2001. Tracer diffusion coefficients in sedimentary rocks: Correlation to porosity and hydraulic conductivity. Journal of Contaminant Hydrology 53, 85−100.

Bourg, I.C., Sposito, G., Bourg, A.C.M., 2006. Tracer diffusion in compacted, water-saturated bentonite. Clays and Clay Minerals 54, 363-374.

Bourg, I.C., Sposito, G., Bourg, A.C.M., 2007. Modeling cation diffusion in compacted water-saturated sodium bentonite at low ionic strength. Environmental Science & Technology 41, 8118-8122.

Bradbury, M.H., Baeyens, B., 2003. Porewater chemistry in compacted re-saturated MX-80 bentonite – physico-chemical characterization and geochemical modeling. PSI Bericht Nr. 02-10. Paul Scherrer Institut, Villigen, Switzerland, Nagra Techical Report NTB 01-08, Nagra. Wettigen, Switzerland.

Dähn, R., Scheidegger, A.M., Manceau, A., Schlegel, M.L., Baeyens, B., Bradbury, M.H., Morales, M., 2002. Neoformation of Ni phyllosilicate upon Ni uptake on montmorillonite: A kinetics study by powder and polarized extended X-ray absorption fine structure spectroscopy. Geochimica et Cosmochimica Acta 66, 2335-2347.

Gates, W.P., Bordallo, H.N., Aldridge, L.P., Seydel, T., Jacobsen, H., Marry, V., Churchman, G.J., 2012. Neutron Time-of-Flight Quantification of Water Desorption Isotherms of Montmorillonite. Journal of Physical Chemistry C 116, 5558-5570.

Gimmi, T.; Waber, H. N.; Gautschi, A.; Ruebel, A., 2007. Stable water isotopes in pore water of Jurassic argillaceous rocks as tracers for solute transport over large spatial and temporal scales. Water Resour. Res. 43, W04410.

Gimmi, T., Kosakowski, G., 2011. How Mobile Are Sorbed Cations in Clays and Clay Rocks? Environmental Science & Technology 45, 1443-1449.

Glaus, M.A., Baeyens, B., Bradbury, M.H., Jakob, A., Van Loon, L.R., Yaroshchuk, A., 2007. Diffusion of Na-22 and Sr-85 in montmorillonite: Evidence of interlayer diffusion being the dominant pathway at high compaction. Environmental Science & Technology 41, 478-485.

Glaus, M.A., Rosse, R., Van Loon, L.R., Yaroshchuk, A.E., 2008. Tracer diffusion in sintered stainless steel filters: measurement of effective diffusion coefficients and implications for diffusion studies with compacted clays. Clays and Clay Minerals 56, 677-685.

Glaus, M.A., Frick, S., Rosse, R., Van Loon, L.R., 2010. Comparative study of tracer diffusion of HTO, $^{22}Na^{+}$ and $^{36}Cl^{-}$ in compacted kaolinite, illite and montmorillonite. Geochimica et Cosmochimica Acta 74, 1999-2010.

Glaus, M.A., Frick, S., Rosse, R., Van Loon, L.R., 2011. Consistent interpretation of the results of through-, out-diffusion and tracer profile analysis for trace anion diffusion in compacted montmorillonite. Journal of Contaminant Hydrology 123, 1-10.

Glaus, M.A., Birgersson, M., Karnland, O., Van Loon, L.R., 2013. Seeming Steady-State Uphill Diffusion of $^{22}Na^{+}$ in Compacted Montmorillonite. Environmental Science & Technology 47, 11522-11527.

González Sánchez, F., Van Loon, L.R., Gimmi, T., Jakob, A., Glaus, M.A., L.W., D., 2008. Self-diffusion of water and its dependence on temperature and ionic strength in highly compacted montmorillonite, illite and kaolinite. Applied Geochemistry 23, 3840-3851.

Kozaki, T., Sato, H., Fujishima, A., Sato, S., Ohashi, H., 1996. Activation energy for diffusion of cesium in compacted sodium montmorillonite. Journal of Nuclear Science and Technology 33, 522-524.

Kozaki, T., Fujishima, A., Sato, S., Ohashi, H., 1998. Self-diffusion of sodium ions in compacted sodium montmorillonite (vol 121, pg 63, 1998). Nuclear Technology 123, 120-120.

Kozaki, T., Liu, J., Sato, S., 2008. Diffusion mechanism of sodium ions in compacted montmorillonite under different NaCl concentration. Physics and Chemistry of the Earth 33, 957-961.

Liu, J.H., Yamada, H., Kozaki, T., Sato, S., Ohashi, H., 2003. Effect of silica sand on activation energy for diffusion of sodium ions in montmorillonite and silica sand mixture. Journal of Contaminant Hydrology 61, 85-93.

Low, P.F., 1962. Influence of absorbed water on exchangeable ion movement. Clays and Clay Minerals 9, 219–228.

Mazurek, M.; Alt-Epping, P.; Bath, A.; Gimmi, T.; Waber, H. N.; Buschaert, S.; De Cannière, P.; De Craen, M.; Gautschi, A.; Savoye, S.; Vinsot, A.; Wemaere, I.; Wouters, L., 2011. Natural tracer profiles across argillaceous formations. Applied Geochemistry 26, 1035−1064.

Melkior, T., Gaucher, E.C., Brouard, C., Yahiaoui, S., Thoby, D., Clinard, C., Ferrage, E., Guyonnet, D., Tournassat, C., Coelho, D., 2009. Na^{+} and HTO diffusion in compacted bentonite: Effect of surface chemistry and related texture. Journal of Hydrology 370, 9-20.

Nakazawa, T., Takano, M., Nobuhara, A., Torikai, Y., S., S., H., O., 1999. Activation energies of diffusion of tritium and electrical conduction in water-saturated compacted sodium montmorillonite. Radioactive Waste Management and Environment Remediation – ASME.

Norrish, K., 1954. The swelling of montmorillonite. Discussions of the Faraday Society, 120-134.

Oscarson, D.W., 1994. Surface-diffusion - Is it an important transport mechanism in compacted clays. Clays and Clay Minerals 42, 534-543.

Pusch, R., 2001. The microstructure of MX-80 clay with respect to its bulk physical properties under different enviromental conditions., Swedish Nuclear Fuel and Waste Management Co. (SKB), ISSN 1404-0344.

Sato, H., Suzuki, S., 2003. Fundamental study on the effect of an orientation of clay particles on diffusion pathway in compacted bentonite. Applied Clay Science 23, 51-60.

Sen, P.N., 1984. Grain shape effects on dielectric ans electrical-properties of rocks. Geophysics 49, 586-587.

Shackelford, C.D., 1991. Laboratory diffusion testing for waste disposal – A review. Journal of Contaminant Hydrology 7, 177-218.

Shackelford, C.D., Moore, S.M., 2013. Fickian diffusion of radionuclides for engineered containment barriers: Diffusion coefficients, porosities, and complicating issues. Engineering Geology 152, 133-147.

Suzuki, S., Sato, H., Ishidera, T., Fujii, N., 2004. Study on anisotropy of effective diffusion coefficient and activation energy for deuterated water in compacted sodium bentonite. Journal of Contaminant Hydrology 68, 23-37.

Thompson, A.H., Katz, A.J., Krohn, C.E., 1987. The microgeometry and transport-properties of sedimentary-rock. Advances in Physics 36, 625-694.

Van Loon, L.R., Muller, W., Iijima, K., 2005. Activation energies of the self-diffusion of HTO, $^{22}Na^{+}$ and $^{36}Cl^{-}$ in a highly compacted argillaceous rock (Opalinus Clay). Applied Geochemistry 20, 961-972.

Van Schaik, J.C., Kemper, W.D., Olsen, S.R., 1966. Contribution of Adsorbed Cations to Diffusion in Clay-Water Systems. Soil Science Society of America Proceeding 30, 17-22.

Yaroshchuk, A.E., Glaus, M.A., Van Loon, L.R., 2008. Diffusion through confined media at variable concentrations in reservoirs. Journal of Membrane Science 319, 133-140.

Appendix 2

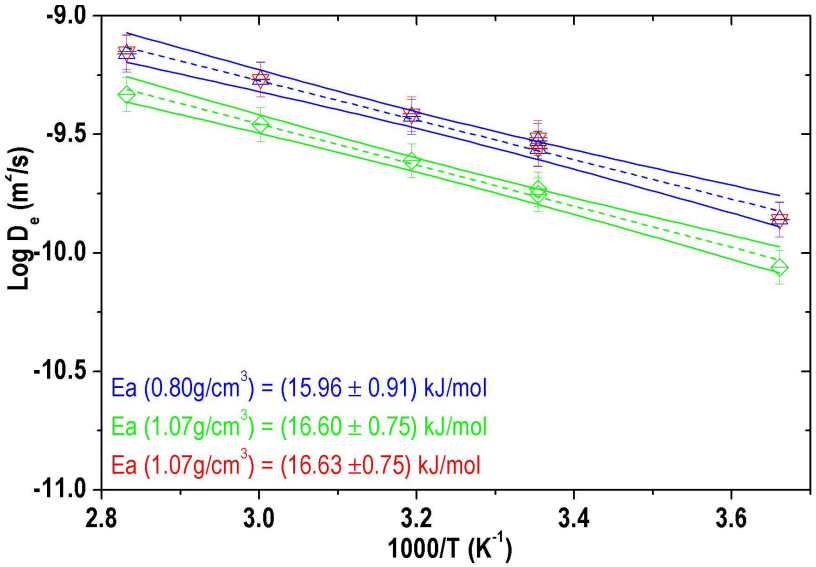

Figure 27. The dependence of the effective diffusion coefficients for HTO through lowly compacted (0.80, 1.07 g/cm^3) Na-montmorillonite on temperature. The background solution was 0.1 M $NaClO_4$.

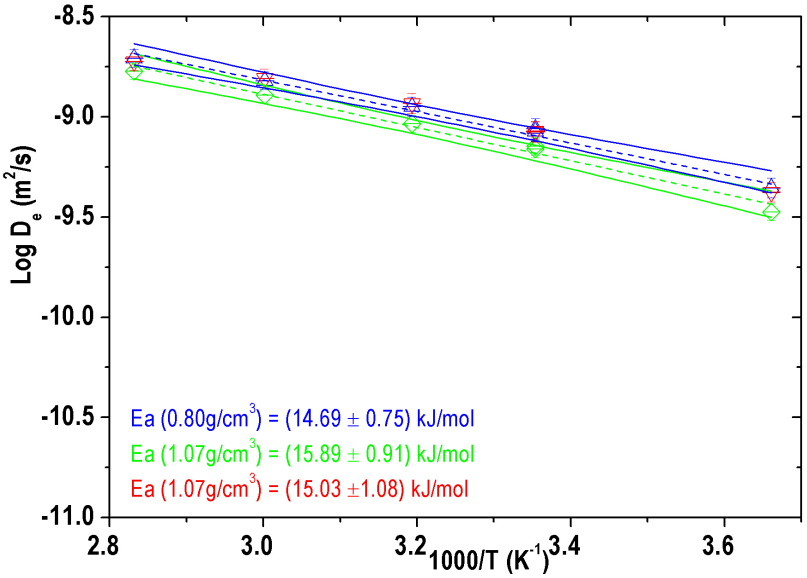

Figure 28. The dependence of the effective diffusion coefficients for ^{22}Na through lowly compacted (0.80, 1.07 g/cm^3) Na-montmorillonite on temperature. The background solution was 0.1 M $NaClO_4$.

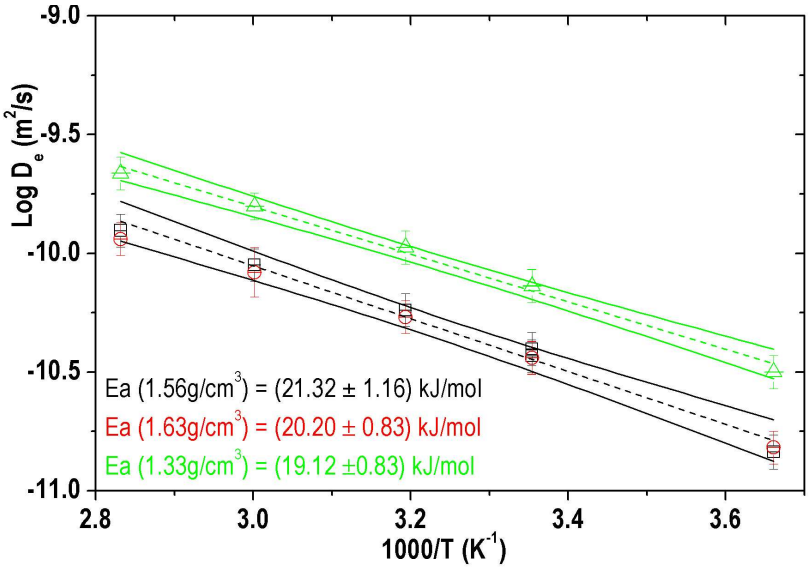

Figure 29. The dependence of the effective diffusion coefficients for HTO through compacted (1.56, 1.63, 1.33 g/cm^3) Na-montmorillonite on temperature. The background solution was 0.1 M $NaClO_4$.

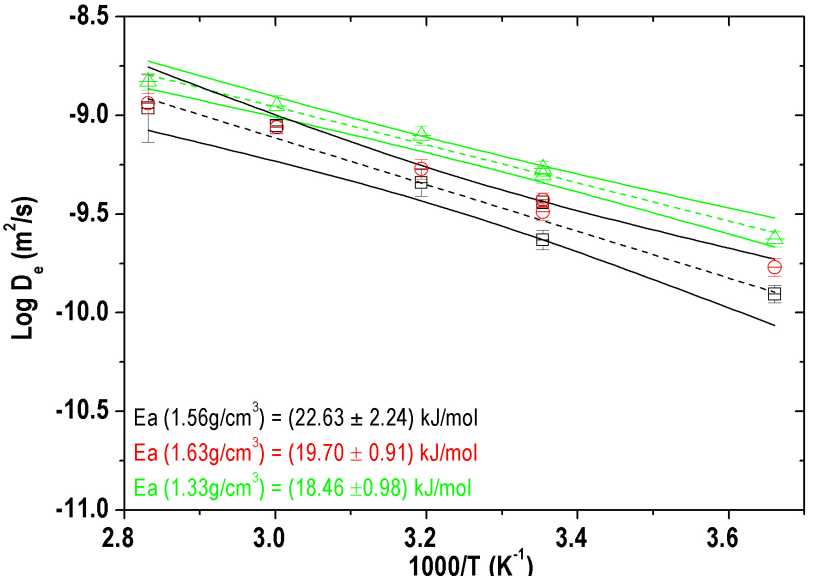

Figure 30. The dependence of the effective diffusion coefficients for ^{22}Na through compacted (1.56, 1.63, 1.33 g/cm^3) Na-montmorillonite on temperature. The background solution was 0.1 M $NaClO_4$.

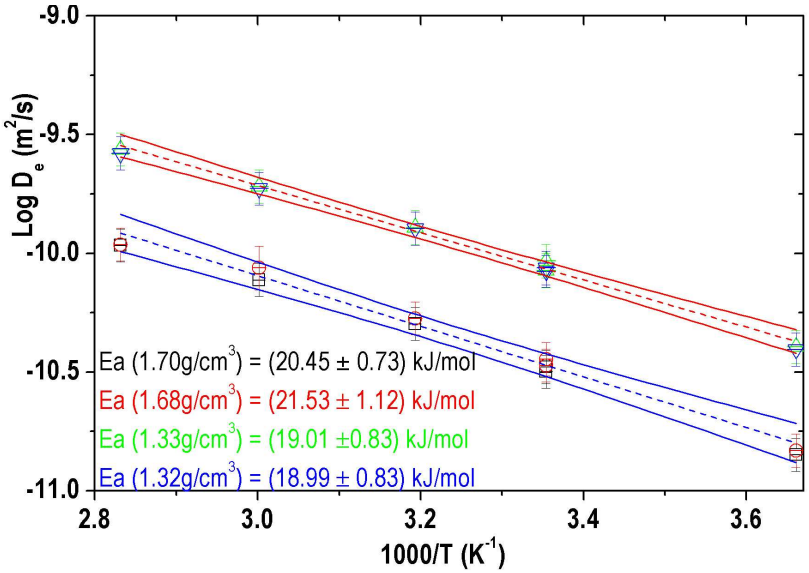

Figure 31. The dependence of the effective diffusion coefficients for HTO through compacted (1.70, 1.68, 1.33, 1.32 g/cm^3) Na-montmorillonite on temperature. The background solution was 1 M $NaClO_4$.

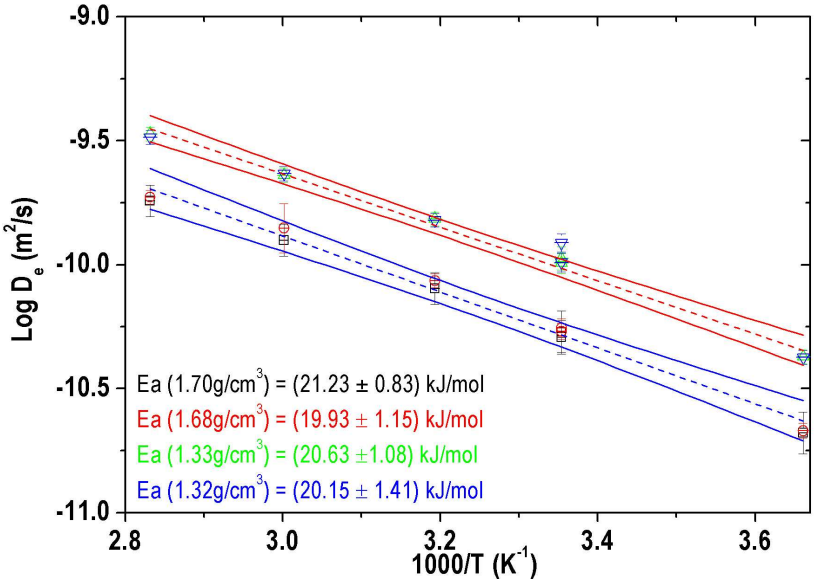

Figure 32. The dependence of the effective diffusion coefficients for ^{22}Na through compacted (1.70, 1.68, 1.33, 1.32 g/cm^3) Na-montmorillonite on temperature. The background solution was 1 M $NaClO_4$.

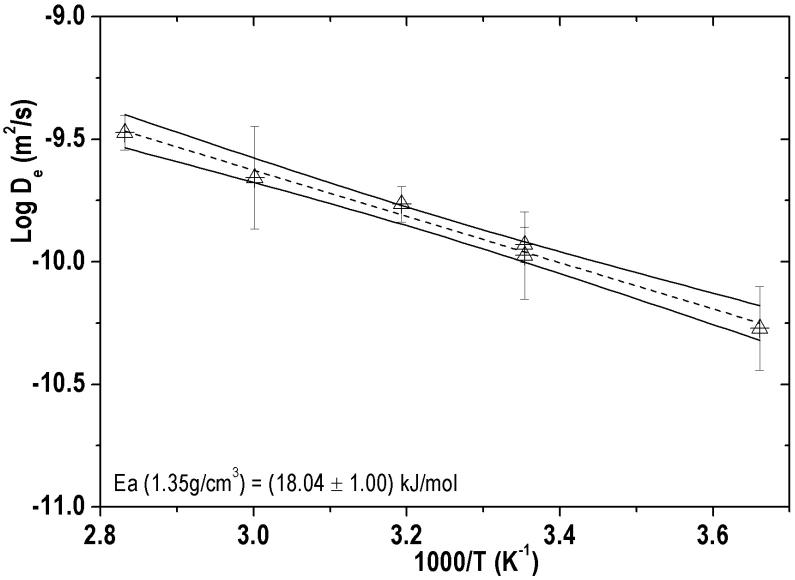

Figure 33. The dependence of the effective diffusion coefficients for HTO through 1.35 g/cm^3 compacted Na-montmorillonite on temperature. The background solution was 5 M $NaClO_4$.

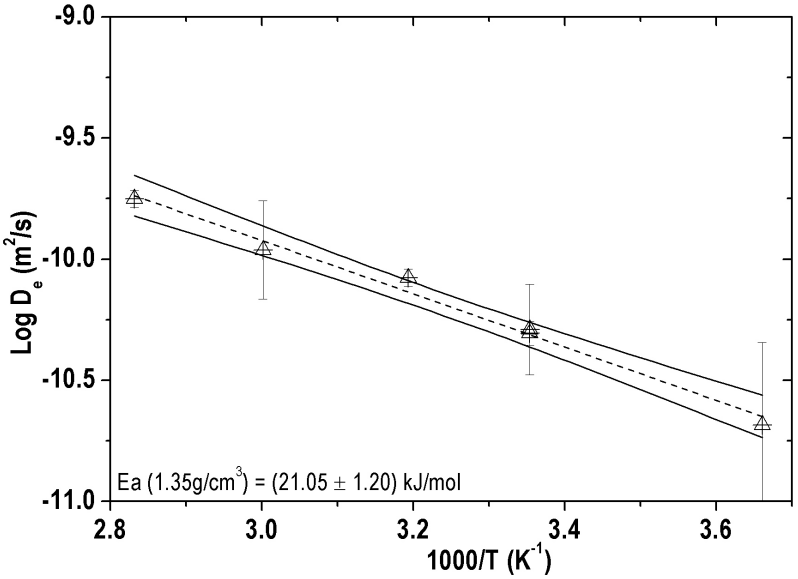

Figure 34. The dependence of the effective diffusion coefficients for ^{22}Na through 1.35 g/cm^3 compacted Na-montmorillonite on temperature. The background solution was 5 M $NaClO_4$.

Table VIII. Results for HTO. *De* is the effective diffusion coefficient in m^2/s, α is the rock capacity factor and Ea is the activation energy.

Sample	1	2	3	4	5	6	7	8	9	10	11
T (°C)	$De \cdot 10^{11}$	$De \cdot 10^{11}$	$De \cdot 10^{11}$	$De \cdot 10^{11}$	$De \cdot 10^{11}$	$De \cdot 10^{11}$	$De \cdot 10^{11}$	$De \cdot 10^{11}$	$De \cdot 10^{11}$	$De \cdot 10^{11}$	$De \cdot 10^{11}$
25	29.6±5.0	18.6±3.0	30.6±5.2	7.3±0.6	3.9±0.6	3.6±0.6	9.3±1.5	8.7±1.4	3.6±0.5	3.3±0.6	10.6±4.1
60				15.8±1.4	8.9±1.4	8.3±1.9	19.1±3.1	18.7±3.0	8.7±1.2	7.7±1.8	
80	69.1±12.1	46.6±7.5	70.4±11.7	21.7±1.9	12.4±1.9	11.5±1.8	27.4±4.4	26.3±4.2	10.9±1.7	10.8±1.7	33.6±5.4
60	53.8±9.0	34.8±5.7	54.0±9.0								22.0±9.8
40	37.6±6.3	24.5±4.0	38.5±6.5	10.6±0.9	5.8±0.9	5.4±0.8	12.9±2.1	12.7±2.0	5.3±0.8	5.0±0.8	17.2±2.9
0	13.8±2.3	8.7±1.4	13.8±2.3	3.2±0.2	1.5±0.2	1.5±0.2	4.0±0.6	3.9±0.6	1.5±0.2	1.4±0.2	5.3±2.0
25	27.6±4.6	17.6±2.9	27.6±4.6	7.3±0.6	3.7±0.6	3.6±0.6	8.5±1.4	8.4±1.3	3.4±0.5	3.2±0.5	11.7±1.9
$\alpha_{25°C}$ (-)	0.79±0.3	0.75±0.3	0.61±0.4	0.98±0.2	0.61±0.1	0.62±0.1	1.11±0.5	0.40±0.4	0.56±0.1	0.47±0.1	0.58±0.2
Ea ($kJmol^{-1}$)	15.9±0.9	16.6±0.7	16.6±0.7	19.1±0.8	21.3±1.2	20.2±0.8	19.0±0.8	19.0±0.8	21.5±1.1	20.4±0.7	18.0±1.0

Table IX. Results for ^{22}Na. *De* is the effective diffusion coefficient in m^2/s, α is the rock capacity factor, K_d is the sorption distribution coefficient, κ the capacity ratio for sorption and Ea is the activation energy.

Sample	1	2	3	4	5	6	7	8	9	10	11
T (°C)	$De \cdot 10^{11}$	$De \cdot 10^{11}$	$De \cdot 10^{11}$	$De \cdot 10^{11}$	$De \cdot 10^{11}$	$De \cdot 10^{11}$	$De \cdot 10^{11}$	$De \cdot 10^{11}$	$De \cdot 10^{11}$	$De \cdot 10^{11}$	$De \cdot 10^{11}$
25	84.4±9.7	71.2±7.3	84.1±9.7	49.8±5.0	36.3±2.8	37.3±3.0	10.6±1.1	12.2±1.0	5.4±0.4	5.1±0.3	5.9±0.4
60				111±14	88.3±7.3	86.8±6.5	23.0±1.5	23.3±1.6	14.0±3.1	12.6±0.8	
80	196±19	169±15	188±18	148±14	109±41	115±14	33.7±2.2	32.6±2.1	18.7±1.2	18.1±1.1	17.7±1.4
60	151±16	128±12	155±17								10.9±4.8
40	112±13	92.2±9.0	116±13.3	78.7±8.9	45.6±7.0	53.4±6.2	15.3±1.0	15.1±1.0	8.6±0.5	8.0±0.5	8.4±0.7
0	44.1±5.0	33.5±3.2	41.9±4.6	23.6±2.2	12.4±1.3	16.9±1.7	4.2±0.3	4.2±0.3	2.1±0.1	2.1±0.2	2.1±1.4
25	87.1±10.2	69.1±6.9	84.6±9.8	53.7±4.9	23.4±2.7	32.5±3.3	10.2±0.9	10.2±1.0	5.6±0.5	5.4±0.4	4.9±0.6
$\alpha_{25°C}$ (-)	8.7±2.1	8.9±2.7	9.7±2.1	17.3±1.5	15.8±1.3	18.4±1.6	1.6±0.4	1.9 ±0.4	1.5 ±0.1	2.0±0.1	0.7±0.3
K_d (cm^3/g)	10.0±2.6	7.7±2.6	8.5±1.9	12.6±1.1	9.8±0.8	11.0±0.9	0.8 ±0.3	1.0 ±0.3	0.7 ±0.08	0.9±0.08	0.1±0.2
κ_{exp} (-)	11.2±2.08	13.4±2.7	14.7±2.1	32.0±1.5	34.6±1.3	43.1±1.6	2.1±0.4	2.7±0.4	2.8±0.1	4.1±0.1	0.4±0.3
κ_{calc} (-)	11.2±1.1	17.3±1.7	17.3±1.7	25.3±2.5	35.2±3.5	39.0±3.9	2.5±0.3	2.5±0.2	4.3±0.4	4.2±0.4	0.5±0.1
Ea ($kJmol^{-1}$)	14.7±0.7	15.9±0.9	15.0±1.1	18.5±1.0	22.6±2.2	19.7±0.9	20.1±1.4	20.1±1.4	19.9±1.1	21.2±0.8	21.0±1.2

4 Chapter 4: Water diffusion in Na-montmorillonite as a function of water content - A neutron scattering study

Martina BESTEL[*1,2] and Fanni JURÁNYI[1]

[1]Laboratory for Neutron Scattering, Paul Scherrer Institut, 5232 Villigen PSI, Switzerland

[2]Institute of Geological Sciences, University of Bern, 3012 Bern, Switzerland

[*]*Corresponding author: mbestel@gmx.de*

Abstract - Swelling clays are major components of engineered barriers in nuclear waste repositories. In a way, they act like a sponge and can absorb large quantities of water. Swelling clays have complex pore structures. Therefore the interpretation of diffusion coefficient of pore water on the macroscopic scale - which is relevant for applications - is difficult. Local diffusion coefficients provide here valuable information. Published data are available only for samples with low hydration where virtually all water belongs to one water population. At higher hydration (lower bulk dry density), water in two or more populations is present in interlayers and interparticle pores. In this work, local diffusion coefficients of water at room temperature were derived from quasielastic neutron scattering experiments (SINQ, PSI, Villigen). The data analysis for Na-montmorillonite samples in which two water populations exists are dicussed. For the first time in the literature, experimentally obtained local diffusion coefficients of water for such highly hydrated samples are presented, and compared to the ones in less hydrated samples.

Key words - Swelling clays, low bulk density, high water content, local diffusion coefficient, quasielastic neutron scattering

Introduction

Na-montmorillonite is a major component of the bentonite barrier used to isolate nuclear waste repositories from the environment. The waste barrier contains swelling clays which are expandable and have self-sealing properties. Therefore, the water diffusion and the release of radionuclides are significantly slowed down. Na-montmorillonite is composed of plate-shaped, small particles which are surrounded by interparticle pores. The crystalline sheets of the particles are held together by charge-compensating cations (like Na^+). These cations form, together with the molecular water layer, the so called interlayer and affect the swelling properties of the clay (Salles *et al.,* 2010). At low water content, all water molecules are located at the surfaces forming hydration shell of the compensating cations (Pusch *et al.,* 2001; Bestel *et al.,* to be submitted). Most of them are in the interlayers, since the external surface area is negligible (Bestel *et al.,* to be submitted). As the water content increases, stepwise swelling occurs in the interlayer. In these steps variable number of molecular water layer (up to 4 *W*) can be intercalated (e.g. Kozaki *et al.,* 1998; Bestel *et al.,* to be submitted). Simultaneously, water accumulates in interparticle pores, so that water in interlayer and interparticle pores is present at the same time.

The interactions on atomistic scale (ps, Å) arising from electrostatic constraints (q, -) affect the local diffusion coefficient (D_l, m^2/s): $D_l = q \cdot D_0$ and the structure of the water (González Sánchez *et al.,* 2009). It is expected, that water in different pore environments have different diffusion coefficients. Therefore understanding and predicting of water diffusion coef-

ficient through the clay on the macroscopic scale is challenging, especially at large water content, i.e. where more than one water population exists. Until now, D_l for Na-montmorillonite with only interlayer water (maximal 1 or 2 *W*) was published (González Sánchez *et al.,* 2008; Bordallo *et al.*, 2008). Bordallo *et al.* (2008) succeeded in measuring diffusion of surface and interlayer water in Na-montmorillonite with quasielastic neutron scattering (QENS) and obtained values for the surface water close to bulk water. Their attempt to obtain local diffusion coefficients in clay samples where two water populations exist was not successful. Bourg *et al.* (2006) proposed a model to connect the apparent diffusion coefficient (D_a, m²/s) measured by tracer diffusion experiments with the local ones. The fractions of interlayer water (f_{ILW}, -) and interparticle water (1-f_{ILW}, -) were additively treated as weighting factors of the local diffusion coefficients:

$$\frac{D_a}{D_0} = \frac{1}{G}\left((1 - f_{ILW}) + \delta_{ILW} f_{ILW}\right) \quad (38)$$

with D_0 (m²/s) the diffusion coefficient in bulk water, δ_{ILW} the constrictivity near basal surfaces in interlayer (the constrictivity for BLW in the interparticle pore compartment is assumed to be one) and *G* (-) the geometrical factor. Latter is defined as $G = \tau^2 \cdot \delta^{-1}$ describing the tortuosity (τ, -) and the constrictivity (δ, -) of the diffusion path. In a previous study we determined the fraction of water in the different pore environments (Bestel *et al.,* to be submitted), while this study is focused on the local diffusion coefficients. The idea of this study was to use the quantified amount of surface water (SW) in interlayer pores and bulk-like water (BLW) in larger (e.g. interparticle) pores with Fixed Window Scans (FWS) on a neutron backscattering spectrometer (Bestel *et al*., to be submitted). The measurement is based on different freezing properties of

these two water populations. It was assumed to obtain more precise values than from d-spacing and surface area measurements (Bestel *et al.*, to be submitted). For samples with low total water contents, similar values were obtained when comparing the results from spectroscopy with results from diffraction. For samples with high water contents (more than 2 water layers in the interlayer), the amount of BLW is increasing to significantly higher values compared to the ones from diffraction. It turned out, that during the FWS measurement water most likely redistribute in samples with high water content, and therefore the obtained fraction is relevant only below about -10 ºC (Anderson, 1967). This conclusion is not yet verified and for this reason the QENS data analysis using these values is also presented. The aim was to obtain D_l from QENS for Na-montmorillonite with 1 to 4 *W*. For the first time in the literature, the fractions of molecular water layers and the fraction of both, surface water (n_{SW}) and bulk-like water (n_{BLW}) were taken into account in order to obtain D_l.

Table X. Experimental set up. ΔE: energy resolution, Q: scattering wave vector.

Instrument	FOCUS
technique	QENS
wavelength (Å)	6.00
ΔE (μeV)	40-50
Q (A^{-1})	0.45-1.65

Material and Methods

Montmorillonite powder was conditioned to the homoionic Na-form. Details and characterisation are described in Bestel *et al.*, (to be submitted). The conditioned clay power was hydrated to a gravimetric water content *w* (g/g) of 0.07, 0.15, 0.32 and 0.49 corresponding to 1, 2, 3 and 3&4 water layers in the interlayer determined by neutron diffraction measurements. To this end,

the hydrated powder was compacted to the bulk dry density ρ_{bd} of 2.06 (1 *W*), 1.67 (2 *W*), 1.29 (3 *W*) and 1.00 g/cm^3 (3&4 *W*). The bulk dry density is defined as the dry clay mass (g) per volume of the sample V_{sample} (cm^3), the latter being 5 cm · 1.5 cm · 0.06 to 0.1 cm. The corresponding water saturation *S* (-) was found to be 0.55 (1 *W*), 0.62 (2 *W*), 0.77 (3 *W*) and 0.76 (3&4 *W*). For the experiments the samples were encapsulated in an aluminum sample holder.

Local diffusion coefficients were obtained from quasielastic neutron scattering (QENS) experiments on FOCUS (SINQ, PSI, Villigen). For the used set up of the instrument see table X. Vanadium was used to calibrate the detector efficiency and to determine the energy resolution ΔE. Measurements for the empty holder and the dry clay were used as background. Experiments were performed at room temperature (300K).

Model to fit Quasielastic Neutron Scattering data

For the samples with SW only and one distinct Bragg peak of 1 *W*, 2 *W* the respective scattered intensity as a function of the scattering wave vector *Q* (Å^{-1}) and the energy transfer *E* (meV) $S^W(Q,E)$ is defined as:

$$S^W(Q,E) = [A(Q)\cdot\delta(E) + B(Q)\cdot S(Q,E)] \otimes R(Q,E) + BG(Q) \quad (39)$$

where $A(Q)\cdot\delta(E)$ is the contribution from the elastic intensity of the dry clay and from the instrument, *R(Q,E)* is the measured resolution function, *BG* (Q) (-) is the background and $S(Q,E)$ is the inelastic contribution from the water. The vibrational contribution is included in *B(Q)*. The different types and motions from isotropic rotation $S_R(Q,E)$ and translational diffusion $S_T(Q,E)$ are assumed to be separated on the time scale in the inelastic contribution from

the water $S(Q,E) = S_R(Q,E) \otimes S_T(Q,E)$. The translational diffusion is defined as (Bée, 1988):

$$S_T(Q,E) = \frac{1}{\pi} \frac{\Gamma^T(Q)}{\varpi^2 + \Gamma^T \Gamma^T(Q)} \quad (40)$$

where Γ^T (meV) is the translational half width at half maximum (line broadening) of the Lorentzian curves. It is known, that the line broadening at large *Q*-values is different from Fick's law because the diffusion process at atomistic scales becomes important. The isotropic rotational diffusion describing the isotropic rotation on a sphere around the center of the water molecule is assumed. This is mathematically described by the Sears expansion (Sears, 1966):

$$S_R(Q,E) = j_0^2(Qa) \cdot \delta(E) + \frac{1}{\pi} \sum_{n=1}^{3} (2n+1)\, j_n^2(Qa) \frac{n(n+1) \cdot \left(\frac{\hbar}{6 \cdot \tau_r} \right)}{E^2 + \left(n(n+1) \cdot \left(\frac{\hbar}{6 \cdot \tau_r} \right) \right)^2} \quad (41)$$

where j_n are spherical Bessel functions, a=0.98Å is the O-H distance, $\delta(E)$ is the Dirac delta funtion, and τ_r (ps) is the rotational relaxation time.

To keep the number of fit parameter on an acceptable level the following assumptions were done:

• Intensity reduction due to vibrational motion so that *B(Q)* is the same for all types of water

• Relative intensity of different water population from Fixed Window Scans and Neutron diffraction measurements is fixed

• Interparticle water has bulk-like properties.

The surface water as 1 to 4 *W* in the interlayer and the bulk-like water in the interparticle pores

are spatially separated. The exchange between them is neglectable during the observation time of QENS. Therefore their contribution to the energy spectrum can be treated additively as further terms in the case of more than one water population. For sample 3 *W* and for sample 3&4 *W* the scattering intensity is defined as:

$$S^{W}(Q,E) = [A(Q)\cdot\delta(E) + B(Q)\left(S_{SW}(Q,E)\cdot n_{\mathrm{SW}} + S_{BLW}(Q,E)\cdot n_{\mathrm{BLW}}\right)] \otimes R(Q,E) + BG(Q) \quad (42)$$

with the inelastic contributions $S_{SW}(Q,\omega)$ and $S_{BLW}(Q,\omega)$ and the fractions n_{SW} (3W and 3&4W) and n_{BLW}, respectively. For sample 3&4 *W* the scattering intensity for the 4 *W* ($S^{W}(Q,E)$) was additionally obtained from

$$S^{W}(Q,E) = [A(Q)\cdot\delta(E) + B(Q)\left(S_{3W}(Q,E)\cdot n_{3\mathrm{W}} + S_{4W}(Q,E)\cdot n_{4\mathrm{W}} + S_{BLW}(Q,E)\cdot n_{\mathrm{BLW}}\right)] \otimes R(Q,E) + BG(Q) \quad (43)$$

with the inelastic contributions $S_{3W}(Q,\omega)$ and $S_{4W}(Q,\omega)$ and the fractions n_{3W} and n_{4W}, respectively. The local diffusion coefficient for the 3 *W* state was fixed to the former obtained value of $1.5\cdot10^{-9}$ m²/s in order to obtain D_l for 4 *W* (Tab. XI, Appendix).

Cebula et al. (1981), Anderson et al. (1999) and González Sánchez *et al.* (2008) obtained good results for montmorillonite using the jump diffusion model (Hall and Ross, 1981; Singwi and Sjölander, 1960). For that reason, the Singwi-Sjölander diffusion model which accounts for the described deviation from Fick's law at larger *Q*-values was used to obtain Γ^{T} as a function of *Q* (Singwi and Sjölander, 1960):

$$\Gamma^{T}(Q) = \frac{\hbar\cdot D_l\cdot Q^2}{1 + D_l\cdot Q^2\cdot\tau_t} \quad (44)$$

The jump diffusion model describes the fixed time τ_t (ps) that a hydrogen atom spends at a quasi-equilibrium position before it jumps to the next quasi equilibrium position with mean

jump length l (Å) (Singwi and Sjölander, 1960):

$$l = \sqrt{6 \cdot D_l \cdot \tau_t} \qquad (45)$$

Results & Discussion

In the next paragraph, the results for local diffusion coefficient D_l of 1 to 4 water layers in the Na-montmorillonite interlayer from equations 39-44 are presented and discussed (Tab. XI, Appendix).

The local diffusion coefficient D_l for the samples 1 *W* and 2 *W* were derived using one water population (Eq. 39). The D_l value from equation 44 is lower for 1 *W* compared to the sample with 2 *W*. Both obtained values are lower compared to that in highly compacted Na-montmorillonite (González Sánchez *et al.*, 2008). The obtained l from equation 45 was similar for samples 1 *W* and 2 *W*. However, it has to be mentioned, that the experimental setup has been optimized regarding D_l and it is not ideal for obtaining l due to the limited Q range. Therefore the fitted residence times and calculated mean jump lengths are less reliable than the diffusion coefficients.

The sample 3*W* is the best for discussing the data analysis with different models of one (Eq. 39, model I) and two (Eq. 40, model II) water populations. Model I does not account for the differences in the dynamics of interlayer and interparticle water, and results in a kind of average value. Contrary to that it is expected that the data contains summed intensities from all water populations since the exchange of water molecules is neglectable on the time scale of the QENS experiment. In this sample the interlayer of all particles is filled with 3 water layers. This water population (3W) has to be distinguished from the interparticle water with bulk-like prop-

erties. The parameters of interparticle water (D_{BLW}, translational and rotational jump lengths) were fixed to the values from bulk water and the ratio of 3 *W* and BLW was fixed to the value obtained from the Fixed Windo Scan measurements. The number of fitted parameters was the same for both models. The isotropic rotation, $BG(Q)$ and the inelastic contribution were identical for the obtained D_l for both models. The elastic intensity *A(Q)* increases towards Q=0 $Å^{-1}$ for model I, while it is constant using model II. Both behaviors are explainable. Either there is a true small angle scattering from the clay structure or (part of) the second water population is apparently immobile. Consequently the line width Γ^T and the obtained average D_l is smaller for model II compared to model I (Fig. 35). Comparing the residuals model II fits slightly better. The main deviation might arise from paramagnetic scattering of Fe in the clay structure (Bordallo *et al.,* 2008). Both D_l values (from model I and from model II) are between the values of sample 2*W* and Na-illite (González Sánchez *et al.,* 2008), as it is expected. The mean jump length is higher than for Na-illite and lower than for highly compacted Na-montmorillonite. The local diffusion coefficient is stable when changing the fitting area of *Q*. The average D_l was deduced from different fixed values for some parameters. Some of the parameters are coupled (like $BG(Q)$ and rotational time), but fixing some parameters to a reasonable value, and repeating the fit for different values, we have seen that D_l is hardly affected. From this we can conclude that adding the signal from the different water populations (W, SW, BLW) lead to such slow diffusion coefficients.

The sample 3&4 *W* has water in the interlayer both in 3 and in 4 layer form, which might have measurably different diffusion properties. Here also 2 models have been used for data analysis: in equation 42 (model II), like before two water populations are distinguished and equation 43 (model III) with 3 water populations. In more detail, in model II it is assumed, that

both the 3 and 4 layer form has the same or similar diffusion coefficients, i.e. only interlayer and interparticle water is distinguished, whereas in model III they are handled separately. To keep the number of fit parameters low enough, the parameters of the 3 *W* state is fixed to the numbers obtained with model II for sample 3 *W*. And again in both models it is assumed, that the interparticle water has bulk like properties. The obtained D_l value was constant (within the error bar) for different fitting parameter and similar for 3 and 4 *W* suggesting similar dynamical behavior. The low value from model III is possibly due to the too low n_{4W} in the sample.

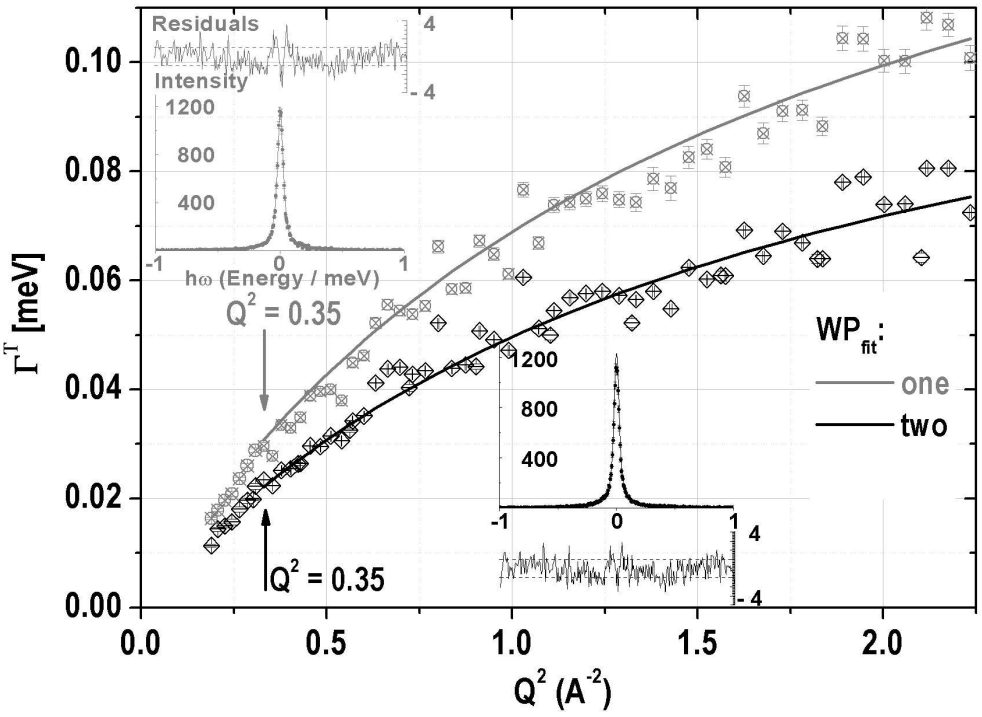

Figure 35. The translational line widths (Γ^T) versus momentum transfer (Q^2) from models I (equation 39) and II (equation 42) with corresponding number of water populations (WP_{fit}). The solid lines are the fits to the data. The inserted diagrams are the QENS spectra and residuals of the fit for the lowest Q^2-value included in the fit.

Finally the consequences of the large discrepancy in the water distribution as obtained from FWS and diffraction measurements for samples containing more than 2 layer water in the interlayer has to be discussed. The results from the Fixed Window Scan measurements might characterize the samples in a different state than they were during the QENS measurements due to possible water redistribution in the clay during cooling as reported in Anderson, 1967 and Svensson and Hansen (2010). In this case the ratio obtained from diffraction should be used instead of the ones from the Fixed Window Scans. Temperature dependent diffraction measurements are foreseen to clarify this issue before finalizing the data treatment for samples 3W (model II) and 3&4W (model II and model III).

Conclusion & Outlook

Na-montmorillonite samples with different amount of pore water has been measured by quasielastic neutron scattering in order to determine local diffusion coefficients in the interlayer of up to four intercalated molecular water layers. For samples with high water content (from three to four molecular water layers) the fractions of two different water populations of surface and bulk-like water were involved in a model. Local diffusion coefficients from models with one and two water populations were compared for a sample which contains not only interlayer but also interparticle water. The translational line width and local diffusion coefficient from the model with one water populations are evidently largerer. The larger line width is accompanied by the presence of a true or apparent small angle scattering. Based on the fit results it was not possible to declare the model with one water population as erroneous. In comparison to Na-montmorillonite with 1 and 2 water layers and highly compacted Na-illite from literature the obtained average local diffusion coefficient for both models are realistic. The reason for this

might be that the used ratio between the different water populations is not the correct one describing the sample at ambient conditions. More realistic value might be the one from diffraction, where the amount of interparticle water is only few percent.

The obtained data set together with the measured water distribution and results from tracer diffusion can give a solid base for testing upscaling models like of Bourg *et al.* (2006).

Acknowledgment

This work is based on experiments performed at the Swiss spallation neutron source SINQ, Paul Scherrer Institute, Villigen, Switzerland. The authors acknowledge the financial support of the Swiss National Science Foundation (SNF).

References

Anderson, D.M., 1967. Interface between ice and silicate surfaces. Journal of Colloid and Interface Science 25, 174-191.

Anderson, M.A., Trouw, F.R., Tam, C.N., 1999. Properties of water in calcium- and hexadecyltrimethylammonium-exchanged bentonite. Clays and Clay Minerals 47, 28-35.

Bée M., 1988. Quasielastic Neutron Scattering: Principles and Applications in Solid State Chemistry, Biology and Material Science In: Institute of Physics Publishing. ISBN 0852743718

Bestel, M., Gimmi, T., Glaus, M.A., Van Loon L.R., Zamponi, M., Diamond, L.W., Jurányi, F., to be submitted. Water distribution in Na- and Cs-montmorillonite. Clays and Clay Mineralogy.

Bordallo, H.N., Aldridge, L.P., Churchman, G.J., Gates, W.P., Telling, M.T.F., Kiefer, K., Fouquet, P., Seydel, T., Kimber, S.A.J., 2008. Quasi-elastic neutron scattering studies on clay interlayer-space highlighting the effect of the cation in confined water dynamics. Journal of Physical Chemistry C 112, 13982-13991.

Cebula, D.J., Thomas, R.K., White, J.W., 1981. Diffusion of water in Li-montmorillonite studied by Quasi-elastic neutron-scattering. Clays and Clay Minerals 29, 241-248.

Bourg, I.C., Sposito, G., Bourg, A.C.M., 2006. Tracer diffusion in compacted, water-saturated bentonite. Clays and Clay Minerals 54, 363-374.

Gonzalez Sanchez, F., Juranyi, F., Gimmi, T., Van Loon, L., Unruh, T., Diamond, L.W., 2008. Translational diffusion of water and its dependence on temperature in charged and uncharged clays: A neutron scattering study. The Journal of Chemical Physics 129, 174706-174706.

Gonzalez Sanchez, F., Gimmi, T., Juranyi, F., Van Loon, L., Diamond, L.W., 2009. Linking the diffusion of water in compacted clays at two different time scales: tracer through-diffusion and quasielastic neutron scattering. Environmental Science & Technology 43, 3487-3493.

Hall, P.L., Ross, D.K., 1981. Incoherent neutron-scattering functions for random jump diffusion in bounded and infinite media. Molecular Physics 42, 673-682.

Kozaki, T., Fujishima, A., Sato, S., Ohashi, H., 1998. Self-diffusion of sodium ions in compacted sodium montmorillonite (vol 121, pg 63, 1998). Nuclear Technology 123, 120-120.

Pusch, R., 2001. The microstructure of MX-80 clay with respect to its bulk physical properties under different enviromental conditions. Swedish Nuclear Fuel and Waste Management Co. (SKB), ISSN 1404-0344.

Salles, F., Bildstein, O., Douillard, J.M., Jullien, M., Raynal, J., Van Damme, H., 2010. On the Cation Dependence of Interlamellar and Interparticular Water and Swelling in Smectite Clays. Langmuir 26, 5028-5037.

Sears, V.F., 1966. Theory of cold neutrons scattering by homonuclear diatomic liquids. I. Free rotation. Canadian Journal of Physics 44, 1279-1297.

Singwi, K.S., Sjolander, A., 1960. Diffusive motions in water and cold neutron scattering. Physical Review 119, 863-871.

Svensson, P.D., Hansen, S., 2010. Freezing and thawing of montmorillonite - A time-resolved synchrotron X-ray diffraction study. Applied Clay Science 49, 127-134.

Wuttke, J., Budwig, A., Drochner, M., Kaemmerling, H., Kayser, F.-J., Kleines, H., Ossovyi, V., Carlos Pardo, L., Prager, M., Richter, D., Schneider, G.J., Schneider, H., Staringer, S., 2012. SPHERES, Julich's high-flux neutron backscattering spectrometer at FRM II. Review of Scientific Instruments 83.

Appendix 3

Table XI. Sample properties for Na-montmorillonite (Na-mnt) with W: number of molecular water layers and *w*(g/g): gravimetric water content per dry clay mass taken from Bestel *et al.* (to be submitted). The average local diffusion coefficients (D_l) (grey font) and mean jump lengths (l) for 300K (grey font) were obtained for the fixed values (black font) of D_l, D_{BLW} and n_{SW} (%), n_{BLW} (%): the water fraction of surface (SW) and bulk-like water (BLW) from equations 39-45. In comparison the data from González Sánchez *et al.* (2008) [1].

	Na-mnt										Na-mnt [1]	Na-illite [1]
W	1	2	3		3&4						2	9
w (g/g)	0.07	0.14	0.31		0.49						0.16	0.14
	n_{SW}	n_{SW}	n_{SW}	n_{BLW}	n_{SW}	n_{BLW}	n_{3W}	n_{4W}	n_{BLW}		n_{SW}	
%	100	100	100	30	60	40	47	20	33		100	
	$D_l \cdot 10^9$	$D_l \cdot 10^9$	$D_l \cdot 10^9$	$D_{BLW} \cdot 10^9$	$D_l \cdot 10^9$	$D_{BLW} \cdot 10^9$	$D_l \cdot 10^9$	$D_l \cdot 10^9$	$D_{BLW} \cdot 10^9$		$D_l \cdot 10^9$	$D_l \cdot 10^9$
m^2/s	0.5±0.1	0.9±0.1	1.8±0.1	2.4	1.3±0.1	2.4	1.5	1.4±0.1	2.4		1.2 ± 0.1	2.2 ± 0.1
l (Å)	1.91±0.39	1.90	2.07±0.10	1.98±0.02	2.33		2.46				2.82±0.15	1.61±0.13

5 Erklärung

Gemäss Art. 28 Abs. 2 RSL 05

Vorname, Name: Martina Bestel

Matrikelnummer: 09-105-263

Studiengang: Erdwissenschaften

Titel der Arbeit: Water–montmorillonite systems: Neutron scattering and tracer through-diffusion studies

Ich erkläre hiermit, dass ich diese Arbeit selbstständig verfasst und keine anderen als die angegebenen Quellen benutzt habe. Alle Stellen, die ich wörtlich oder sinngemäss aus Quellen entnommen wurden, habe ich als solche gekennzeichnet. Mir ist bekannt, dass andernfalls der Senat gemäss Artikel 36 Absatz 1 Buchstabe r des Gesetzes vom 5. September 1996 über die Universität zum Entzug des auf Grund dieser Arbeit verliehenen Titels berechtigt ist.

Bern, den 06.05.2014

6 Curriculum Vitae

Name:	Martina
Surname:	Bestel
Date of birth:	21.09.1982
Place of birth:	Sangerhausen (Germany)
Email:	mbestel@gmx.de

Education:

2009/2014	Dissertation phil. nat. at the Institute of Geological Science, University of Bern (Switzerland). "Water–montmorillonite systems: Neutron scattering and tracer through-diffusion studies" at the Paul Scherrer Institute (Villigen-Switzerland)
2003/2009	Diploma degree in Geology, Institute of Geological Science, Free University of Berlin (Germany)

Work experience:

2009/2014	Ph. D. student at the Laboratory for Neutron scattering and the Laboratory for Waste Management, Paul Scherrer Institute, (Villigen-Switzerland)
2009/2012	Student assistent at the Institute of Geological Science, University of Bern (Switzerland)
2007/2009	Student assistent at the Institute of Geological Sciences, Free University of Berlin (Germany)
2002	Internship at "Environmental measurement & consult", (Erfurt-Germany)

Publications:

1.	Bestel, M., Gimmi, T., Glaus, M.A., Van Loon L.R., Zamponi, M., Diamond, L.W., Jurányi, F., to be submitted. Water distribution in Na- and Cs-montmorillonite. Clays and Clay Mineralogy.
2.	Bestel, M., Frick, S., Glaus, M.A., Gimmi, T., Van Loon, L.R., and Diamond, L.W., to be submitted. Combined tracer through-diffusion of HTO and ^{22}Na through Na-montmorillonite with different bulk dry den-

sities. Applied Geochemistry.

3. Bestel, M., Gawronski, T., Abart, R. and Rhede, D., 2009. Compositional zoning of garnet porphyroblasts from the polymetamorphic Wölz Complex, Eastern Alps. Mineralogy and Petrology, 97, 173-188.